

THERMODYNAMIC CHARACTERISTICS OF FERROELECTRIC
AND ANTIFERROELECTRIC TRANSITIONS IN
LEAD PEROVSKITES

By

JOHN WILLARD NORTHRIP

Bachelor of Science
Southwest Missouri State College
Springfield, Missouri
1954

Master of Science
Oklahoma State University
Stillwater, Oklahoma
1958

Submitted to the Faculty of the Graduate School of
the Oklahoma State University
in partial fulfillment of the requirements
for the degree of
DOCTOR OF PHILOSOPHY
August, 1964

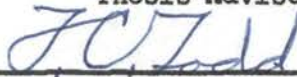
JAN 8 1965

THERMODYNAMIC CHARACTERISTICS OF FERROELECTRIC
AND ANTIFERROELECTRIC TRANSITIONS IN
LEAD PEROVSKITES

Thesis Approved:

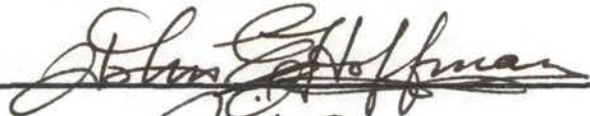


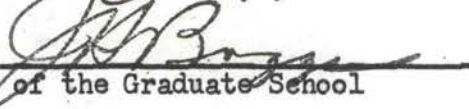
Thesis Adviser











Dean of the Graduate School

570279
ii

ACKNOWLEDGMENT

I wish to express the deepest gratitude to Dr. E. E. Kohnke for his valuable guidance and encouragement during the planning and execution of this study. I would also like to express my thanks to the many other members of the staff of Oklahoma State University who through their advice and suggestions have aided in its completion. Special thanks are due to Gary Baum for his aid in the experimental procedures and the equipment design. I must also express the utmost gratitude to the National Science Foundation and Sandia Corporation, who through their contributions of finances, equipment, and sample materials have made the study possible.

TABLE OF CONTENTS

Chapter		Page
I.	INTRODUCTION	1
II.	CRYSTALLOGRAPHY AND CHEMISTRY OF PEROVSKITES	6
	Lead Perovskite Materials	10
III.	THERMODYNAMICS OF PHASE TRANSITIONS IN FERROELECTRICS AND ANTIFERROELECTRICS	17
	Thermodynamics of Phase Transitions	17
	Applications of the Above Considerations to Ferroelectric and Antiferroelectric Transitions	24
IV.	DIELECTRIC MEASUREMENTS	31
	Dielectric Susceptibilities	31
	Dielectric Loss	34
	Measurement Equipment	36
	Experimental Samples	38
	Measurement Procedures and Calculating Techniques	39
	Results	40
V.	POLARIZATION MEASUREMENTS	57
	Experimental Equipment	60
	Calculation Techniques	60
	Experimental Results	63
VI.	THERMAL MEASUREMENTS	68
	Description of Equipment	69
	Description of Samples	71
	Measurement Techniques	74
	Experimental Results	84
VII.	RESULTS OF RELATED WORK	97
	Clevite Work on $Pb_{0.99}Nb_{0.02}(Zr_{0.68}Ti_{0.07}Sn_{0.25})_{0.98}O_3$	97
	Clevite Lead Zirconate Titanate Stannate Compositional Studies	102
	Sandia Studies On Lead Hafnate Titanate Compositions	103

Chapter	Page
VIII. CONCLUSIONS	106
Free Energy Relationships in $\text{Pb}_{0.99}\text{Nb}_{0.02}(\text{Zr}_{0.68}\text{Ti}_{0.07}\text{Sn}_{0.25})_{0.98}\text{O}_3$	106
Results for the Lead Hafnate Titanate Samples . . .	116
Qualitative Theory of FE-AFE Transitions in Lead Perovskites	116
Resume of Experimental Techniques	119
BIBLIOGRAPHY	122

LIST OF TABLES

Table		Page
I.	Tolerance Factors for Principal Perovskite $A^{+2}B^{+4}O_3$ Ferroelectrics	8
II.	Phase Boundary Relationships	30
III.	Dimensions of Samples Used in Dielectric Measurements . .	39
IV.	Data From Preliminary Thermal Measurements	88
V.	Heat of Transition Data	96

LIST OF FIGURES

Figure	Page
1. Representation of a Ferroelectric (a) and Antiferroelectric (b) Dipole Array	10
2. Compositional Phase Diagram for $\text{Pb}(\text{Zr}_{1-x}\text{Ti}_x)\text{O}_3$	13
3. Compositional Phase Diagram for $\text{Pb}(\text{Zr}_{0.70-x}\text{Ti}_x\text{Sn}_{0.30})\text{O}_3$	14
4. Compositional Phase Diagram for $\text{Pb}(\text{Hf}_{1-x}\text{Ti}_x)\text{O}_3 + 1 \text{ wt } \% \text{ Nb}_2\text{O}_5$	16
5. U and G vs. T for $p = 0$ and $E = 0$	20
6. Variation of Free Energy with Polarization for a Ferroelectric Material	32
7. Polarization vs. Bias Voltage Showing Nonlinear Saturation Effect	33
8. Block Diagram of Dielectric Measurement Apparatus	37
9. Dielectric Data for PZST	41
10. Phase Diagram for PZST as a Function of Field and Temperature	43
11. Dielectric Constant at the Transition vs. Field for PZST	45
12. Behavior of PZST Above the Curie Temperature as a Function of Applied Electric Field	46
13. Dielectric Constant vs. Field for Sample 95HN2	48
14. Dielectric Constant vs. Field for Sample 96HN2	49
15. Dielectric Constant vs. Field for Sample 97HN2	50
16. Dielectric Constant vs. Field for Sample 98HN4	51
17. Dielectric Constant vs. Field for Sample 100HN2	52
18. Curie Temperature vs. Bias Field for Lead Hafnate Titanate Compositions	53

Figure	Page
19. Peak Dielectric Constant vs. Bias Field for Lead Hafnate Titanate Compositions	54
20. Tentative Temperature vs. Field Phase Diagram for 96HN2	56
21. Double Hysteresis Loop Observed During Field Enforced AFE-FE Transition	59
22. Sawyer-Tower Circuit for 60 cps Hysteresis Loops	61
23. Circuit for Slow Loop Hysteresis Measurements	62
24. Hysteresis Parameters for the 95/5 Lead Hafnate Titanate Composition	64
25. Hysteresis Parameters for the 96/4 Lead Hafnate Titanate Composition	65
26. Hysteresis Loops and Portions of Double Hysteresis Loops Showing Field Enforced Ferroelectric Phase in the 96/4 Lead Hafnate Titanate Composition	67
27. Calorimeter Design	70
28. Construction of Sample Assembly	72
29. Determination of Loss Factor in Preliminary Measurements	77
30. Exponential Cooling Curve for Quartz Check Sample	78
31. Block Diagram of Automated Thermal Measurement Apparatus	82
32. Amplifier Schematic for Automated System	83
33. Input Power and Rate of Change of Temperature as Function of Temperature for PZST	85
34. Exponential Cooling for Lead Hafnate Titanate Samples	86
35. Measurement of Thermal Loss Factor for Lead Hafnate Titanate Samples	87
36. Specific Heat vs. Temperature for $\text{Pb}(\text{Hf}_{0.95}\text{Ti}_{0.05})_3 + 1 \text{ wt. } \% \text{ Nb}_2\text{O}_5$	89
37. Specific Heat vs. Temperature for $\text{Pb}(\text{Hf}_{0.96}\text{Ti}_{0.04})_3 + 1 \text{ wt. } \% \text{ Nb}_2\text{O}_5$	90
38. Specific Heat vs. Temperature for $\text{Pb}(\text{Hf}_{0.97}\text{Ti}_{0.03})_3 + 1 \text{ wt. } \% \text{ Nb}_2\text{O}_5$	91

Figure	Page
39. Specific Heat vs. Temperature for $\text{Pb}(\text{Hf}_{0.98}\text{Ti}_{0.02})\text{O}_3 + 1 \text{ wt. } \% \text{ Nb}_2\text{O}_5$	92
40. Specific Heat vs. Temperature for $\text{PbHfO}_3 + 1 \text{ wt. } \% \text{ Nb}_2\text{O}_5$	93
41. Specific Heat vs. Temperature for PZST	94
42. Excess Power vs. Time Plot Used to Calculate Curie Transition Energy for PZST	95
43. Polarization vs. Temperature and Pressure for PZST	99
44. Electric Field vs. Pressure Phase Diagram for PZST	100
45. Electric Field vs. Temperature Phase Diagram for PZST	101
46. Comparison of Transitions Observed with Increasing Temperature and Increasing Field for PZST	109
47. C_p/T for PZST Sample	113
48. Free Energy vs. Temperature for PZST	113
49. Relative Free Energies of the Various Phases for a PZST Sample at Zero Field	115
50. Relative Free Energies of the Various Phases for a PZST Sample with External Field of 5 Kv/cm	115

CHAPTER I

INTRODUCTION

Although the study of ferroelectricity is of relatively recent origin, it is a field which has shown phenomenal growth. The unique properties of these materials (high dielectric constant, strong electro-mechanical coupling, charge storage capabilities, etc.) have led to a large amount of published work ranging from materials research and fundamental theory to device applications. Several good reviews of this work have already been published (16, 17, 18, 19, 22) so no comprehensive review of past literature will be listed here.

From a crystallographic viewpoint, certain materials are characterized by the presence of a spontaneous electric dipole within the unit cell. That is, the center of negative charge does not coincide with the center of positive charge at zero electric field. Since the magnitudes of these internal dipoles change with temperature, giving rise to detectable surface charges, the materials have come to be called "pyro-electrics." In 1917, during studies of the dielectric and piezoelectric anomalies of Rochelle salt, Anderson (1) and Cady (6) discovered that its spontaneous internal polarization could be reversed by the application of an electric field at certain temperatures. This gave rise to hysteresis loops similar to those observed in ferromagnetism and thus the phenomenon was given the name "ferroelectricity." This correspondence, however, is sometimes misleading since ferromagnetism

occurs principally at the electronic level while ferroelectricity is basically an ionic phenomenon. It is interesting to note that in much European literature the term used is "seignettelectricity" from the French term for Rochelle salt (Seignette salt).

Thus, a ferroelectric is a material exhibiting a reversible spontaneous electrical dipole within each unit cell. The existence of this polarization at the macroscopic level is usually masked by surface charges and is revealed by applying an electric field to reverse the dipoles, causing a current to flow in the external circuit. The interaction of this internal polarization with the ionic positions in the crystal lattice gives rise to the striking electrical, mechanical, optical, and thermal effects associated with ferroelectricity.

During the course of ferroelectric investigations another class of materials was found in which the basic cell exhibited a spontaneous dipole but with neighboring dipoles antiparallel. In such materials there is no macroscopic polarization but many of the other phenomena characterizing ferroelectricity are present. In correspondence to their ferromagnetic analogues, these materials are called antiferroelectrics.

Most ferroelectric and antiferroelectric materials have been grouped into four chemical classes:

1. Rochelle salt and its isomorphous salts. These materials are characterized by having both an upper and a lower temperature limit to the ferroelectric region and are piezoelectric in the non-ferroelectric state. Present theories attribute their ferroelectric properties to orientations involving the hydroxyl groups in this complex structure.

2. Potassium dihydrogen phosphate and isomorphous compounds. These materials exhibit their ferroelectric properties only at temperatures well below zero Centigrade. Their behavior is attributed to an orientation of the phosphate radicals by the hydrogen bonds. Ammonium dihydrogen phosphate was one of the first studied antiferroelectric materials.
3. The perovskite compounds. These materials have so far been the most important group from an application viewpoint since they exhibit strong ferroelectric properties at room temperature, have high polarizations, and are mechanically stable. Their ferroelectric properties are attributed to slight perturbations of the basic cubic perovskite structure. More will be said about this class of compounds in the next chapter.
4. Miscellaneous structures. This includes many compounds, usually of a complex layered structure, which cannot be conveniently grouped under a single structure. In general, these compounds have low polarizations with a corresponding decrease in the anomalies observed in all properties.

Almost all ferroelectric materials exhibit a phase transition into a more symmetric phase at some temperature. This more symmetric phase is no longer ferroelectric; it exhibits normal dielectric behavior with the exception that the dielectric constant decreases with rising temperature. Because of this decrease, this upper phase has been called "paraelectric." It should be pointed out, however, that the internal behavior of the paraelectric phase does not differ from that of a dielectric in the same way that a paramagnetic material differs from a diamagnetic one.

The temperature at which the ferroelectric or antiferroelectric phase becomes paraelectric is known as the Curie temperature. This phase transition has been studied quite thoroughly in many materials. It has been found in some materials to be first order, in some second order, and in at least one case a "higher than second order" transition was reported (11). The transition is most easily detected by the pronounced peak of dielectric constant occurring at that temperature or by the discontinuous release of polarization charge if the transition is of first order. All other properties connected with the spontaneous internal polarization (piezoelectric behavior, optical birefringence, etc.) also undergo drastic changes at this temperature.

Besides the Curie transition there are other phase transitions which may occur within a ferroelectric or antiferroelectric material. These transitions involve minor shifts within the lattice and usually cause a shift in the direction of internal polarization (the ferroelectric axis). These again are accompanied by anomalies in all the properties connected with polarization but usually to a much lesser degree than in the Curie transition. Some of these changes will be discussed more fully in the next chapter, which deals with the behavior of materials having the perovskite structure.

A few materials exhibit phase transitions in which they change from the ferroelectric to the antiferroelectric state. This phenomenon was first observed in sodium niobate (7), which is antiferroelectric between -60°C and -200°C and ferroelectric below -200°C . Within the last few years it has been found that several lead perovskite solid solutions also exhibit this behavior. It is these materials which are of interest here.

It is the purpose of this research to study some of the thermodynamic characteristics of the ferroelectric and antiferroelectric phases in these lead perovskites. A survey of the chemical and crystallographic characteristics of the perovskite structure has been made with special emphasis on the role of ionic properties in the determination of ferroelectric behavior. A review of the thermodynamics of ferroelectrics and antiferroelectrics is given and a proposal outlined for the relationships between the various phases which would lead to the observed phase diagrams for ferroelectric and antiferroelectric phases.

Much of this study has been devoted to the refinement and interpretation of the experimental techniques used in studying the various phase transitions. Measurements have been made of dielectric constant and loss as functions of both temperature and electric field. An important finding of this work has been the development of the "loss conductance as a more sensitive and accurate indicator of material characteristics than the more conventional loss tangent or dissipation factor. Polarization measurements have been made in the vicinity of the ferroelectric-antiferroelectric transitions in an effort to explain some of the anomalous hysteresis loops observed in this region. A calorimetric study has been made to determine the specific heat and heats of transition of these materials in order to approximate the temperature dependence of the free energies of the various phases.

Finally, a correlation of this work with other work on perovskite solid solutions has been made in an effort to determine some of the patterns of behavior of this important family of materials.

CHAPTER II

CRYSTALLOGRAPHY AND CHEMISTRY OF PEROVSKITES

The perovskite family of materials has played a very important role in the history of ferroelectricity. Because of their large polarizations and high electromechanical coupling coefficients, these materials have become the most commercially useful of all ferroelectric materials. Barium titanate, the first ferroelectric perovskite discovered, has been the subject of a vast amount of research which has led to much of our basic knowledge about ferroelectrics in general. The fact that many of the perovskites are soluble with one another leads to a whole range of solid solutions which allow a variation of the ferroelectric properties to fit the convenience of the user. It is in this realm of solid solutions that the present study is most interested.

The basic perovskite lattice is of simple cubic structure having the composition ABO_3 . The structural unit cell can be pictured as a cube having A atoms at the corner, a B atom in the body center position, and oxygen atoms in the face centers.

In making a transformation into a ferroelectric or antiferroelectric phase, the basic perovskite cube must become slightly distorted. A one dimensional distortion of the cube leaves the lattice in the tetragonal symmetry. If this distortion is a lengthening of a cube edge, the material becomes ferroelectric; if it represents a compression, the material becomes antiferroelectric. A two dimensional shear of the cube

leads to the orthorhombic phase in which the polarization axis lies along a face diagonal. If the original cube is given a three dimensional shear, the symmetry becomes rhombohedral with the polarization axis being one of the body diagonals.

The use of ceramic samples of perovskite materials leads to certain interesting crystallographic results. In the absence of electric fields or orienting stresses, the sample is nearly isotropic because of the random orientation of the ceramic grains. The application of an electric field to a sample in the ferroelectric phase, however, aligns many of the ferroelectric domains ("poles" the sample) and produces a distance anisotropy. This poled sample represents a symmetry characterized by an infinite-fold rotational axis; i. e., the material is isotropic in the plane perpendicular to the axis of rotation. This is true regardless of the actual crystalline symmetry characterizing the ferroelectric state.

To fit the cubic pattern of the perovskite structure, the A atoms must have a coordination number of twelve and the B atoms a coordination number of six. From the viewpoint of valence, the sum of the A-valence and the B-valence must be six, giving rise to both $A^{+1} B^{+5} O_3$ and $A^{+2} B^{+4} O_3$ compounds.

The concept of ionic size plays an important part in the determination of the ferroelectric properties of perovskite compounds. If the ions fit ideally into the unit cube described above, it can be seen that the sum of the A-ion diameter and an oxygen diameter makes up a face diagonal of the cube, while the sum of a B-ion diameter and an oxygen diameter makes up a cube edge. For this reason, perfect packing of the ions requires the following relation to hold:

$$R_A + R_O = \sqrt{2} (R_B + R_O)$$

Since the perovskite structure is observed in a large number of compounds, this relation cannot hold ideally for all of them. It is precisely this deviation from perfect packing which allows a slightly distorted cubic structure possessing spontaneous polarization within the unit cell to exist as a stable configuration. The deviations from ideal packing are usually described in terms of a tolerance factor, t , defined as follows:

$$t = \frac{R_A + R_O}{\sqrt{2} (R_B + R_O)}$$

A value of t greater than one signifies that the B ion is small enough to "rattle around" within the ionic framework of the A and O ions. A value of t less than one indicates that the B ion is large enough to deform the basic BO_6 octahedra of the structure. In a first approximation therefore, high values of t have been associated with ferroelectricity and low values with antiferroelectricity. The tolerance factors for the principal ferroelectric and antiferroelectric perovskite compounds are given in Table I, obtained from Megaw (19).

TABLE I

TOLERANCE FACTORS FOR PRINCIPAL PEROVSKITE $A^{+2} B^{+4} O_3$ FERROELECTRICS

A Ion	B Ion			
	Ti	Zr	Hf	Sn
A Ion	(0.64)	(0.77)	(0.76)	(0.74)
Ca (1.16)	0.89	0.84	0.84	0.85
Sr (1.37)	0.97	0.91	0.91	0.92
Ba (1.52)	1.02	0.96	0.96	0.97
Pb (1.32)	0.98	0.93	0.93	*0.92

* not produced as a stable perovskite compound

The ferroelectric properties of these materials cannot be explained completely on the basis of ionic size. Although the tolerance factor for lead titanate is less than one, this compound exhibits the strongest ferroelectric properties observed to this time. For this reason, attention must be directed to other properties of the ions, such as their polarizability. Roth, in his classification of ABO_3 compounds (21), discusses the effect of the polarizability of the A ion on the structural properties of the compound formed. He finds that for A ions of low polarizability ($>0.60 \text{ \AA}^3$) a cubic or pseudocubic structure is stable over the whole range of B radii. For Pb^{+2} , on the other hand, which has a polarizability of 0.90 \AA^3 , ferroelectric and antiferroelectric structures occur for all B radii in the range between 0.65 \AA and 0.85 \AA .

This dependence of ferroelectric properties on polarizability also shows up in the x-ray structural studies of the ion displacements in $BaTiO_3$ and $PbTiO_3$ (27). In $BaTiO_3$, the phase change from cubic to tetragonal involves a shift of the Ba^{+2} ion of 0.05 \AA with reference to the oxygen lattice. In $PbTiO_3$ this shift is 0.47 \AA . Thus the increase of polarizability of the lead ion allows ionic motion an order of magnitude greater than that observed in $BaTiO_3$.

A third factor which enters into the formation of ferroelectric structures in perovskite compounds is the concept of directional or covalent bonding. Megaw (20) has pointed out that any covalent character in the bonding of the ions leads to a minimal energy for certain bond directions which can influence the ability of the material to undergo certain types of distortions.

From the viewpoint of electrostatics, the phenomenon of ferroelectricity represents a cooperative interaction involving the orientation

of a dipole in the field caused by surrounding dipoles. If dipoles are arranged in a one-dimensional array as shown in Figure 1 (a) below, the minimum energy is found when they are aligned in a parallel manner. This then represents a ferroelectric array. If they are placed side by side as in Figure 1 (b), the minimum energy is represented by an anti-parallel (antiferroelectric) arrangement. In a two or three dimensional array, the relative strengths of these two interactions determine whether the material exhibits ferroelectric or antiferroelectric behavior.



Figure 1. Representation of a Ferroelectric (a) and Anti-ferroelectric (b) Dipole Array.

The interaction between the dipoles and the internal field must be strong enough to override all factors which tend to disorient or destroy them in order to produce a stable ferroelectric or antiferroelectric phase. Thus it can be seen that ferroelectricity represents a balancing of strong mechanical and electrical interactions in the production of a stable distorted structure having spontaneous internal polarization.

Lead Perovskite Materials

The materials of greatest interest in this study are the solid solutions of lead zirconate titanate, lead zirconate titanate stannate, and lead hafnate titanate. These compose a system of perovskite materials having a common A ion with the variation in properties being attributed to the varying characteristics of the B ions. Some of these characteristics are given in the following paragraphs.

The Ti^{+4} ion is the smallest of the perovskite B ions considered, with a Goldschmidt radius of 0.64 Å. The electronegativity of this element is 2.27, meaning that its bonds with oxygen tend to be about equally ionic and covalent. Because of its ionic size, the presence of Ti^{+4} in solid solutions tends to favor the ferroelectric state. In fact, lead perovskite solid solutions containing more than twelve per cent of this ion tend to be ferroelectric under all conditions.

Zirconium possesses about the same electronegativity as titanium but has an ionic radius of 0.77 Å. The consequent increase in the tolerance factor induced by the presence of this ion in lead perovskites tends to favor antiferroelectricity in its solid solutions.

The Hf^{+4} ion, although much heavier than the Zr^{+4} ion, is almost the same size, having a radius equal to 0.76 Å. However, it is somewhat less electronegative (2.1), which according to the criteria of Sanderson (23) and Wells (29) leads to a more ionic character in its bonds with oxygen and to a somewhat smaller polarizability. This means that within the framework of the perovskite lattice the hafnium ion carries a slightly larger charge than the zirconium ion but is not quite as susceptible to the distortions of its electron clouds. This ion still behaves very similarly to the Zr^{+4} ion with relation to its antiferroelectric character.

The Sn^{+4} ion behaves quite differently from the other three ions discussed here because of its basically different electron configuration. The four valence electrons in the tin atom represent two s-electrons and two p-electrons from the same shell, while for the others they are two s-electrons and two d-electrons from the next smaller shell. Thus while the ionic radius of this ion (0.74) is nearly the same as that of the

zirconium or hafnium ion, it does not show the tendency to induce anti-ferroelectricity nearly so strongly as these ions. The electronegativity of tin is 3.10 leading to a much greater covalent character in its oxygen bonds and a greater susceptibility to ionic deformation.

The compounds and solid solutions involving the above ions have been the subject of many studies. These have in general attested to the strong ferroelectric character of lead titanate and the antiferroelectric tendencies of lead zirconate and lead hafnate. Certain studies, however, revealed deviations from the expected similarities in the characteristics of the zirconate and hafnate solutions, especially in the very low titanate regions.

In his work on lead zirconate titanate, Sawaguchi (24) developed the phase diagram for the low titanate region given in Figure 2. It can be seen from this figure that for solid solutions containing from 3 to 6% titanium, the material undergoes an antiferroelectric to ferroelectric transition on heating. That is, the room temperature phase of these compositions is antiferroelectric, but they also exhibit a high temperature ferroelectric phase before reaching the Curie temperature.

In a later study, Jaffe, Roth, and Marzullo (15) developed a similar diagram for lead zirconate titanate containing 30% lead stannate (Figure 3). They found that the addition of the stannate not only increased the compositional region exhibiting antiferroelectric behavior, but also reversed the slope of the phase boundary separating the ferroelectric and antiferroelectric phases. Thus for compositions containing between 7 and 12% titanium, the room temperature phase is ferroelectric and transforms into an antiferroelectric phase on increasing temperature before reaching the Curie transition temperature. Later work at Sandia

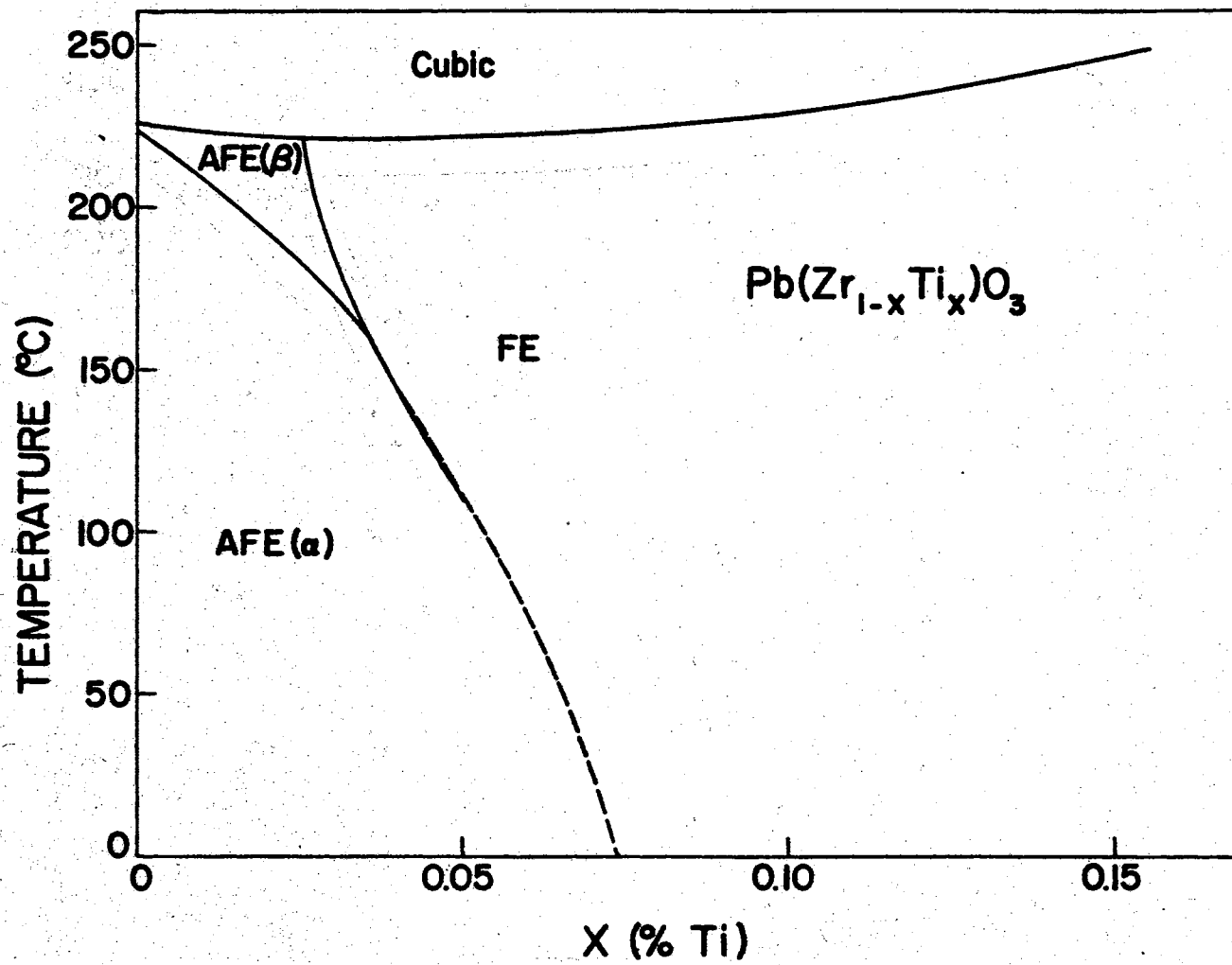


Figure 2. Compositional Phase Diagram for $\text{Pb}(\text{Zr}_{1-x}\text{Ti}_x)\text{O}_3$. (After Sawaguchi (24)).

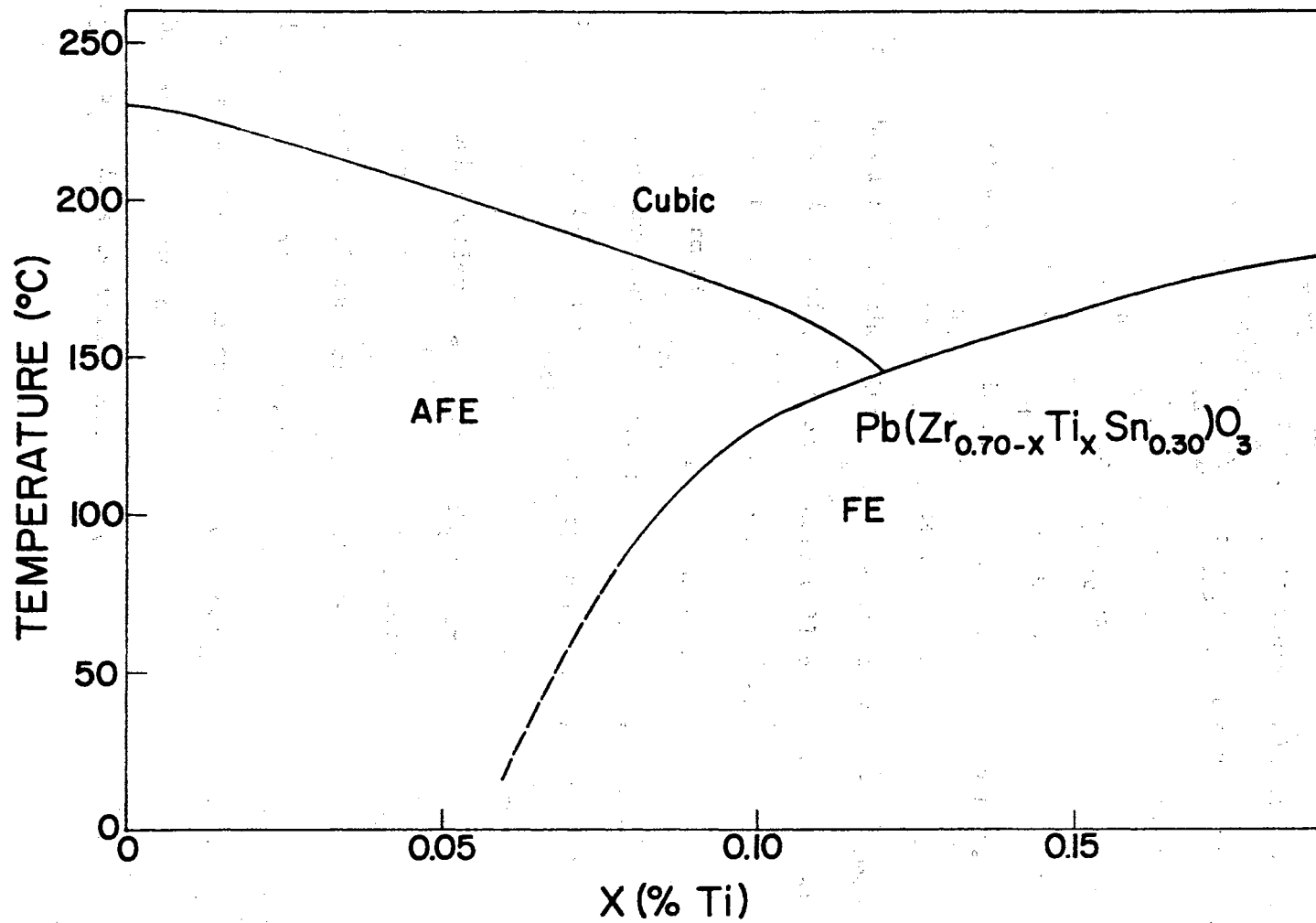


Figure 3. Compositional Phase Diagram for $\text{Pb}(\text{Zr}_{0.70-x}\text{Ti}_x\text{Sn}_{0.30})\text{O}_3$ (After Jaffe (15)).

Corporation and Clevite Research Laboratories revealed that this behavior was also exhibited by solid solutions containing smaller percentages of stannate.

Early work on lead hafnate by Shirane and Pepinsky (26) indicated that this material behaved much like lead zirconate. This was to be expected from the similarities in the character of the ions. However, later work at Sandia Corporation by Hall (12) showed that solid solutions of lead hafnate and lead titanate showed the ferroelectric to antiferroelectric phase relationship characteristic of the lead zirconate titanate stannate solutions (Figure 4).

This leads to a situation in which temperature dependence of the phase stability of lead zirconate can be reversed either by adding lead stannate to the solution or by substituting the extremely similar hafnium ion for the zirconium ion. The present study on some of the thermodynamic characteristics of the transitions was initiated in an effort to examine the factors responsible for this behavior.

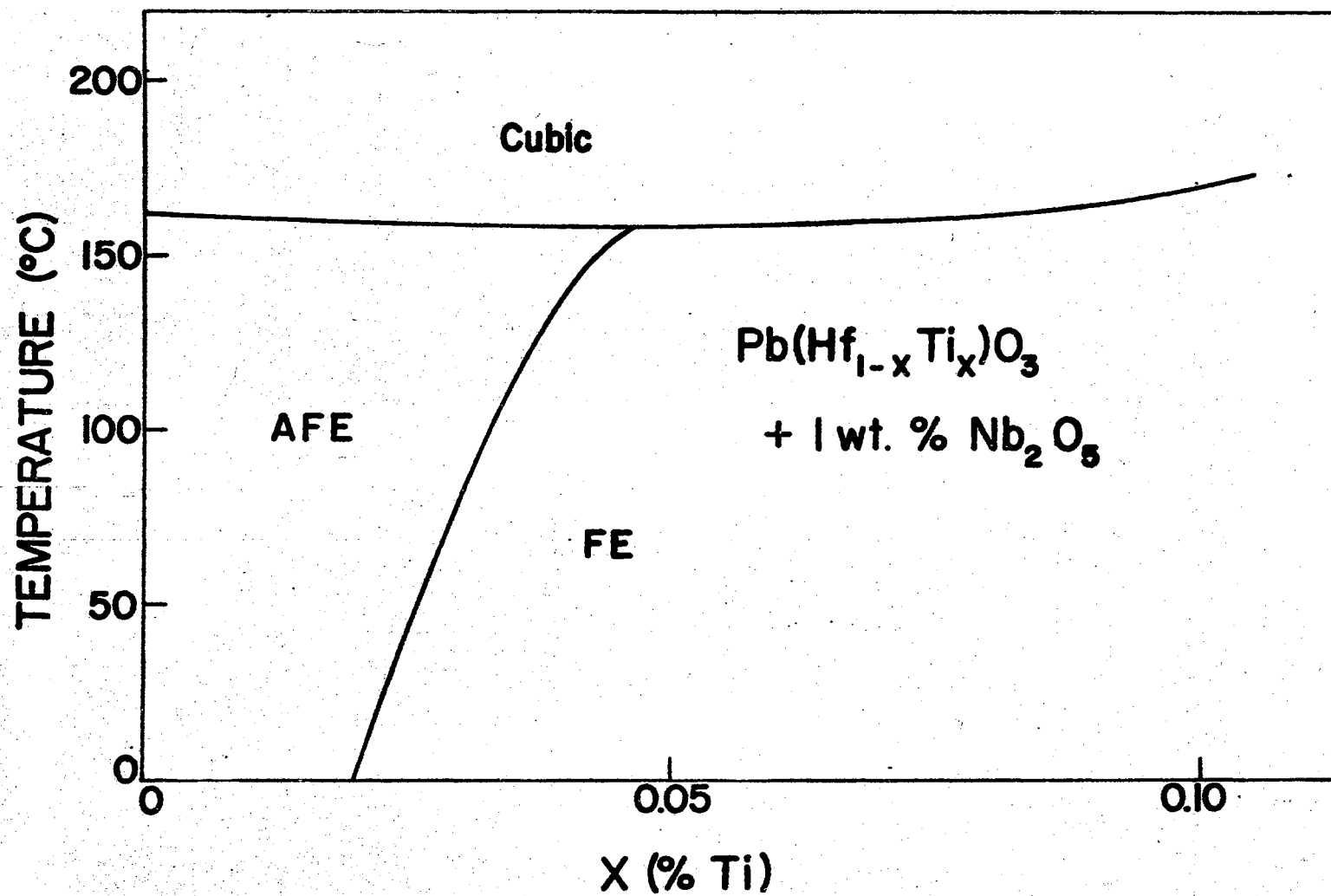


Figure 4. Compositional Phase Diagram for $\text{Pb}(\text{Hf}_{1-x}\text{Ti}_x)\text{O}_3 + 1 \text{ wt. \% Nb}_2\text{O}_5$ (After Hall (12)).

CHAPTER III

THERMODYNAMICS OF PHASE TRANSITIONS IN FERROELECTRICS AND ANTIFERROELECTRICS

The purpose of this chapter is to outline some of the basic thermodynamic considerations which are of importance in discussing phase transitions in ferroelectric and antiferroelectric materials. This will be done by first considering the relationships common to all phase transitions together with some of the factors which determine transition rates. Then the thermodynamic properties of ferroelectrics and antiferroelectrics will be related with an emphasis on the factors which govern the relative stability of the various phases observed in the lead perovskites. Finally, a discussion of the application of the Gibbs phase rule to these systems will be given, together with a description of the information which may be obtained from the various types of phase diagrams.

Thermodynamics of Phase Transitions

Phase transitions in materials are usually discussed in terms of the Gibbs free energy. For convenient illustration one takes a simple homogeneous, isotropic medium where energy exchanges between the system and its surroundings which arise from changes of temperature, pressure, or electrical potential difference lead to a free energy given by,

$$G = U - TS + pV - vQ$$

U = internal energy

T = temperature

S = entropy

p = pressure

V = volume

v = electrical potential difference

Q = dipolar charge

This may also be represented for polarizable materials in terms of energy densities by the relation:

$$G' = U' - TS' + p - EP$$

where the primes represent densities for the symbolized quantities and

E = applied electric field

P = polarization (dipolar charge per unit area).

Using these definitions, the common thermodynamic relations for variation of free energy may be derived:

$$\left(\frac{\partial G}{\partial T}\right)_{p,v} = -S$$

$$\left(\frac{\partial G}{\partial p}\right)_{T,v} = V$$

$$\left(\frac{\partial G}{\partial v}\right)_{T,p} = -Q.$$

A transition occurring with a discontinuity in one of the above quantities is called a first order transition. A transition in which all of the above quantities are continuous, but where one of their derivatives (the second derivative of free energy with respect to an intensive parameter) is discontinuous, is called a second order transition. Higher order transitions may be defined similarly.

The type of phase relationship which is of most interest to this study is known as polymorphism. Polymorphism is the existence of several crystalline modifications of the same substance. Phase transitions

between polymorphic modifications represent the simplest crystalline reactions since they involve no macroscopic motion of ions. The polymorphic structure which has the lowest free energy under a given set of conditions will be the most stable structure. All of the other forms will tend to transform into this structure, although there may be energy barriers which cause the reaction to go extremely slowly.

At absolute zero, zero pressure, and zero electric field, the relative stability is determined primarily by the structure energies of the various polymorphic forms. It should be noted that this is not the total lattice energy but may be represented as the difference between the energy of the given structure and that of a minimum energy optimum packing configuration. There will be one of the polymorphic forms which represents a minimum structural energy and this will be the most stable form of the material in the absence of intensive variables.

As the temperature increases the temperature-entropy product becomes the dominant term in the free energy equation. Although the internal energy increases with temperature, the magnitude of the change is ordinarily much smaller than that of the temperature-entropy product. Thus the free energy becomes a monotonically decreasing function of temperature. If the entropy of the form most stable at absolute zero is greater than the entropy of other forms at all temperatures, this form will always be the most stable and no transitions will occur. However, if this is not the case, there may exist a situation in which for $U_2 > U_1$, $U_2 - TS_2 = U_1 - TS_1$. This is illustrated in Figure 5.

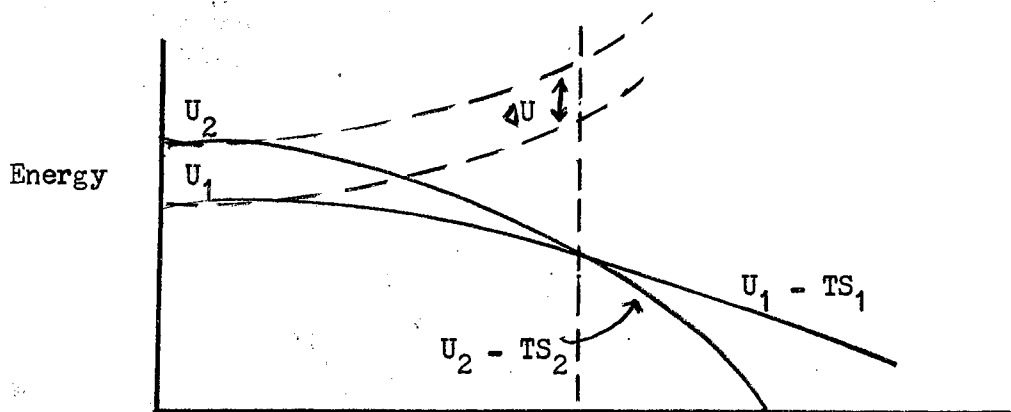


Figure 5. U and G vs. T for $p = 0$, $E = 0$.

Under these conditions there will be a transition from phase 1 to phase 2. Since this transition is accompanied by a discontinuous change in entropy as shown by the slopes of the free energy curves, it is of first order and involves a positive heat of transformation. That this quantity is always positive for transformations occurring on rising temperature can be seen from the relation:

$$U_2 - U_1 = TS_2 - TS_1 = T(S_2 - S_1).$$

The temperature is a positive quantity and S_2 must be greater than S_1 in order for the curves to cross, so both factors on the right hand side of the equation are positive. Thus a polymorphic transition on rising temperature must be accompanied by an absorption of heat. If more than two structures are possible for the given material, there may be temperature regions in which each is stable.

Under ordinary conditions an increase in the electric field applied to a material produces a monotonic decrease in free energy in the same manner as an increase in temperature. In this case the extensive variable of interest is the dipole charge on the sample, or the polarization of the material. For materials lacking spontaneous polarization, the induced polarization, that polarization which is due to the application of an

external electric field, is given by

$$P(E) = \int_0^E \frac{dP}{dE} dE = \int_0^E \epsilon_0 \chi(E) dE.$$

Thus materials having high susceptibility will, other factors being equal, be more stable at high fields than materials of low susceptibility. In ferroelectric materials the spontaneous polarization adds to this effect immensely, assuming the polarization be aligned with the field. If the spontaneous polarization is oriented antiparallel to the external field, however, the effect is to increase the free energy rather than to decrease it. For materials possessing spontaneous polarizations and very high coercive fields, it is possible that the free energy could actually be increased appreciable by the application of an electric field.

On the other hand, the influence of an increase of pressure on the free energy is opposite to that of temperature and electric field, due to the positive sign of the pressure-volume product in the free energy equation. Thus an increase of pressure produces an increase of free energy and the most stable structures at high pressures will be those of minimum volume.

The experimental determination of the relative free energies of several phases in a polymorphic system is greatly hindered by the wide variation in transformation rates observed in such systems. In general, there exists an energy barrier between two phases which have equal free energies and an activation energy is required to allow the transformation to take place. Because of the relative immobility of ions within a solid lattice, this may lead to an extremely slow rate of transition in cases where drastic rearrangements are necessary to form the new phase. For

this reason, these transformations often exhibit large hysteresis and quite often a phase may exist as a stable configuration for long periods of time at temperatures where it no longer represents the minimum free energy in a polymorphic family.

Buenger (5) has given a crystallographic classification of phase transitions in solids according to the types of microscopic bonding changes necessary to form the new phase. He places all polymorphic transitions into four groups:

I. Transformations of secondary coordination. These represent, in general, changes in the weak bonded or non-nearest neighbor configurations. In this type of transformation the strong bonded (contacting atom) configurations remain undisturbed and merely shift their spatial relations to one another. A good example of this type of transformation is the ferroelectric transition in potassium dihydrogen phosphate, in which the phosphate tetrahedra change orientation, causing minor changes in the length of the hydrogen bonds. This type of transition is relatively rapid and will take place at quite low temperatures unless the rearrangement requires an actual reconstruction of the secondary bonds.

II. Transformations of disorder. This class includes changes in rotational disorder (such as the alpha to beta quartz transformation) and transformations of substitutional disorder (such as those occurring in alloys). In general, the first of these proceed rapidly while the last are quite sluggish and take place only at high temperatures.

III. Transformations of first coordination. These transformations represent a change in the bond structure of nearest neighbors and distortions of the strongly bonded structural configurations. If the change is merely a dilatation of the strongly bonded group (the case in perovskite

transitions) the transition may proceed rather rapidly. However, even the simplest first coordination transitions usually become rather sluggish at low temperatures. If the transformation requires a bond rearrangement among nearest neighbors, the rate of change is exceedingly slow, allowing seemingly stable structures to exist under conditions where they are not energetically favorable.

IV. Transformations of bond type. In these transformations the polymorphic structures possess entirely different bonding characteristics. This is exemplified in the diamond and graphite configurations of carbon. Transformations of this type usually proceed rather slowly and are often difficult to initiate. It is quite possible that the ferroelectric transformations in perovskites fall partially into this class. In structures such as the perovskites, the ratio of ionic to covalent character in the oxygen to metal bonds is a function of bond length. Thus, the distortions of the basic cubic lattice may cause a partial change of bond type.

The use of ceramic or powdered materials may also affect the transition rates appreciably. If the transition is controlled by the nucleation rate, i. e., if the new phase spreads rapidly throughout the lattice once it is nucleated, the transition rate is usually somewhat slower in finely divided material. However, if the rate is controlled by the ability of the new phase to grow throughout the lattice after being nucleated at a surface, ceramics and powders transform much more readily than large single crystals.

Applications of the Above Considerations to Ferroelectric and Antiferroelectric Transitions

In the special case of polymorphic systems involving ferroelectric (FE) or antiferroelectric (AFE) phases, certain relationships are introduced into the above free energy picture. The presence of a large spontaneous polarization in the FE phase allows the electric contribution to play a more dominant role in the transition behavior than is normal in polymorphic transitions. The application of an electric field lowers the free energy curve of the FE phase much more than that of either the AFE or cubic (PE) phase. This causes a shift in transition temperatures in such a manner as to increase the temperature range over which the FE phase is stable, e. g., ferroelectric Curie temperatures are raised by the application of an electric field. The only exception to this rule might be in the case of small fields applied in the opposite direction to the polarization of the FE sample. Since the field and polarization vectors are antiparallel in this case, the free energy of the phase would be raised instead of lowered. However, this leads to an instability in that the decrease of free energy obtained by switching is greater than that obtained by a transformation to a new phase. Thus it would seem that switching should occur first and the ultimate change in transition temperature should be nearly independent of the field direction.

In the transitions from AFE to a PE phase, the application of an electric field tends to favor the PE phase. As will be discussed in the section on dielectric measurements, the polarizability of the lattice in the cubic phase is greater than that in the antiferroelectric phase. Thus from the free energy equation, the application of an electric field

lowers the PE free energy more than that of the AFE phase. This is verified by the observation that antiferroelectric Curie temperatures are lowered by the application of an electric field.

In the perovskite structure a transition from PE to FE is accompanied by an increase in volume, while a transition from PE to AFE results in a decrease of volume. Thus the application of a hydrostatic pressure (which increases the free energy of each phase by an amount proportional to the phase volume) leads to a favoring of the AFE phase over the PE and FE phases, and a favoring of the PE phase over the FE phase.

The variation of the free energies of the different phases with temperature depends on the relationships between the various factors which determine the entropy of the system. Since there is negligible macroscopic ionic motion associated with the phase transformations in perovskite solid solutions, the configurational entropies of the three phases are approximately equal. The entropy difference between the phases must then be accounted for by either an order-disorder transformation or by differences in the phase vibrational entropies. In the potassium dihydrogen phosphate family of ferroelectric materials, the constancy of the entropy change at the Curie transition throughout the family indicates that the dominant mechanism is the order-disorder one (18). In perovskites on the other hand, the entropy change at the transition varies widely from material to material, suggesting that in this family the vibrational entropy is dominant.

Following the reasoning of Buerger (5), it can be seen that the cubic phase represents the highest entropy of the possible phases of a perovskite structure. As an unpoled ferroelectric approaches the Curie temperature the thermal vibrations and expansion of the lattice lower the

coercive force to the point that domains have a certain probability of becoming thermally switched. At the transition this switching takes place rapidly enough that the time average of each ionic position becomes the same as the position in the cubic state. This is equivalent to saying that the ferroelectrically active ions oscillate about positions which are equivalent to their positions in the cubic phase. Thus the cubic phase may be regarded as a disordered equivalent of the polar phase and therefore the phase of highest entropy. This is borne out by the fact that the cubic phase is always the most stable phase at high temperature.

The entropy relationship between the FE and AFE phases is more difficult to determine from basic principles. Although the AFE phase shows no net polarization, it can be considered as being composed of two sublattices possessing equal and opposite spontaneous polarizations. Thus, in perovskites, both the FE and the AFE phases represent a polar distortion of the original nonpolar lattice. The differences of the entropy associated with these phases then result from small differences in bond structure and in the vibrational configurations of their lattices. It is to be expected that these phases will have nearly equal entropies for many compositions. Thus the reversal of direction of the phase transition with temperature which was discussed in the previous chapter does not result from a drastic change in the energy relations in either phase, but rather from a small change which allows a slight entropy dominance of one phase to become an entropy dominance of the other. Further remarks on this subject will be included in the final chapter, which gives some of the conclusions which can be reached from experimental results.

Application of Gibbs Phase Rule Concepts to this System

The Gibbs phase rule may be stated in generalized form as

$$F = C - P + N$$

where

F = number of degrees of freedom in the system

C = number of chemical components

P = number of phases present

N = number of intensive variables.

The number of degrees of freedom represents the number of variables which may be changed independently without causing the appearance or disappearance of a new phase. This equation does not specify a definite relationship between phases, but rather is used to correlate data from experimental studies.

The phase relationships for a given system are usually given in the form of graphs called phase diagrams. In these plots, which use compositional relations and intensive parameters as variables, each phase extends over that set of points specifying the conditions under which it is most stable. In general, the number of dimensions, D, required by such a plot is given by

$$D = C + N - 1.$$

Thus the phase relation in a two component system under fixed external conditions may be specified on a straight line, while those for a three component system under fixed external conditions require a plane (the common triangular compositional phase diagrams). A plane is also required to plot the relations in a two component system as a function of one external variable (temperature, pressure, etc.). To show the phase

relationships in a solid solution family such as the lead zirconate titanate stannates as a function of temperature, pressure, and electric field would require a five dimensional phase diagram.

In a phase diagram of D dimensions, a single phase will be stable in a D dimensional region, transition conditions between two phases will be represented by a $D-1$ dimensional phase boundary, and equilibrium between three phases can occur only over a $D-2$ dimensional region. For example, in a two dimensional phase diagram a single phase is represented by an area, the boundary between two phases by a line, and the coexistence of three phases by a single point. This agrees with the Gibbs phase rule which specifies that for $C + N = 3$ (the necessary condition for a two dimensional phase diagram), a single phase has two degrees of freedom, a pair of phases has only one degree of freedom, and three phases can exist together only under an isolated set of conditions.

In working with systems involving ferroelectric solid solutions, the chemist or ceramist is, in general, interested in the variation of properties with composition. Phase diagrams used by ceramists generally depict either relationships involving composition alone or relationships between composition and one intensive variable, usually temperature. The physicist or engineer, on the other hand, is usually interested in the characteristics of a single sample, which represents a single composition because of the low internal mobility of the ions. Phase diagrams of interest to the physicist depict the relationship between phases as two intensive parameters are varied (transition temperature vs. electric field, etc.).

The derivation of specific thermodynamic data from phase diagrams involving composition as a variable is complicated by the fact that a

change of composition affects not only the internal energies of the various phases, but also the other extensive parameters (entropy, molar volume, polarization). Thus the slopes of the boundaries between phases as functions of composition are not easily interpreted in terms of the parameters involved in the free energy equations.

In phase diagrams involving two or more intensive variables, the slopes of the phase boundaries can be used to determine the relationships between the corresponding extensive parameters. For first order transitions such as those observed in this study, this is given by a generalized Clausius-Clapeyron equation:

$$\left(\frac{\partial X_i}{\partial X_j}\right) = -\frac{\Delta x_j}{\Delta x_i}$$

where X_i and X_j represent intensive variables (generalized forces), $(\partial X_i / \partial X_j)$ represents the slope of the phase boundary with all other intensive variables held constant, and Δx_i and Δx_j represent the discontinuous changes in the corresponding extensive variables at the transition.

The various types of phase diagrams and the information to be obtained from each are given in Table II. Using these relationships and the measurements of polarization, cell volume, and specific heat of the material, a free energy diagram explaining the phase relationship as a function of the intensive parameters can be developed.

TABLE II

PHASE BOUNDARY RELATIONSHIPS

Type of Phase Diagram	Intensive Parameter Boundary Slope	Extensive Parameter Relationship (1st order Transition)
Transition temperature vs. pressure	$\left(\frac{\partial T}{\partial P}\right)_E$	$\frac{\Delta V}{\Delta S} = \frac{T\Delta V}{H} *$
Transition temperature vs. electric field	$\left(\frac{\partial T}{\partial E}\right)_P$	$-\frac{V\Delta P}{\Delta S} = -\frac{\Delta P}{\Delta S'}$
Transition pressure vs. electric field	$\left(\frac{\partial P}{\partial E}\right)_T$	$\frac{V\Delta P}{V} = \frac{\Delta P}{\Delta V/V}$

* H = Latent heat of transition.

CHAPTER IV

DIELECTRIC MEASUREMENTS

Measurements of the dielectric susceptibility and loss have played an important role throughout the study of ferroelectrics. It was the extremely high values of susceptibility which first caused interest in these materials and which later led to many of their important applications. The variation of susceptibility with temperature has long been the prime tool for precise determination of transition temperatures.

Dielectric Susceptibilities

In ferroelectric materials, the dielectric constant ($k = \epsilon_0^{-1} dD/dE$) and dielectric susceptibility ($\chi = \epsilon_0^{-1} dP/dE$) become approximately the same. Since these two factors are related by

$$k = \chi + 1$$

and have magnitudes varying from a few hundred to a few thousand, there is little error introduced by using them interchangeably. In general, measurements determine k while most theories deal with χ . In discussing the dielectric susceptibility of a ferroelectric material, however, it is necessary to differentiate between the changes of polarization due to switching and the "true" small signal polarization changes.

The abnormally high dielectric constants of ferroelectric and anti-ferroelectric materials are due to the freedom of certain ions within the pseudocubic lattice structure to move under the influence of small

fields. This leads to large ionic contributions to the susceptibility and also to the extreme variations of dielectric constant with those parameters which affect lattice spacings and orientations.

Using curves representing the variation of free energy as a function of polarization (related to ionic position) such as those in Figure 6 below, the behavior of the dielectric susceptibility in the vicinity of the Curie temperature can be explained.

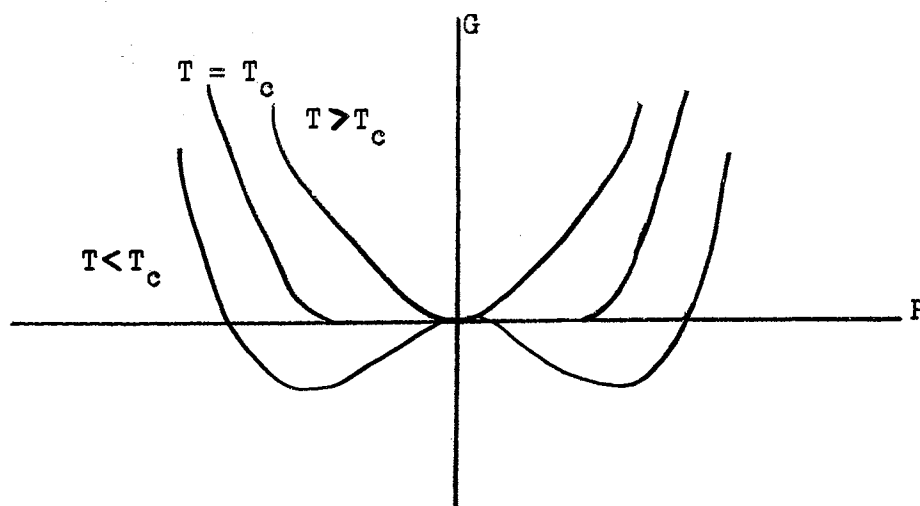


Figure 6. Variation of Free Energy with Polarization for a Ferroelectric Material.

The curves represent a symmetric variation of the free energy about zero polarization with a simple minimum, an extended minimum, and a double minimum. The application of a linear external field to the material superimposes a slope on each of these curves, causing a shift in the position of the minimum. This is equivalent to saying that the ionic motion caused by the application of the external field is highly dependent on the exact shape of the minimum for the temperature concerned. For temperatures below the Curie temperature ($T < T_c$), the material is ferroelectric and the susceptibility is determined by the ability of the ion to move about within one of the symmetric minima. A shift from

one minimum to the other within this temperature region represents switching rather than small signal dielectric behavior. At the Curie temperature ($T = T_c$), the free energy curve is flat at the bottom allowing large ionic shifts with very small fields and thus extremely high dielectric susceptibilities. Above the Curie temperature ($T > T_c$), the free energy exhibits a simple minimum but the ions are still relatively free to move to both sides of this minimum under the influence of a small field. This is the reason the susceptibility in the paraelectric state is higher near the Curie temperature than that of the ferroelectric state.

For antiferroelectric materials, the curves are similar, except that the minima below the Curie temperature are not symmetric. That is, the mechanical constraints in this phase cause one direction of ion shift to be highly favored over the other. This leads to a more restricted ionic motion under the influence of a small external field and thus to lower susceptibilities.

The nonlinearity of dielectric susceptibility may be measured by making small signal capacitance measurements while superimposing a constant biasing voltage on the sample. In the figure below, which is representative of polarization vs. field for a material above the Curie

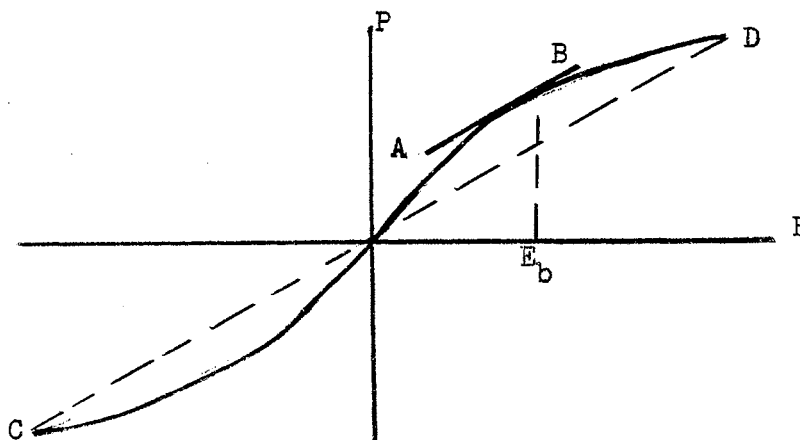


Figure 7. Polarization vs. Bias Voltage Showing Nonlinear Saturation Effect.

temperature, the slope of the line segment AB (the tangent to the curve at $E = E_p$) represents the dielectric susceptibility of the material at a given bias as determined by small signal measurements. This is in sharp contrast to the results of large signal dielectric constant measurements which require much larger bias voltages to achieve the same slope, as is indicated by the line segment CD. Using small signal measurements, the effect of dielectric saturation becomes apparent as a decrease in the measured susceptibility with an increase in the bias voltage. This effect is quite significant near a ferroelectric Curie point.

Measurements of the dielectric susceptibility in the paraelectric region as a function of temperature show that it varies according to the Curie-Weiss Law,

$$\chi = \frac{C}{T - T_0}$$

where C = Curie constant

and T_0 = Curie-Weiss temperature.

For materials in the FE phase, the Curie-Weiss temperature is usually only a few degrees different from the Curie temperature, while for AFE materials this difference may be much greater, sometimes more than fifty degrees.

Dielectric Loss

Most publications of dielectric measurements on ferroelectric materials have reported dielectric loss measurements in terms of $\tan \delta$, the ratio of the loss current to the capacitive current. Variations of loss thus are caused not only by changes in loss mechanism but also by changes in sample capacitance. This leads to no problems for studies

such as those concerned with internal friction in quartz since loss variations of interest occur under conditions where the sample capacitance is constant. In ferroelectrics, on the other hand, many regions of interest are accompanied not only by changes of loss mechanism but also by extraordinary changes of sample capacitance. Thus the loss tangent will be a poor indicator of actual loss values and may at times become misleading. For example, near the Curie temperature of a ferroelectric one would expect rather high dielectric losses since the material is easily influenced by small electric field gradients. However, the exceptionally high dielectric constants in this region lead to very low values of $\tan \delta$. For this reason, it would seem more valid to report ferroelectric data in terms of a dielectric constant and an "equivalent conductance." From the definition of $\tan \delta$ this equivalent conductance can be obtained by the equation

$$g = 2\pi f c \tan \delta$$

g = equivalent conductance

f = measuring frequency

c = total capacitance.

The term equivalent is used here to indicate the contributions of all mechanisms for converting electrical energy to thermal energy, i. e., Joule heating, domain wall motion, irreversible losses in phase transformations, etc. Since all of these mechanisms do not have the same dependence on sample geometry, it seems more satisfactory to speak of the "conductance of a sample" rather than the "conductivity of a material."

This viewpoint is also helpful in experiments where measuring system components contribute currents which are not small compared to the capacitive and loss currents of the sample. Since the measuring system

and sample are equivalently in parallel, their respective capacitances and conductances are additive, while the relationship between the true loss tangent of the sample and the measured loss tangent is more complicated.

Measurement Equipment

Dielectric measurements for this study were made with a General Radio Model 716C capacitance bridge. This was driven by a General Radio Model 1302-A Oscillator. Null detection was accomplished with a General Radio Model 1231 Filter and Amplifier with an oscilloscope as the final null detection device. All measurements were made with a driving frequency of one kilocycle and a peak-to-peak voltage of one volt. Using this system, capacitances were measureable with a sensitivity of about $\pm 1 \mu\text{mf}$, and $\tan \delta$ with a sensitivity of ± 0.0002 .

The sample was maintained in an oil bath containing Dow Corning 200 silicone oil and equipped with an immersion heater and magnetic stirrer. Temperature measurements were made by means of thermometers placed at the sample position. A general laboratory thermometer was used for the lower temperature regions, while one with an expanded scale was used above 140°C for more accurate determination of the transition temperatures. With this bath, measurements could be made in the temperature region $20^{\circ} - 230^{\circ}\text{C}$ with the rate of change of temperature ranging from 3°C per minute at low temperatures to 0.2°C per minute near critical temperature regions.

In order to measure dielectric constant and loss as a function of both temperature and electric field, a system was designed which would allow dc voltages up to two kilovolts to be placed on the sample while making dielectric measurements. This system is shown in Figure 8.

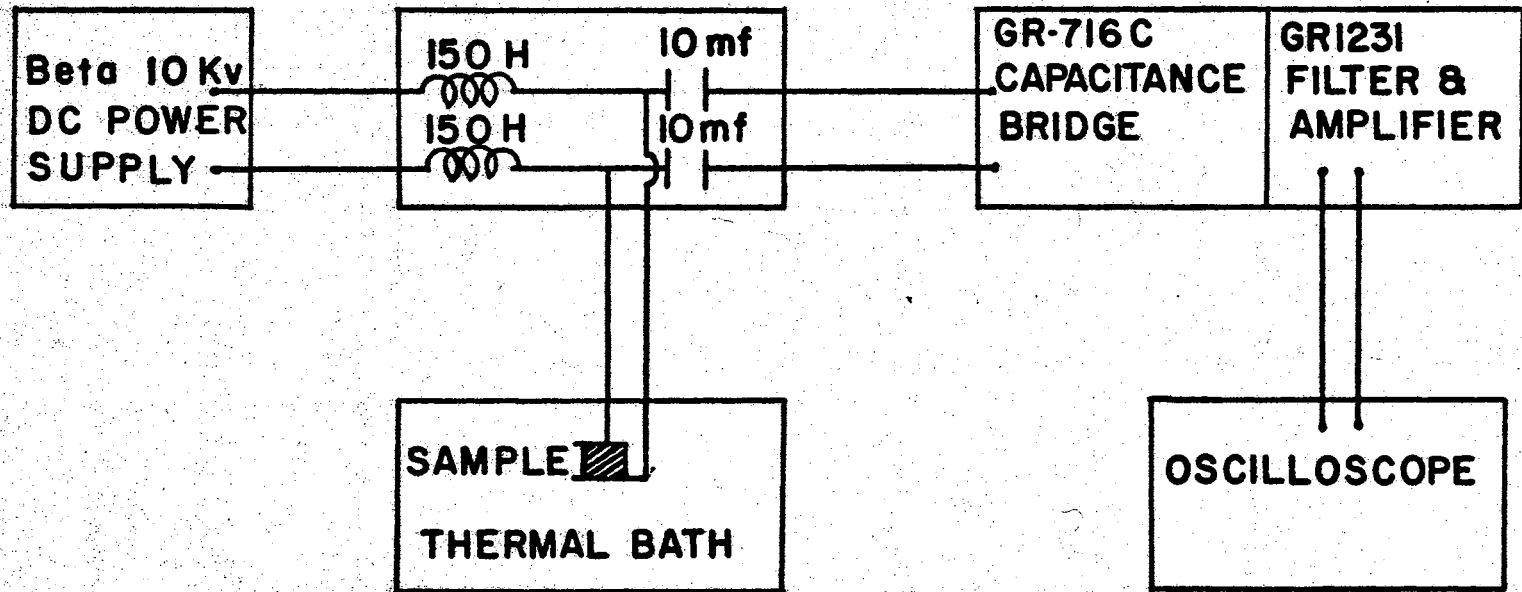


Figure 8. Block Diagram of Dielectric Measurement Apparatus.

The dc voltage was supplied by a Beta 10 kilovolt power supply which was isolated from the sample by two 150 henry chokes. These provided a separating impedance of 1.9 megohms as compared with a maximum sample impedance of about 0.3 megohms at the measuring frequency of one kilocycle. At the same time they allowed the dc voltages to be placed on the sample with negligible loss. The bias voltage was separated from the capacitance bridge by two 10 microfarad, 2 kilovolt oil filled capacitors. These provided dc separation with negligible measuring signal loss. The measuring system introduced stray capacitances of the order of 1000 f into the results which could be measured before introducing the sample and then subtracted from the sample readings.

Experimental Samples

The samples used in this study were furnished by Sandia Corporation in the form of small ceramic discs of lead zirconate titanate stannate and lead hafnate titanate. The compositions had all been made with a small amount of Nb_2O_5 additive to aid in firing and to reduce conductivity. The samples were sintered at approximately 1400°C and were fitted with baked silver electrodes. As a first step in the present investigations, the samples were heated to 500°C for approximately two hours and allowed to cool in the absence of an electric field in order to reduce the effects of past treatment. In measurements at bias voltages, the measurements at low bias were always taken before those at higher bias so that any poling of the sample could be attributed to the bias used in the measurement being made. The actual dimensions of the principal samples used in the dielectric studies are given in Table III.

TABLE III

DIMENSIONS OF SAMPLES USED IN DIELECTRIC MEASUREMENTS

Sample	Diameter (mm)	Thickness (mm)	Density (gm/cm ³)
PZST6	16.09	1.74	7.74
95HN2	13.95	2.65	8.93
96HN2	14.17	2.09	9.00
97HN2	13.92	2.22	9.04
98HN4	14.12	0.88	8.94
100HN2	14.18	1.75	8.99

Measurement Procedures and Calculating Techniques

1. Measurement of the system capacitance and loss tangent were taken with the sample removed. System loss was converted into conductance by the equation given earlier.
2. The sample was placed in the system and the electrical bias to be used for the run placed on it.
3. Measurements of the capacitance and loss tangent of the sample were obtained from room temperature to about thirty degrees above the Curie temperature during both the heating and cooling portions of the run.
4. The sample dielectric constant at each temperature was calculated using the equation:

$$k = \frac{t (\text{Total capacitance} - \text{System capacitance})}{\epsilon_0 A}$$

where t = sample thickness

and A = electrode area.

5. The sample conductance was calculated at each temperature using the relation:

$$g = 2\pi f (\tan \delta) (\text{total capacitance}) - g (\text{system})$$

Because of the large number of measurements made, it was found convenient to use the IBM 650 as the principal means of data reduction.

Results

Lead Zirconate Titanate Stannate

The first samples studied were those of $\text{Pb}(\text{Zr}_{0.68}\text{Ti}_{0.07}\text{Sn}_{0.25})\text{O}_3$. A tentative phase diagram for this material was worked out during the summer of 1961 at Sandia Corporation and it was found to show both FE and AFE phases over large temperature ranges. The present measurements served two purposes: to check out the present measuring system and procedures, and also to refine the phase diagram for the composition.

Figure 9 shows typical curves of the dielectric constant and loss which were exhibited by these samples. The dielectric constant curve indicates the nature of the three transitions of interest. The Curie transition, which exhibits about 3°C temperature hysteresis with rising and falling temperatures, is characterized by the highest peak of dielectric constant. At temperatures above this transition there is a decrease of the dielectric constant following the Curie-Weiss Law.

The FE-AFE transition, which occurs on rising temperature in this material, is accompanied by a small peak in the dielectric constant curve and an extremely large one in the conductance curve. The AFE-FE transition is shown on decreasing temperature by a sudden drop in dielectric constant to values corresponding to those observed with increasing temperature. This phenomenon is also accompanied by a peak in the conductance curve. However, this peak is much smaller than that for the transition observed on rising temperature.

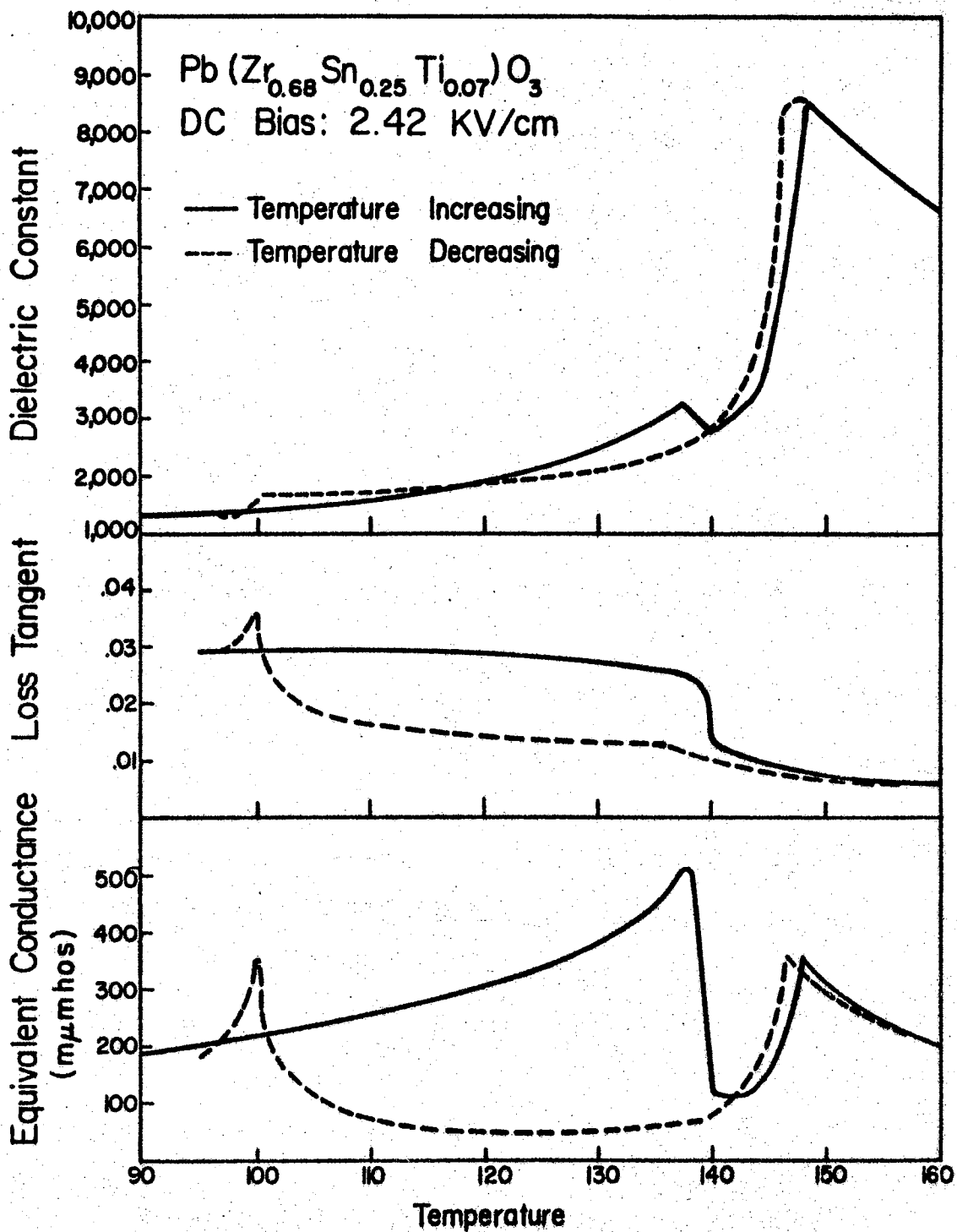


Figure 9. Dielectric Data for PZST.

These curves show the advantage of equivalent conductance as a measure of dielectric loss over the traditional $\tan \delta$. For this material, the loss maximum at the Curie transition is completely lost in the $\tan \delta$ curve. The relative magnitudes of the loss currents at the various transitions are also given their proper perspective in the conductance measurements. Thus, the FE-AFE transition, where mechanical losses would be expected to be greatest, exhibits the highest maximum in loss conductance.

Figure 10 shows the phase diagram for this material as a function of temperature and electric field. This diagram indicates that for low fields the AFE region is stable over a 24 degree range on heating and a range of about 55 degrees on cooling. This large hysteresis is indicative of the fact that the free energies of the FE and AFE phases show virtually the same temperature dependence in the region of interest. As the electric field increases, the AFE phase is less energetically competitive and finally is lost altogether. Thus we see that there are three regions of interest given by this phase diagram:

- a) Low fields - those for which the AFE phase exists over an appreciable range of rising temperatures.
- b) Moderate fields - those for which the FE-AFE transition and the Curie transition occur at temperatures differing by only a few degrees.
- c) High fields - those for which the AFE phase is missing.

It is also interesting to note that the temperature at which polarization disappears (the FE-AFE transition temperature for low and moderate fields and the Curie transition for high fields) apparently has continuous slope at the point where the AFE phase disappears.

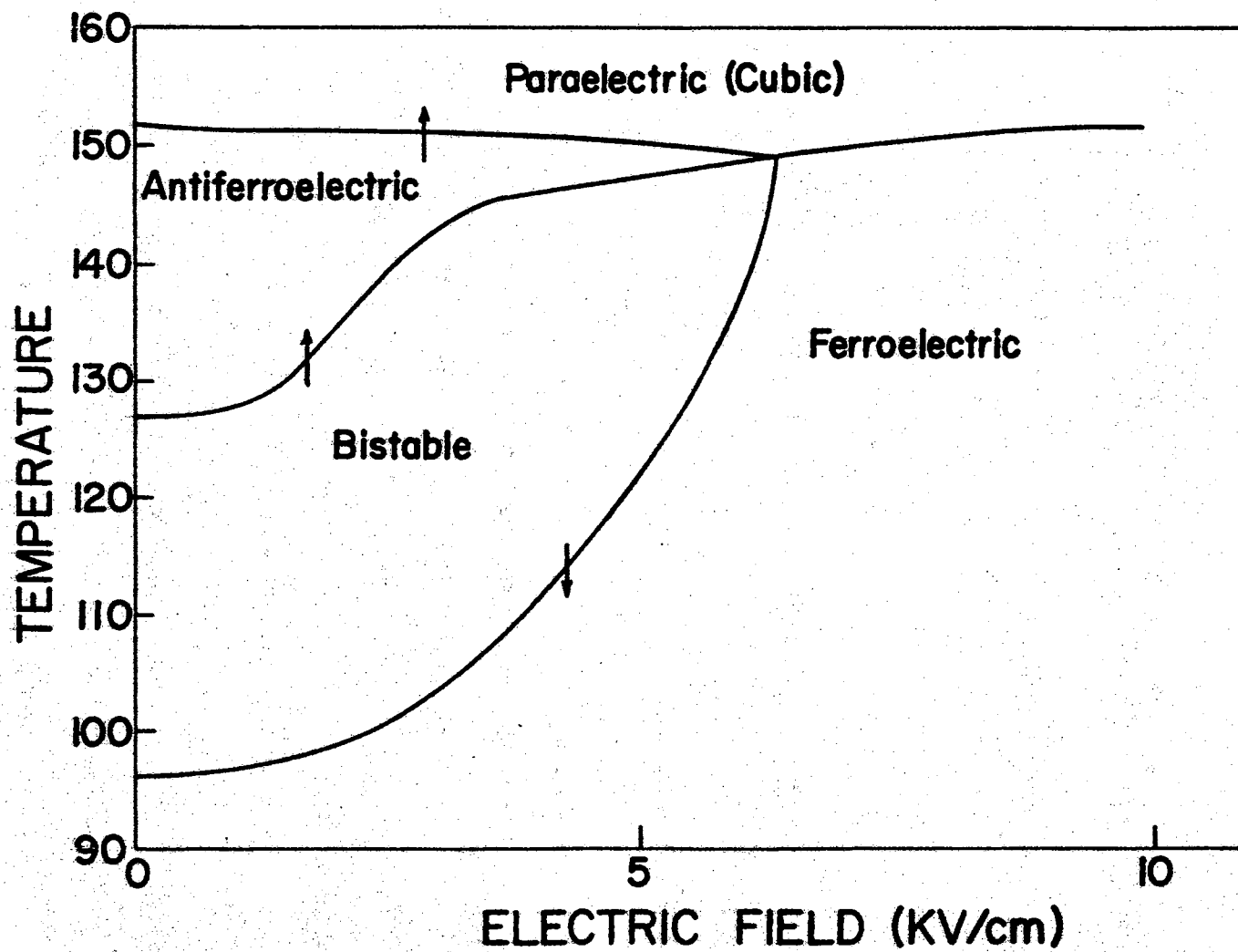


Figure 10. Phase Diagram of PZST as a Function of Field and Temperature.

Figure 11 shows the dielectric constant at the transition as a function of bias. Instead of the normal decrease of the transition dielectric constant for large fields explained by saturation effects, here there is actually an increase. This would seem to require an explanation based on the intrusion of some ferroelectric character into this transition, due to the nearly equal free energies of all three phases in this region. For fields above that at which the AFE phase disappears, normal saturation behavior is again evident.

Figure 12 indicates the behavior of this material in the paraelectric region. This is shown as a dependence of the Curie constant and Curie-Weiss temperature on the applied electrical bias. The Curie constant decreases quite rapidly with increasing bias while the Curie-Weiss temperature increases as the electric field causes the material to assume a dominance of ferroelectric characteristics.

Lead Hafnate Titanate

Measurements were also made on the series of lead hafnate titanate samples furnished by Sandia Corporation. These materials gave results which were not as sharply defined as those obtained with the lead zirconate titanate stannate samples. This was primarily due to the extreme dependence of the FE-AFE nature of these materials on their composition. The samples having a hafnate to titanate ratio of 95/5 were ferroelectric at all temperatures. The 96/4 samples exhibited an FE-AFE transition at low field but this transition was relatively near the Curie point and was not nearly so sharp as in the lead zirconate titanate stannate samples. The 97/3 samples were antiferroelectric under nearly all conditions. Some ferroelectric nature could be imparted to this material by

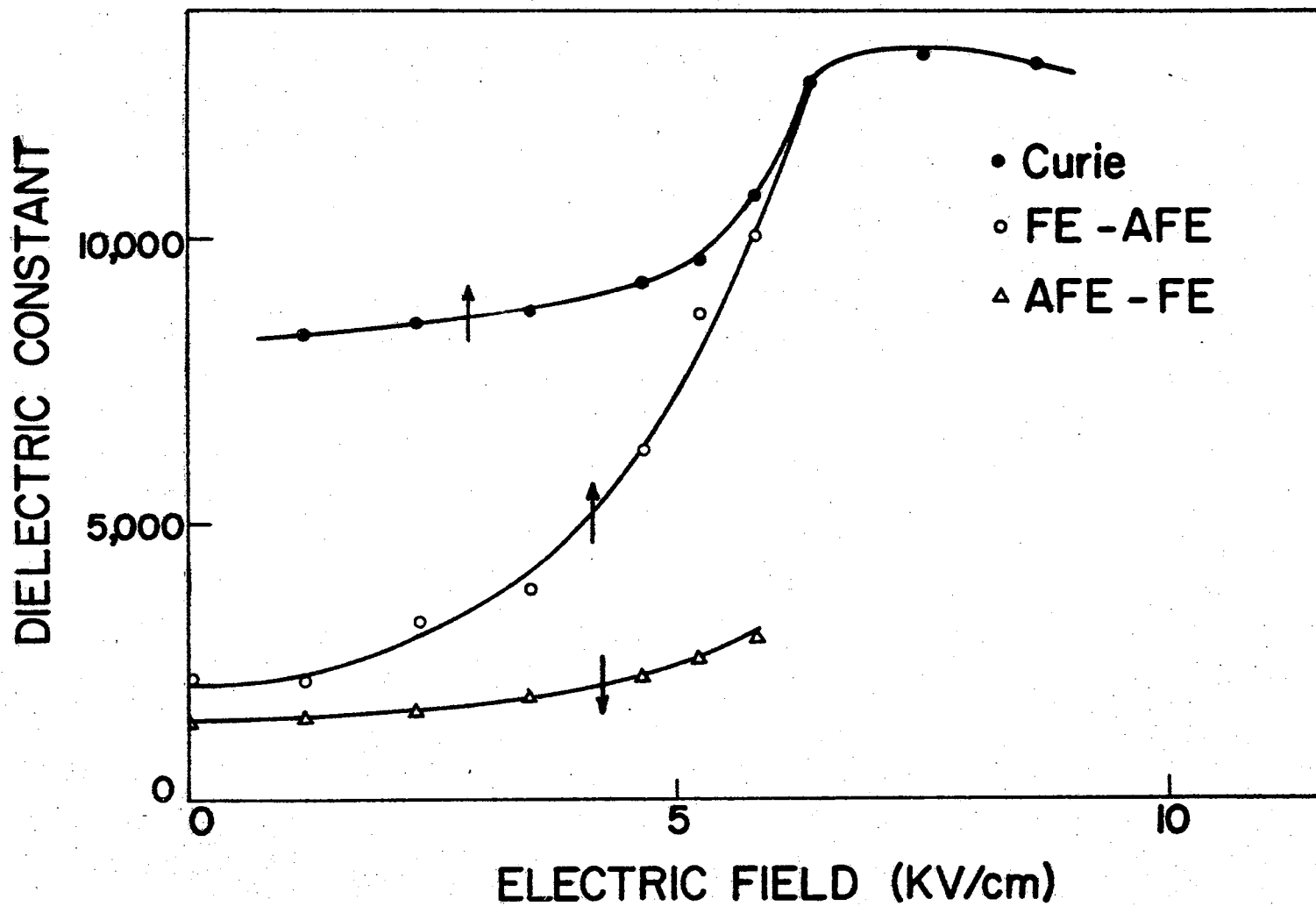


Figure 11. Dielectric Constant at the Transition vs. Field for PZST.

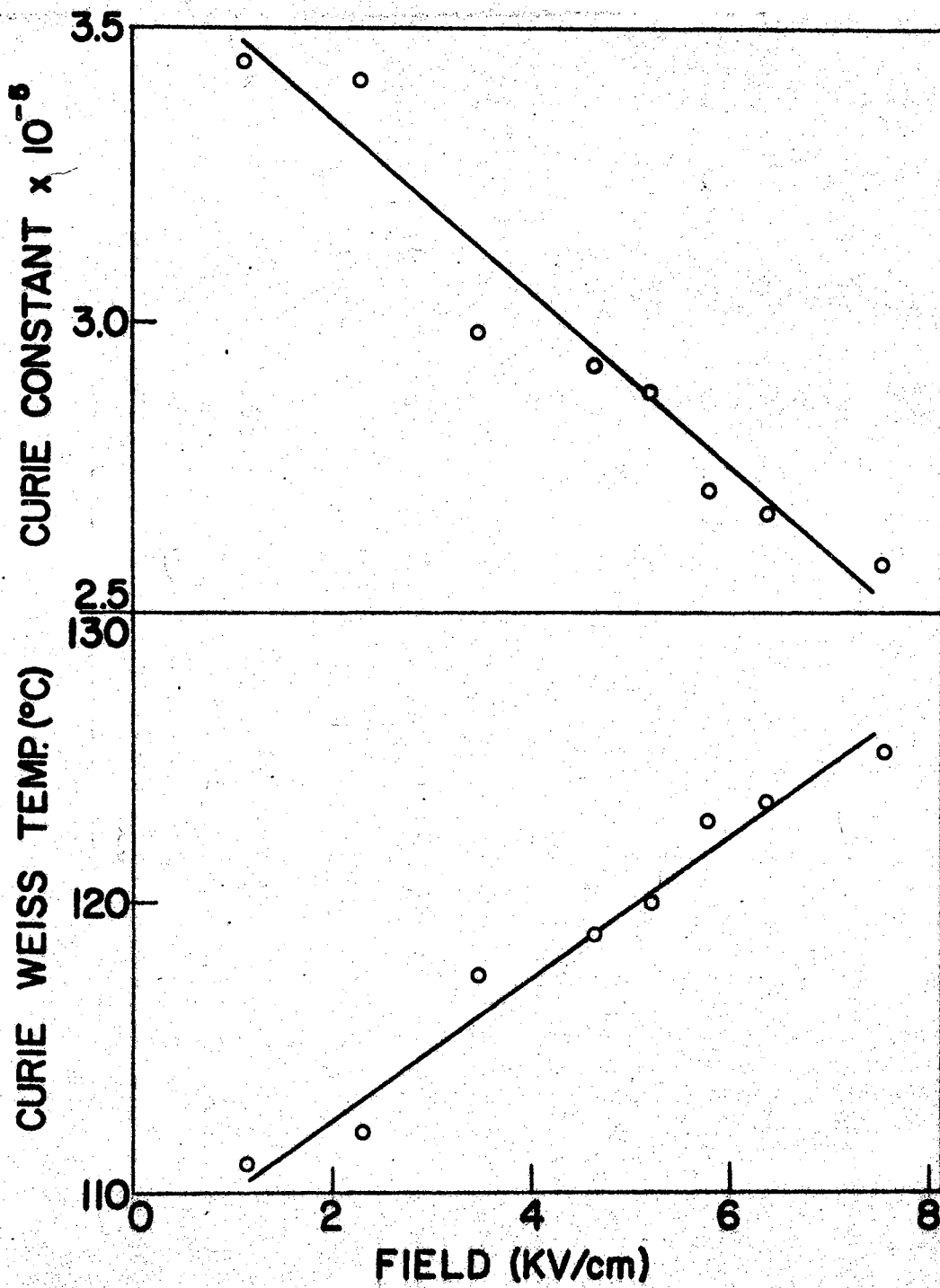


Figure 12. Behavior of PZST Above the Curie Temperature as a Function of Applied Electric Field.

the application of strong fields at room temperature but the FE-AFE transitions observed following this procedure were extremely sluggish, extending from 75° C to 95° C at all observed biases. The samples containing hafnate to titanate ratios greater than 97/3 appeared to be antiferroelectric under all observed conditions.

Figures 13, 14, 15, 16, and 17 show the behavior of these materials. It can be seen that with increasing bias field the peaks become quite broad for the samples exhibiting ferroelectric behavior. Figure 18 indicates the variation of Curie temperature with bias field for these compositions. Transitions from ferroelectric to paraelectric are characterized by an increase in the Curie temperature with bias field. For the 96/4 and 97/3 samples, antiferroelectric to paraelectric transitions cause a corresponding decrease in transition temperature with field. The results for the 98/2 and 100/0 samples were quite interesting in that virtually no bias field dependence of transition temperature was observed; the transitions occurred within one degree for each sample regardless of the bias field.

The effects of dielectric saturation, which are readily apparent in the previous curves, are compiled in Figure 19. This decrease of peak dielectric constant with increasing field is quite strong for the 95/5 samples (30% decrease between zero and five kilovolts per centimeter), becoming less dominant as the materials become more antiferroelectric and the peak dielectric constants at zero bias become smaller. The increase of peak dielectric constant which accompanied the disappearance of the AFE phase in the PZST samples was not noticed in the 96/4 composition, but this was probably due to the lack of sharpness in the FE-AFE and Curie transitions and the consequent blending of their effects. The

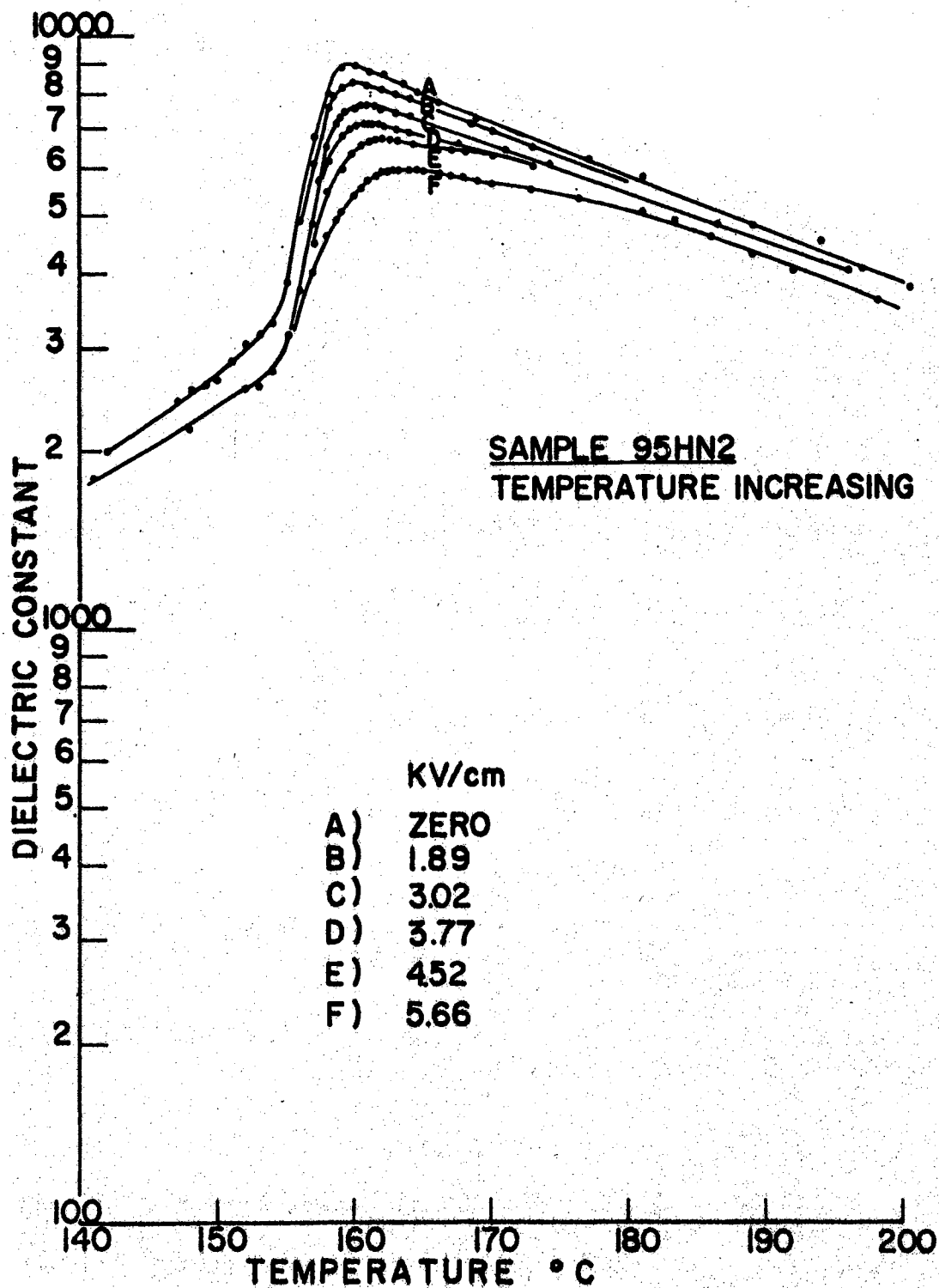


Figure 13. Dielectric Constant vs. Field for Sample 95HN2.

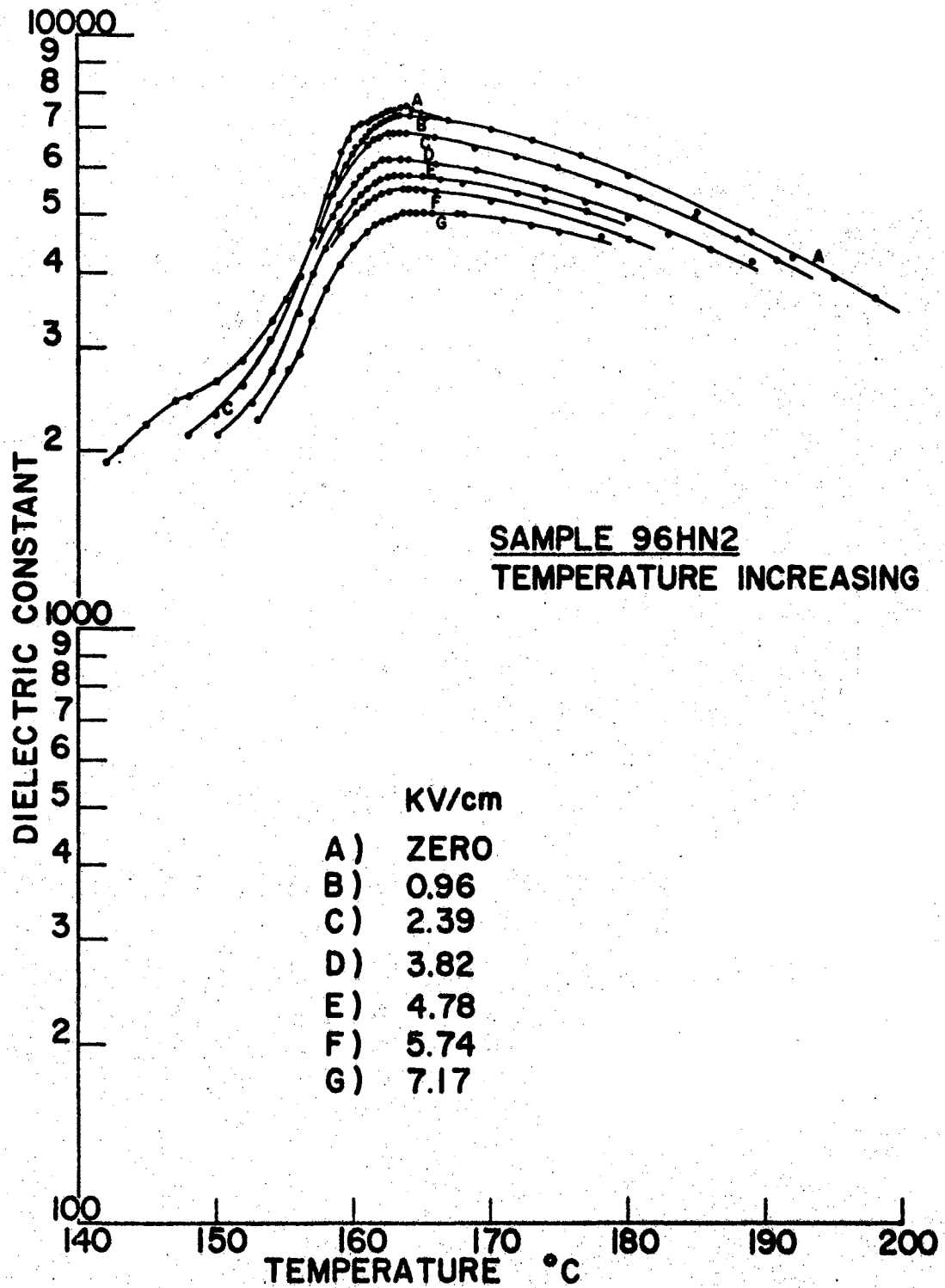


Figure 14. Dielectric Constant vs. Field for Sample 96HN2.

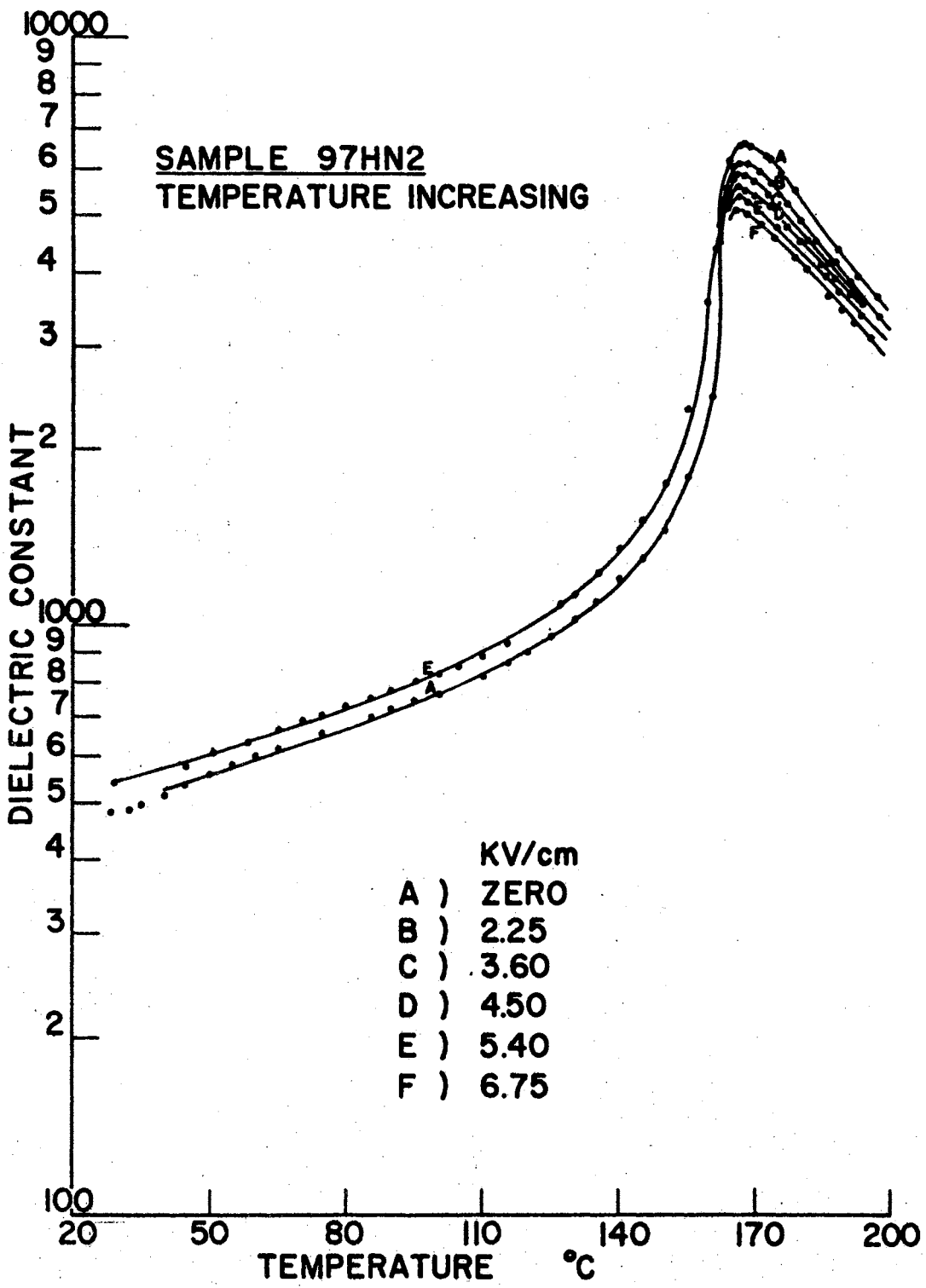


Figure 15. Dielectric Constant vs. Field for Sample 97HN2.

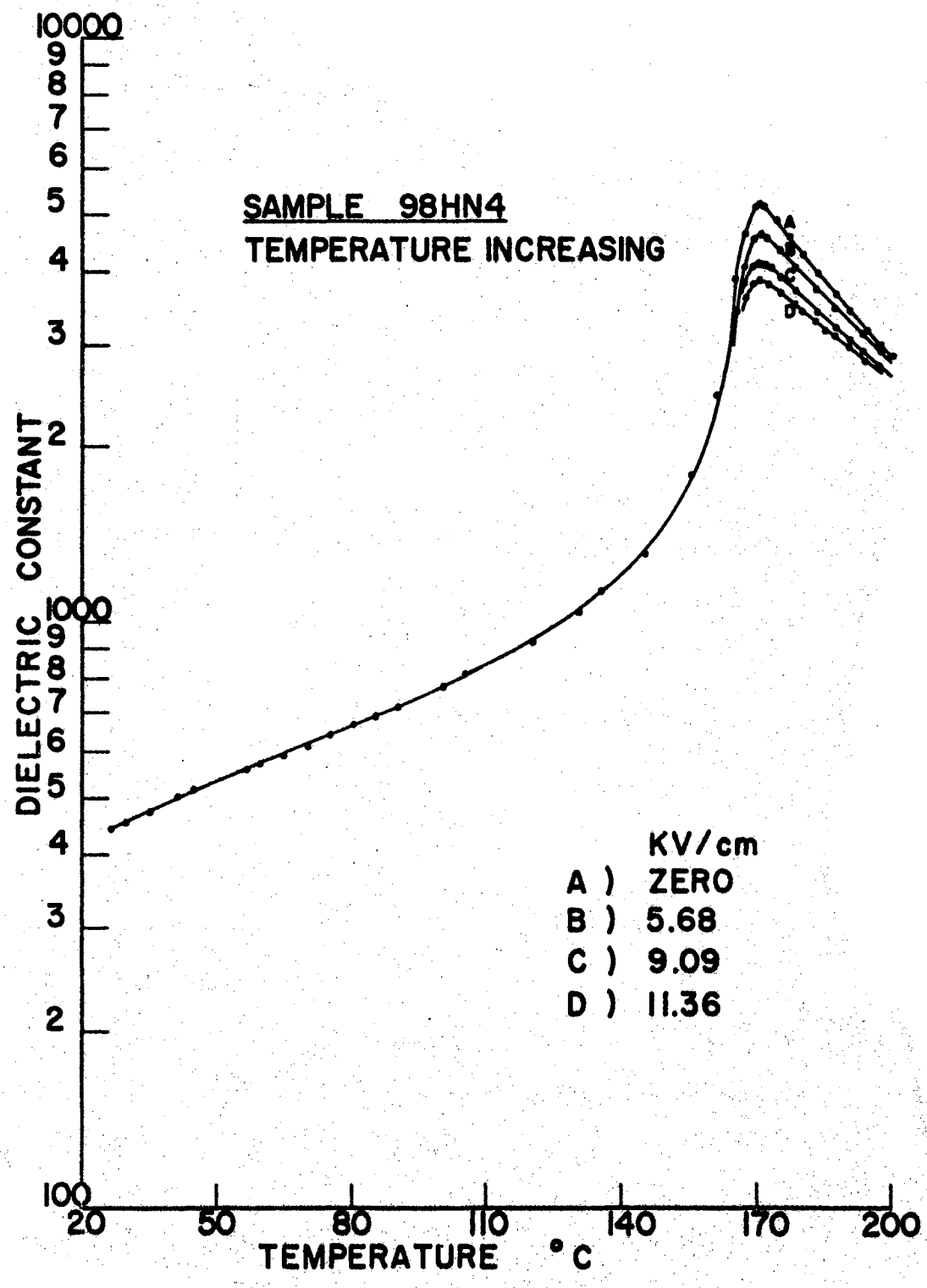


Figure 16. Dielectric Constant vs. Field for Sample 98HN4.

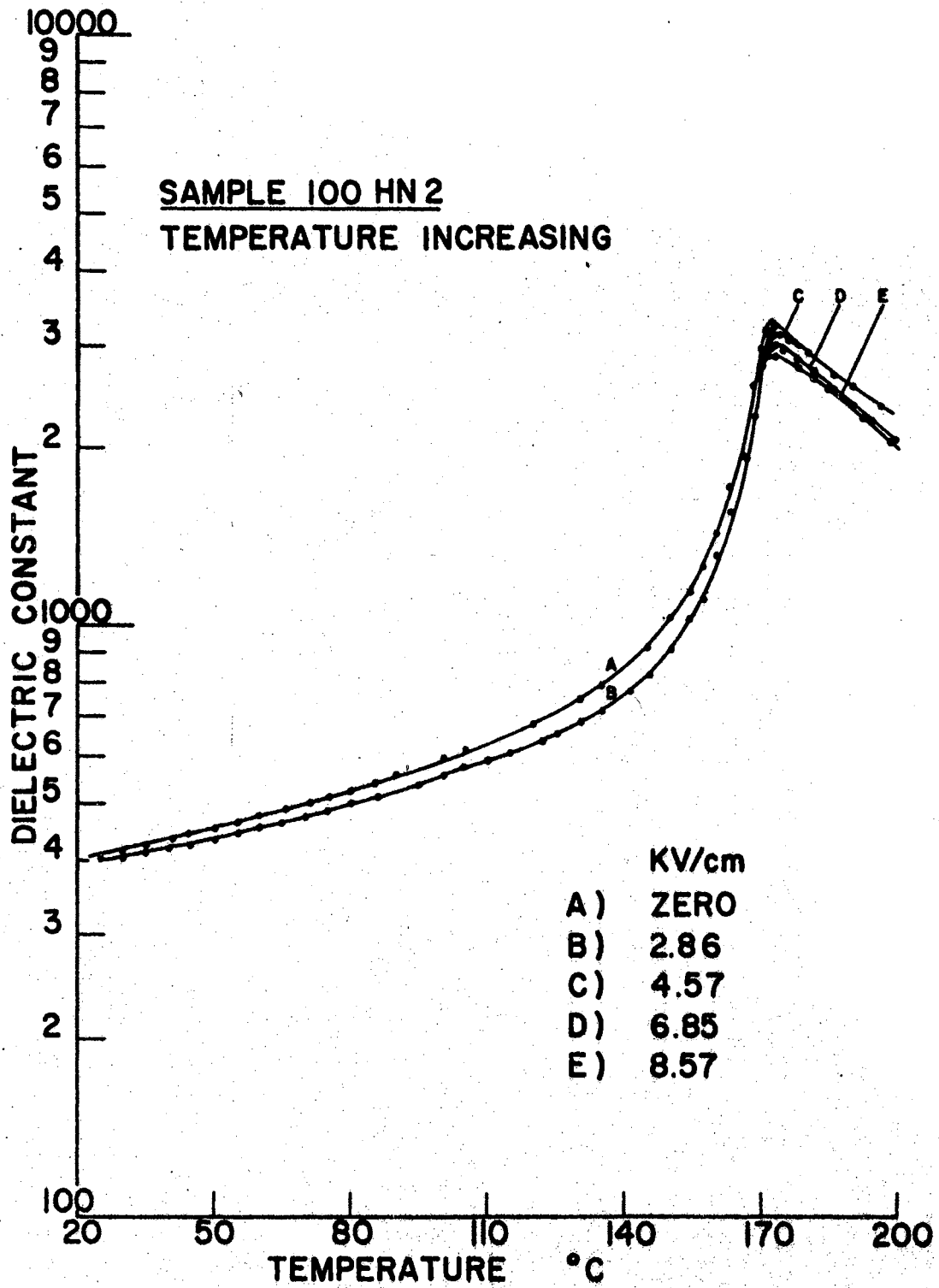


Figure 17. Dielectric Constant vs. Field for Sample 100HN2..

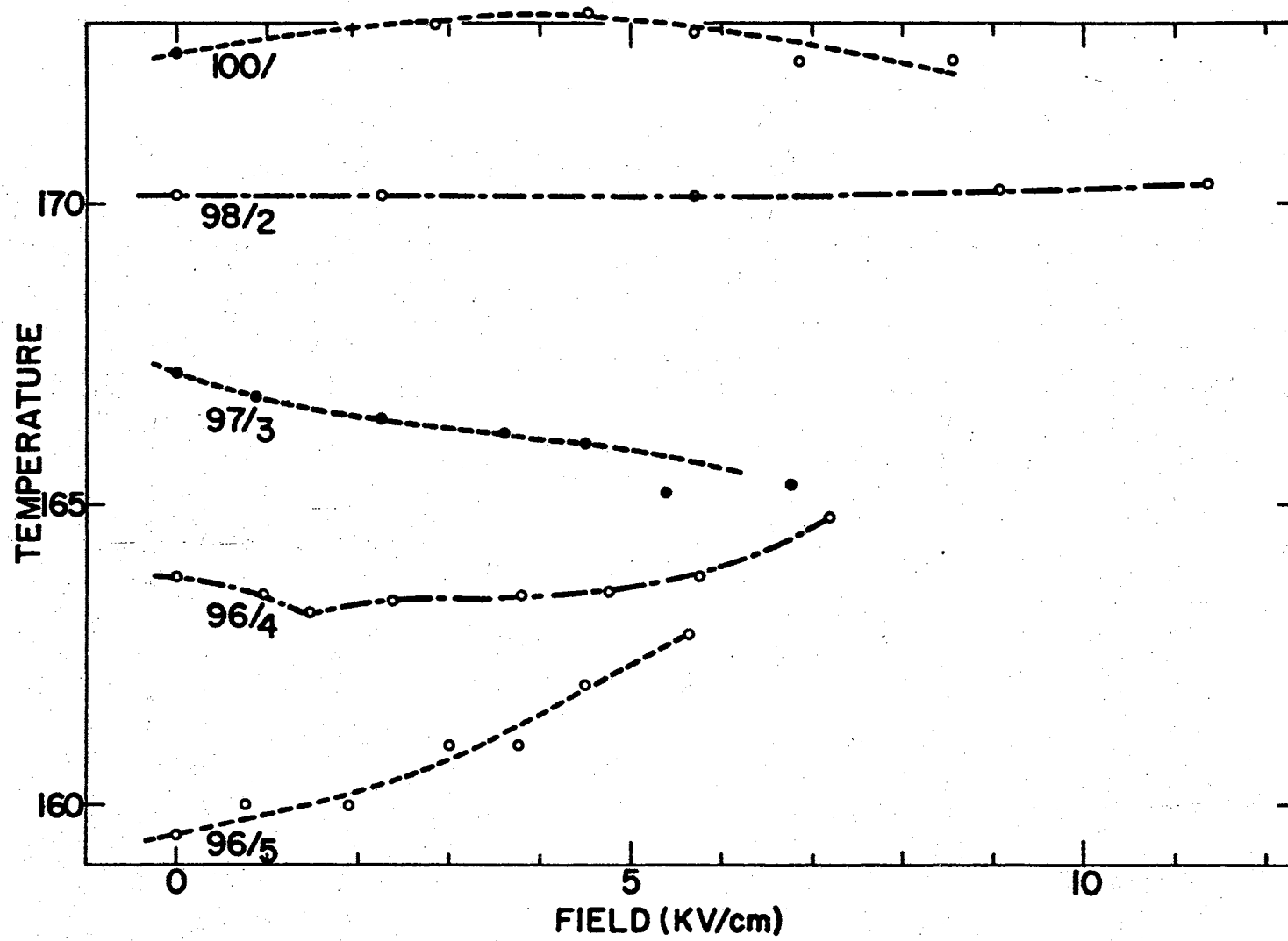


Figure 18. Curie Temperature vs. Bias Field for Lead Hafnate Titanate Compositions.

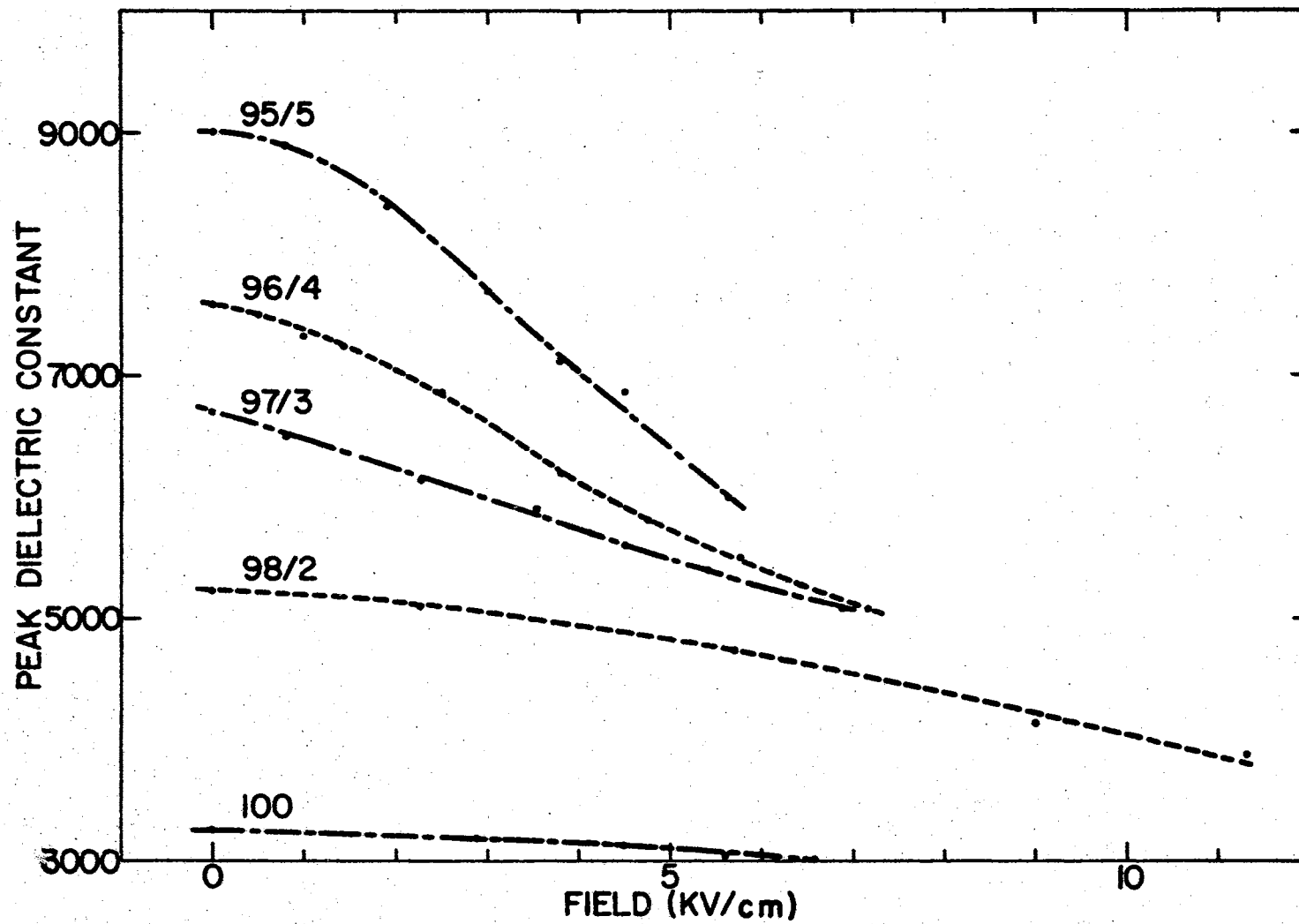


Figure 19. Peak Dielectric Constant vs. Bias Field for Lead Hafnate Titanate Compositions..

95/5, 96/4, and 97/3 materials appear to take on quite similar dielectric characteristics at high fields.

Figure 20 gives a tentative phase diagram for the 96/4 composition. As indicated above, the transitions were not sharp and thus the points indicate only the most probable transition temperatures.

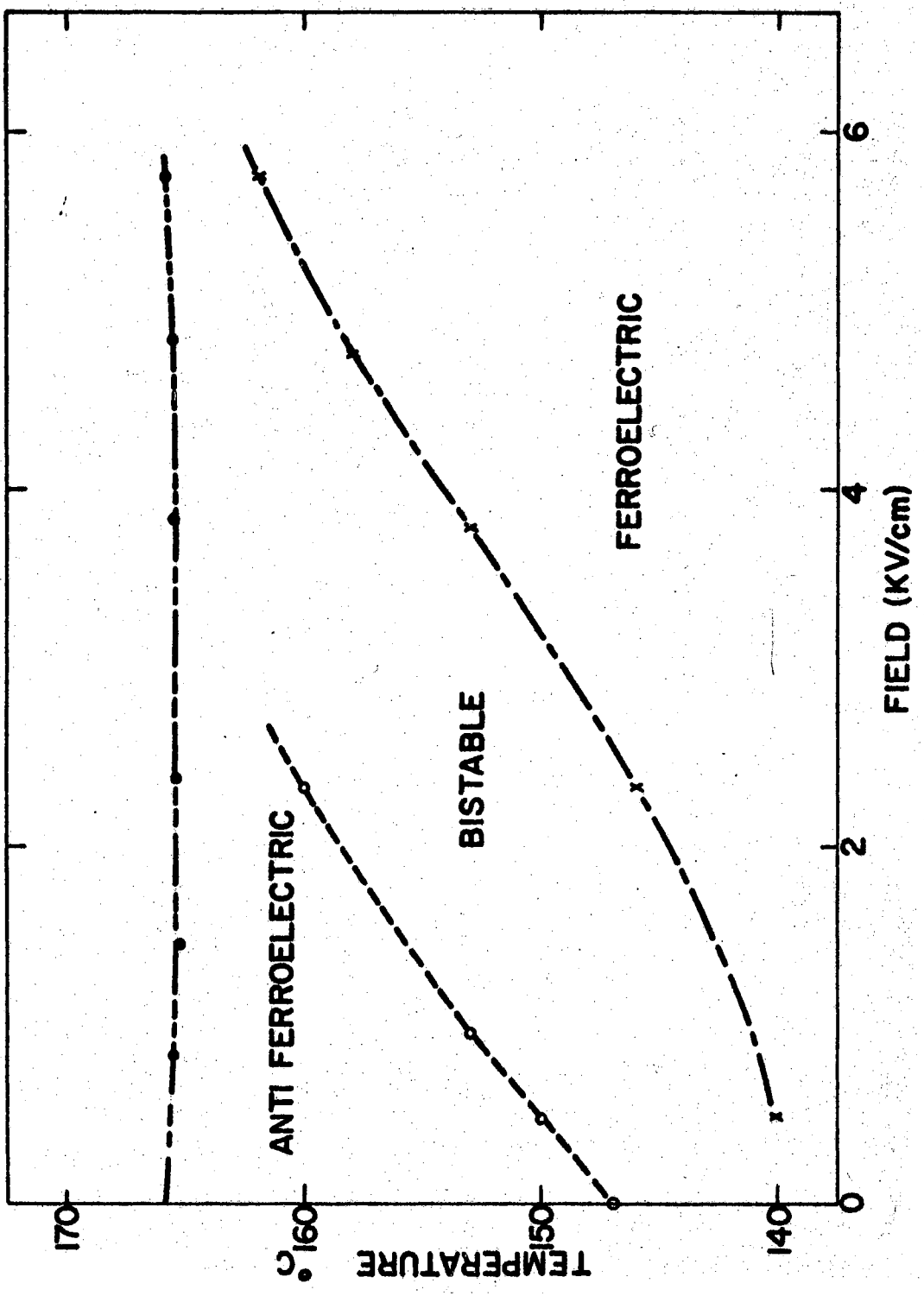


Figure 20. Tentative Temperature-Field Phase Diagram for 96HN2.

CHAPTER V

POLARIZATION MEASUREMENTS

The measurement of polarization has also been of prime interest in the study of ferroelectric materials since these materials are most commonly defined in terms of their possession of a spontaneous reversible internal polarization. This polarization has been used as the basis for the explanation of the other characteristic phenomena associated with ferroelectricity in studies beginning with the interaction theory of Mueller (16) and culminating with the phenomenological theory of Devonshire (9).

Two principal methods have been used to measure the polarization of a given ferroelectric sample. The first uses the detection and measurement of charge flow from the sample when it is caused to transform into the nonferroelectric phase, usually either by heating or the application of pressure. Since the polarization is zero in the nonferroelectric phase, the charge which flows through the measuring circuit during the phase transition must represent the original polarization of the material. This technique has the disadvantage of measuring the polarization only by destroying it.

The second method of measuring polarization in these materials utilizes the reversibility of the spontaneous polarization (25). If the sample is placed in an alternating electric field having sufficient field strength to reverse the polarization on successive half cycles, a

hysteresis loop results. The amount of charge flowing during a single reversal then represents twice the polarization of the material. Also, if the material is subjected to an even number of charge reversals, it can be left in the condition existing before the measurement. Hysteresis loops also have the advantage of giving not only the polarization of the material, but also the electric field necessary to reverse this polarization, the "coercive field." By knowing this field together with the polarization, the energy changes during charge reversal can be found. The area inside a hysteresis loop represents the amount of electrical energy which is converted to thermal energy during one cycle of the applied alternating field.

The random nature of the grain pattern in ceramics leads to basic problems in determining the actual spontaneous polarization of their unit cells. Since perovskite materials have the capability of being polarized along several axes (three in the tetragonal phase, six in the orthorhombic, and four in the rhombohedral), it would seem possible to obtain ceramic polarizations within a few per cent of the single crystal polarization by switching each grain into the lattice direction which most nearly approximates the field direction. In practice, however, mechanical constraints greatly hinder all but the 180° reversals in most materials. In tetragonal barium titanate, for example, only about 15% of the domains not originally optimally aligned can ever be switched 90° . Thus, the polarizations measured on ceramics give only a measure of the actual polarization and precise results must wait until measurements on single crystals are made.

Hysteresis measurements have contributed greatly to the study of FE-AFE transitions through the analysis of the so-called "double loop"

structures given by AFE and cubic materials near a transition point. A typical loop of this type is shown in Figure 21 below.

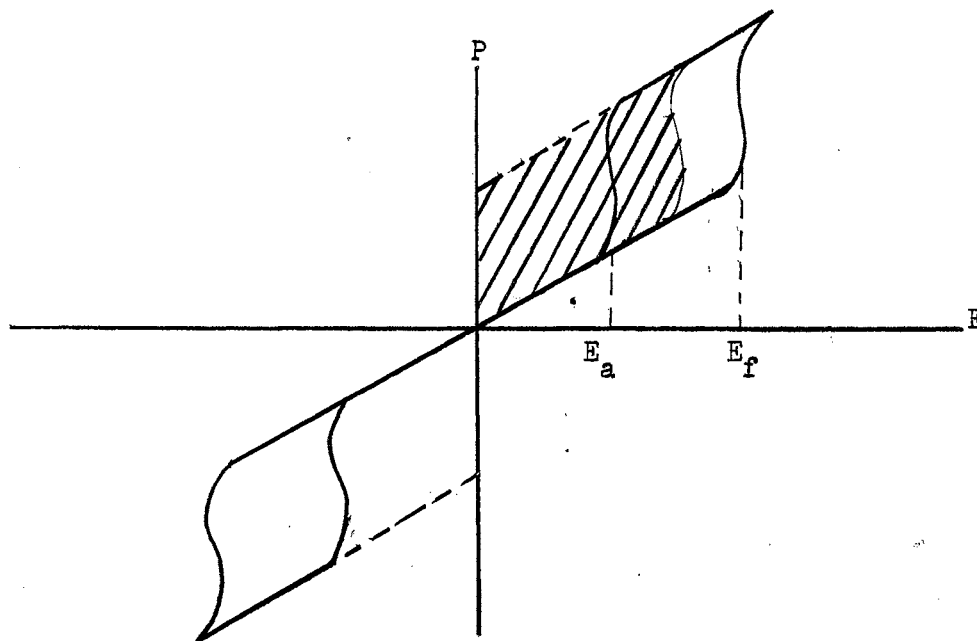


Figure 21. Double Hysteresis Loop Observed During Field-Enforced AFE-FE Transition.

The symbol E_f is used for the field at which the AFE-FE transition takes place, while E_a represents the field at which the FE-AFE transition is observed. If E_f and E_a are approximately equal, a good estimate of the difference in free energies of the two phases is given by the shaded area shown in the figure. In many cases, however, the loops are quite broad and assumptions must be made regarding transition rates and transition probabilities which seriously limit the precision of such estimates.

It has been found that very near the transition temperatures the double loops sometimes reveal a measurable polarization at the zero field point. This phenomenon may be attributed to the coexistence of ferroelectric and antiferroelectric regions within the sample, leading to the superimposing of a normal ferroelectric hysteresis loop on the double antiferroelectric loop.

Experimental Equipment

The systems used for these measurements are shown in Figures 22 and 23. Figure 22 indicates the Sawyer-Tower (25) circuit used to obtain hysteresis loops at 60 cycles. The driving voltage was obtained by connecting to the high voltage transformer of the Beta High Voltage Power Supply immediately before the rectifying stages. In this way a 60-cycle voltage continuously variable from 100 to 2000 volts was available. The resistive divider employed a 100:1 ratio to allow the presentation of the driving voltage as a horizontal sweep of an oscilloscope. The RC integrating network used a 10 microfarad capacitor and a 20 megohm resistor to give an integrating time constant of 200 seconds. The resulting hysteresis loops were then displayed on the oscilloscope and photographed using a Polaroid camera.

For slowlooping measurements the circuit in Figure 23 was used. Driving voltage was supplied by the Beta High Voltage Power Supply and a 400 second integrating circuit was used to detect the polarization changes. A Simpson vacuum tube voltmeter was modified to act as an impedance matching device and allowed the hysteresis loops to be plotted directly on an X-Y recorder. Calibration was done with the aid of a Leeds and Northrup K-3 Potentiometer.

Calculation Techniques

The vertical sweep of the oscilloscope or X-Y recorder indicated the voltage across the capacitor in series with the sample. This capacitor acted to integrate the charge flowing across the sample (the change of sample polarization). The spontaneous polarization

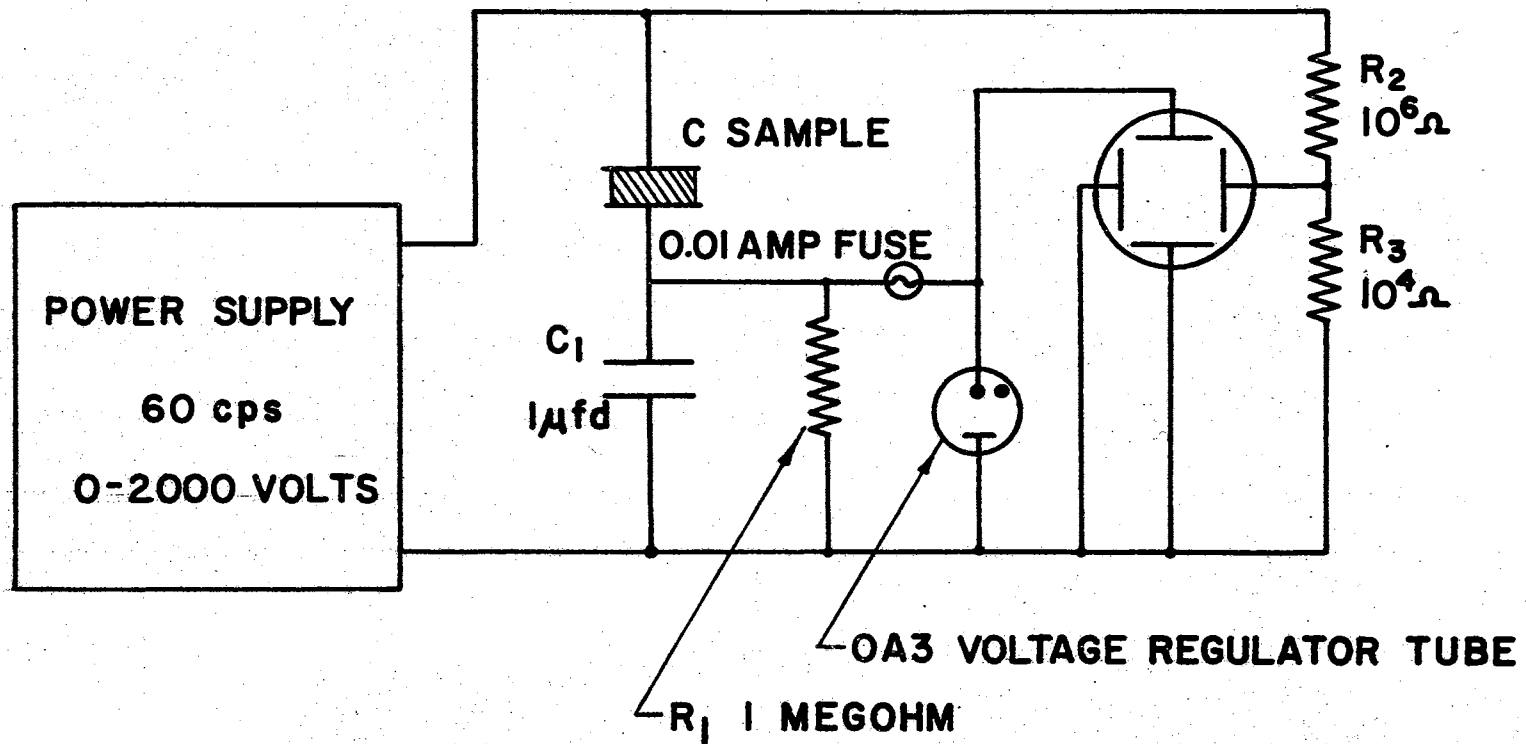


Figure 22. Sawyer-Tower Circuit for 60 cps Hysteresis Loops.

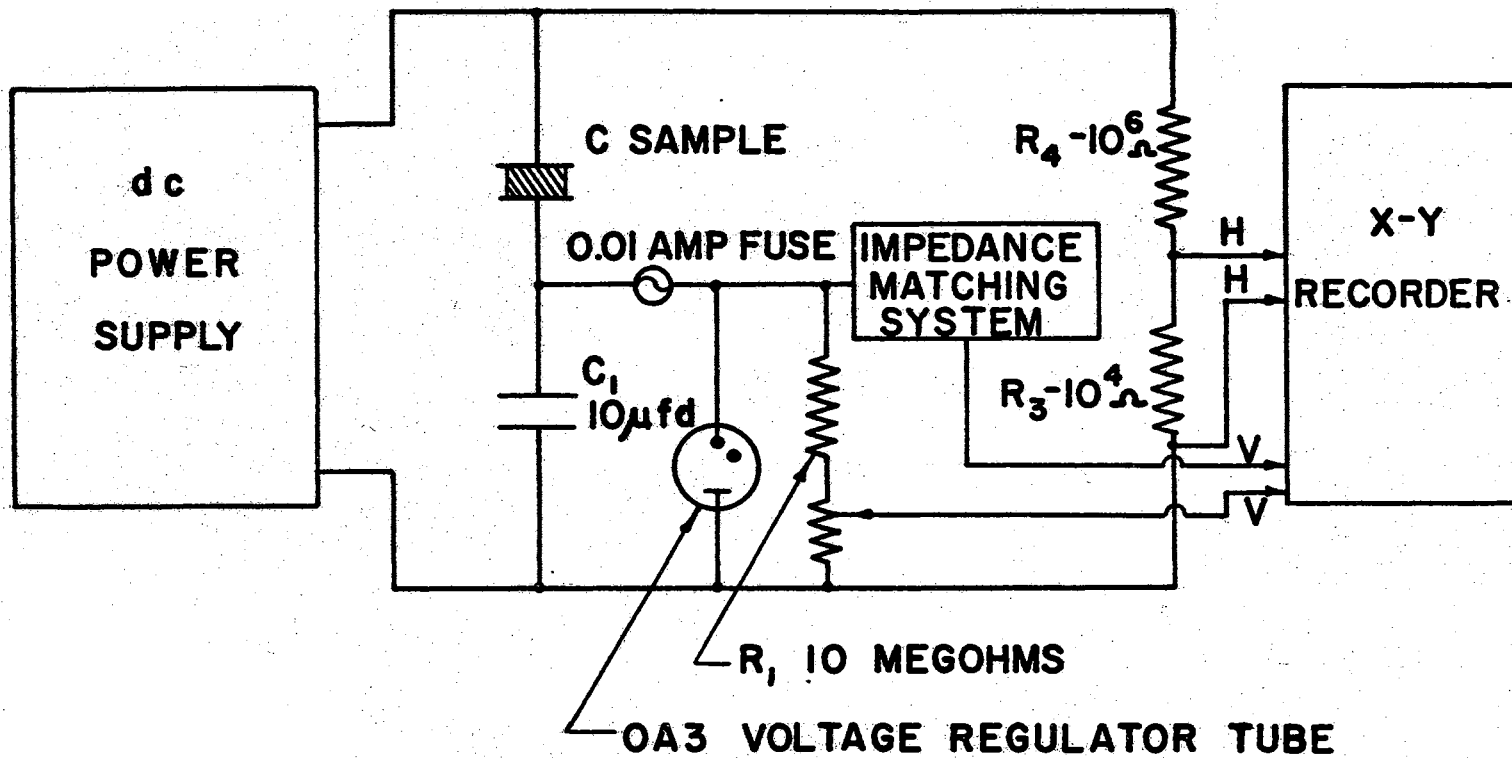


Figure 23. Circuit for Slow-Loop Hysteresis Measurements.

(P_s) was then found by extrapolation of the linear segments at the top and bottom of the loop back to zero field. This polarization is given by

$$P_s = \frac{C_I V_V}{A}$$

where C_I = integrating capacitance

V_V = vertical voltage

A = sample electrode area.

The coercive field of a ceramic sample is usually taken as that field on a symmetric hysteresis loop at which the polarization becomes zero.

This is indicated by the horizontal sweep of the oscilloscope, which is driven by the power source through a voltage divider. If the voltage scale of the oscilloscope and the resistive divider are known, the coercive field is obtained directly.

Experimental Results

Results obtained with this equipment were similar to those previously obtained on this class of materials. Figure 24 indicates the observed polarization and coercive field as a function of the temperature, as obtained in the present investigations on the 95/5 lead hafnate titanate composition. The apparent decrease of polarization at low temperatures and 60 cycles is probably due to a failure to completely saturate the hysteresis loops. The samples were not subjected to voltages much greater than 10 KV/cm in order to insure against electrical breakdown. Figure 25 is a similar plot for the 96/4 sample. Again the differences between the slow loop polarization and that obtained at 60 cycles are probably due to the limitations of the applied voltage.

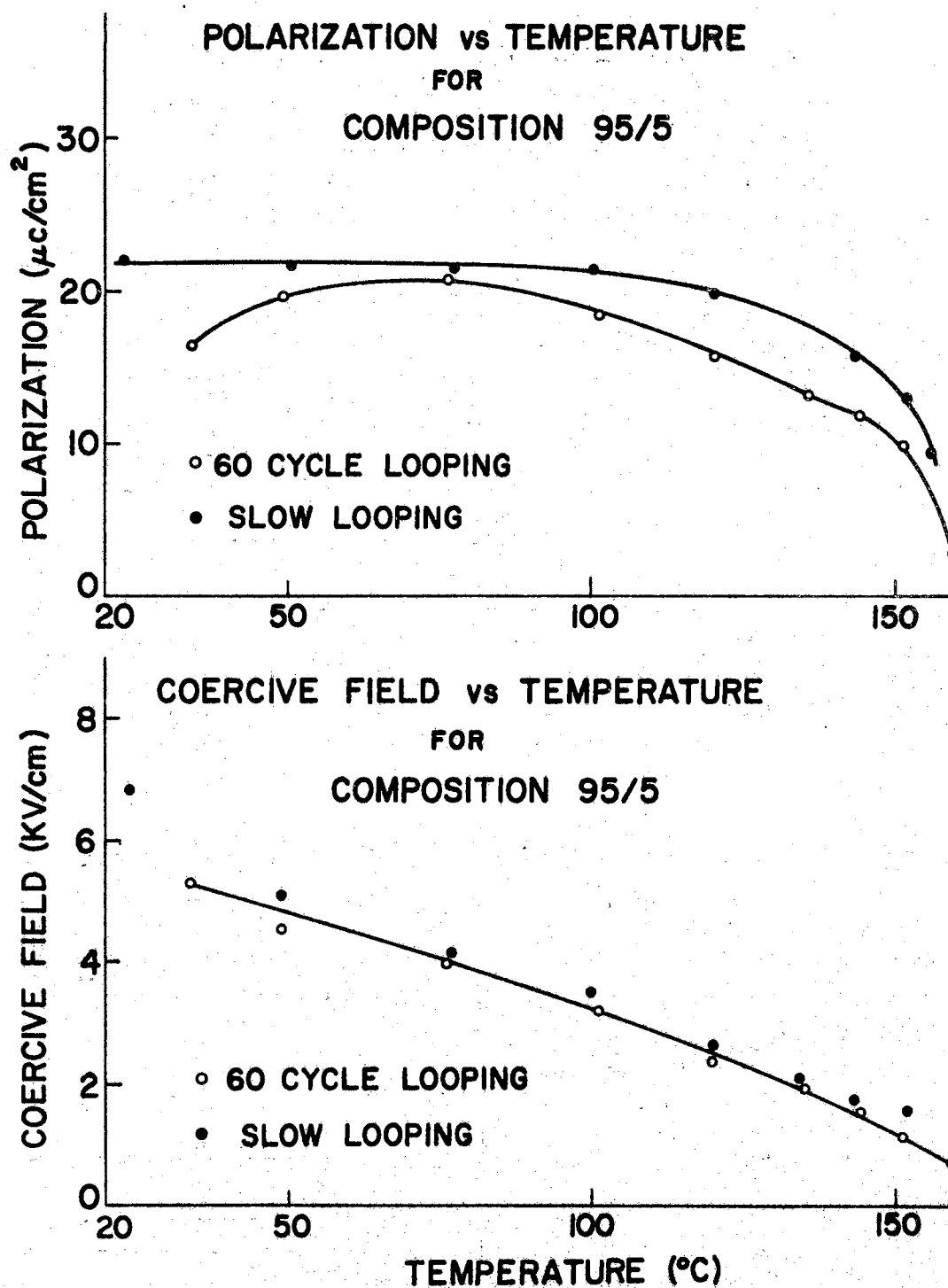


Figure 24. Hysteresis Parameters for the 95/5 Lead Hafnate Titanate Composition.

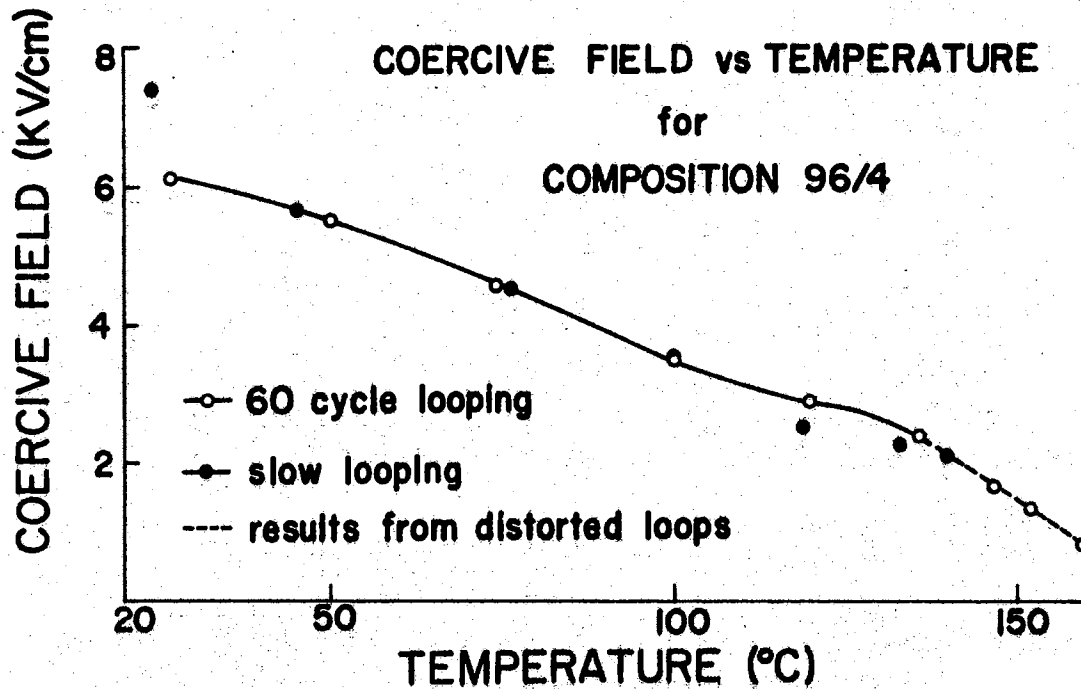
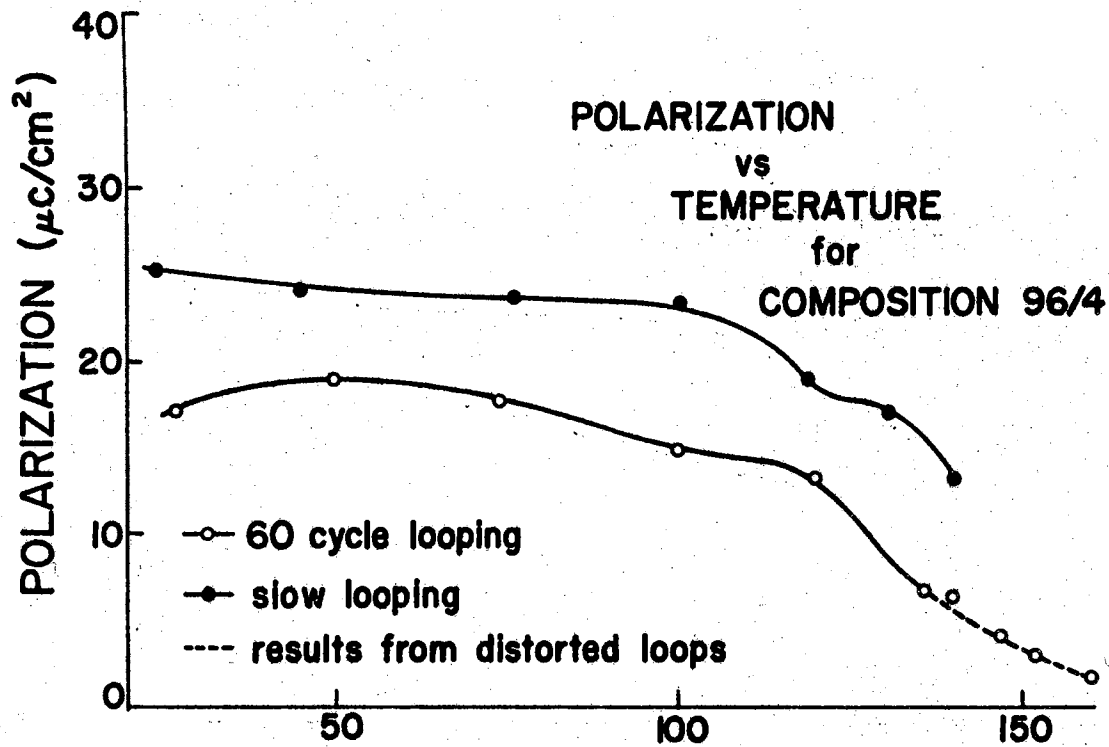


Figure 25. Hysteresis Parameters for the 96/4 Lead Hafnate Titanate Composition.

The loops obtained in the vicinity of the FE-AFE phase transition with the 96/4 material exhibited the characteristic double loop form but failed to close off completely at zero field. In order to establish the presence of some ferroelectric phase material within the sample above the transition temperature, the samples were impressed with only the positive half of the voltage cycle. This enabled the positive half of the double loop to be observed in the absence of any ferroelectric switching. The results of this procedure are shown in Figure 26. The fact that the antiferroelectric loops close off at zero bias under these conditions indicates that a certain portion of the material does remain ferroelectric above the transition temperature. The repeatability of the loops is not sufficient to allow a quantitative description of the phenomenon, but qualitatively it appears that as much as 25% of the sample may remain ferroelectric in the region up to five degrees above the transition temperature.

An attempt was made to apply fields high enough to switch thin samples of the 97/3 and 98/2 material but breakdown of the samples resulted. This has been successfully accomplished at Sandia Corporation and those results are given in a later chapter.

96HN2

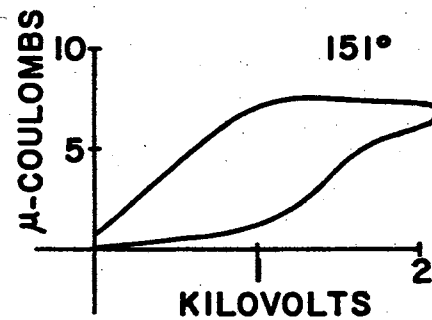
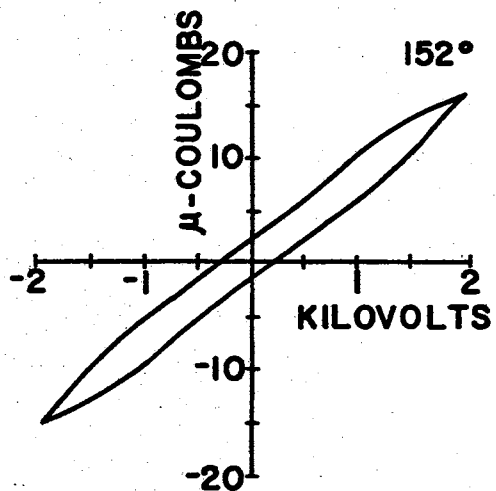
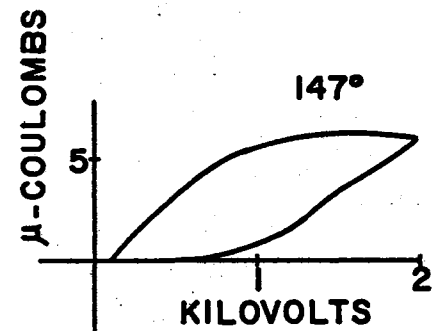
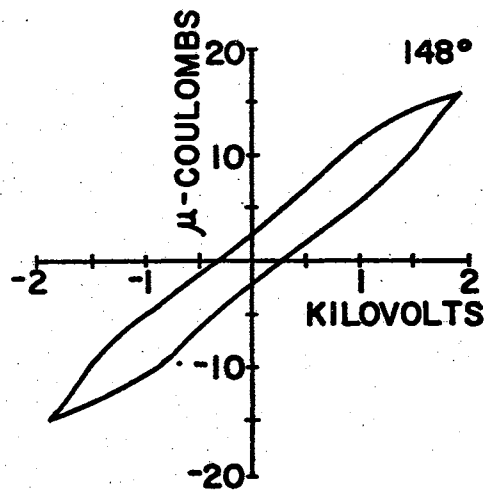


Figure 26. Hysteresis Loops and Portions of Double Hysteresis Loops Showing Field-Enforced Ferroelectric Phase in the 96/4 Lead Hafnate Titanate Composition (Temperature Decreasing).

CHAPTER VI

THERMAL MEASUREMENTS

Calorimetric measurements were made on samples of the materials used in this study in order to determine their specific heats and heats of transformation. The measurements were made in a calorimeter designed specifically for measurements on thin discs of ceramic material.

Many of the basic ideas of adiabatic calorimetry were first developed by Sykes (28). He designed a calorimetric system in which the sample and its container were maintained near the temperature of the calorimeter by means of a heating coil, with a differential thermocouple used between the sample and the calorimeter to detect the growth of temperature differences. By alternately heating the sample above the calorimeter temperature and allowing it to cool slightly below that temperature, Sykes was able to achieve nearly adiabatic conditions of heating. This technique has been modified in the present study by using the ceramic discs themselves to contain the electrical heater and the detection thermocouple, thus doing away with the sample container. The consequent reduction in thermal mass of the sample portion of the calorimeter provides much faster response to changes of input power, allowing the sample to be maintained at the same temperature as the calorimeter for relatively long periods of time.

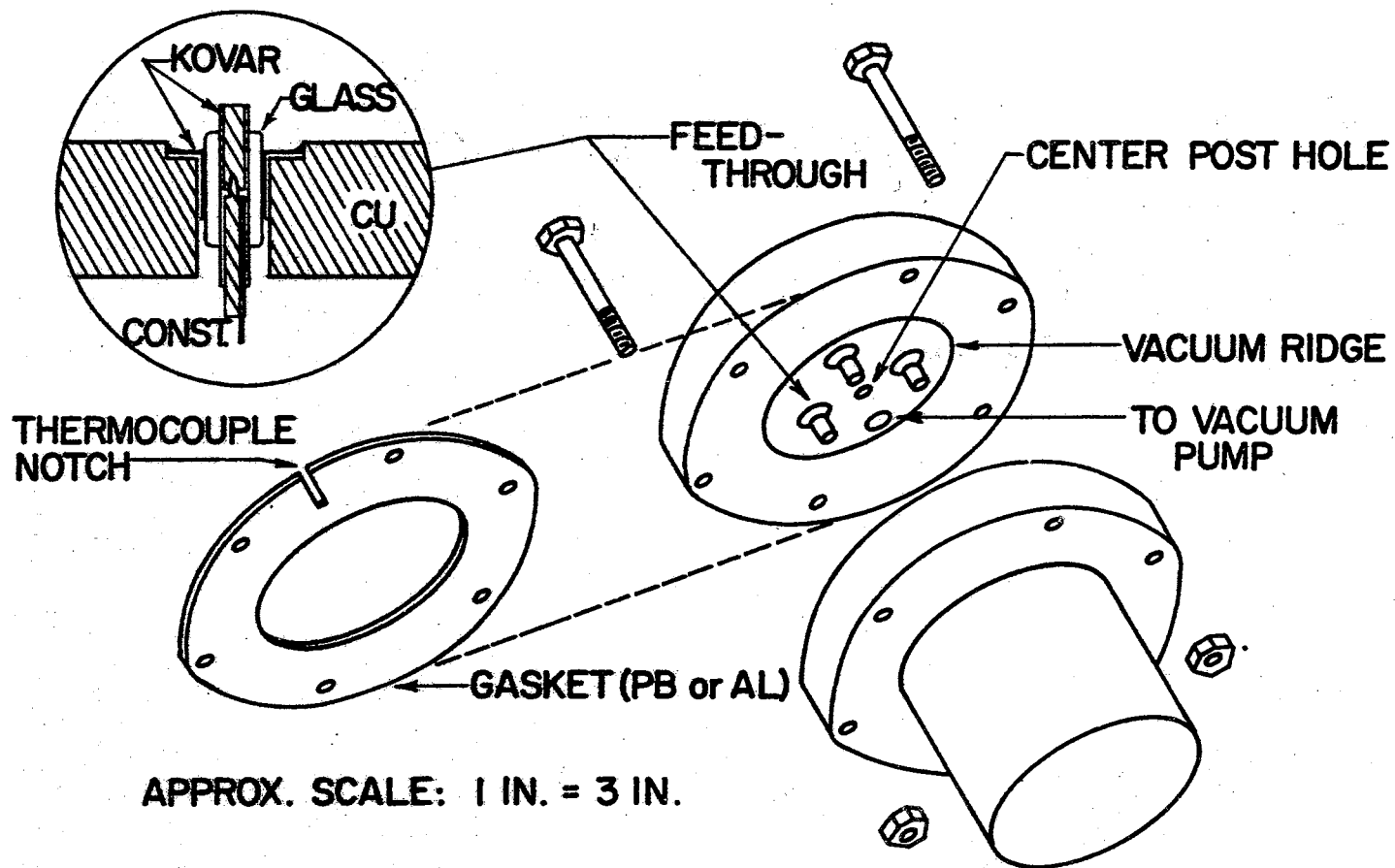
Two different types of measurements were made on the samples used in this study. In the first type, the sample was mounted in the

calorimeter and heated while the calorimeter cup itself remained at room temperature. This permitted the checking of the sample heater and thermocouple and determination of the thermal loss characteristics of the system. This information was used to detect defects in the sample mounting and to aid in the later and more accurate measurements.

In the second type of measurement, the sample was maintained in an adiabatic relationship to the calorimeter while the calorimeter was heated from room temperature to some temperature above the Curie point of the sample material. In this way, the specific heat of the sample could be determined throughout the above temperature range, and the heat of transition absorbed at the Curie point could be obtained. Since these measurements were made under adiabatic conditions, they were more accurate than those of the first type.

Description of Equipment

Figure 27 illustrates the design of the calorimeter. It is constructed of half-inch copper. The outside diameter is five inches and the outside depth five and one-half inches. The inside chamber measures three inches in diameter and three and one-half inches deep. The entire body of the calorimeter is bright nickel plated to resist corrosion and to reduce the radiative emissivity of the chamber. The top of the calorimeter is fitted with three vacuum feedthrough connections for the thermocouples and the heater, as well as a threaded ground post and a metal tube for attachment to the vacuum system. The abutting faces of the calorimeter top and base are fitted with a set of small ridges which permit the use of an aluminum or lead gasket for vacuum sealing. The two parts of the calorimeter are connected to each other by six



APPROX. SCALE: 1 IN. = 3 IN.

ALL PARTS MADE OF COPPER, BRIGHT NICKEL PLATED

Figure 27. Calorimeter Design.

equally spaced 1/4" x 1" bolts. A notch is cut in the gasket to allow the positioning of a copper constantan thermocouple junction near the inside calorimeter chamber as the calorimeter temperature measurement junction.

Heating of the calorimeter was accomplished by means of a three gallon oil bath containing Dow Corning DC200 silicone oil. The bath was fitted with a 1400 watt immersible heater at the bottom of the liquid and was stirred by means of an Eberbach Model 58 variable speed stirrer. A thermometer was placed in the bath near the calorimeter and used for thermocouple calibration. This bath was capable of heating the calorimeter at rates up to ten degrees Centigrade per minute although rates above three degrees per minute were not used during the measurements of interest.

The maximum temperature variation in the region of the calorimeter was less than one degree during all measurements. Considering the thermal diffusivity of the copper, the variation of temperature within the calorimeter chamber was less than this. Since the sample was maintained at the same temperature as the calorimeter cover during adiabatic measurements, radiation exchanges to all parts of the chamber were negligible. The calorimeter was operated under forepump vacuum conditions in order to reduce conduction losses during nonadiabatic measurements.

Description of Samples

Figure 28 illustrates the construction of the sample assembly used in the study. Each sample was built from two discs of the ceramic to be tested. One of these was fitted with a series of grooves and a

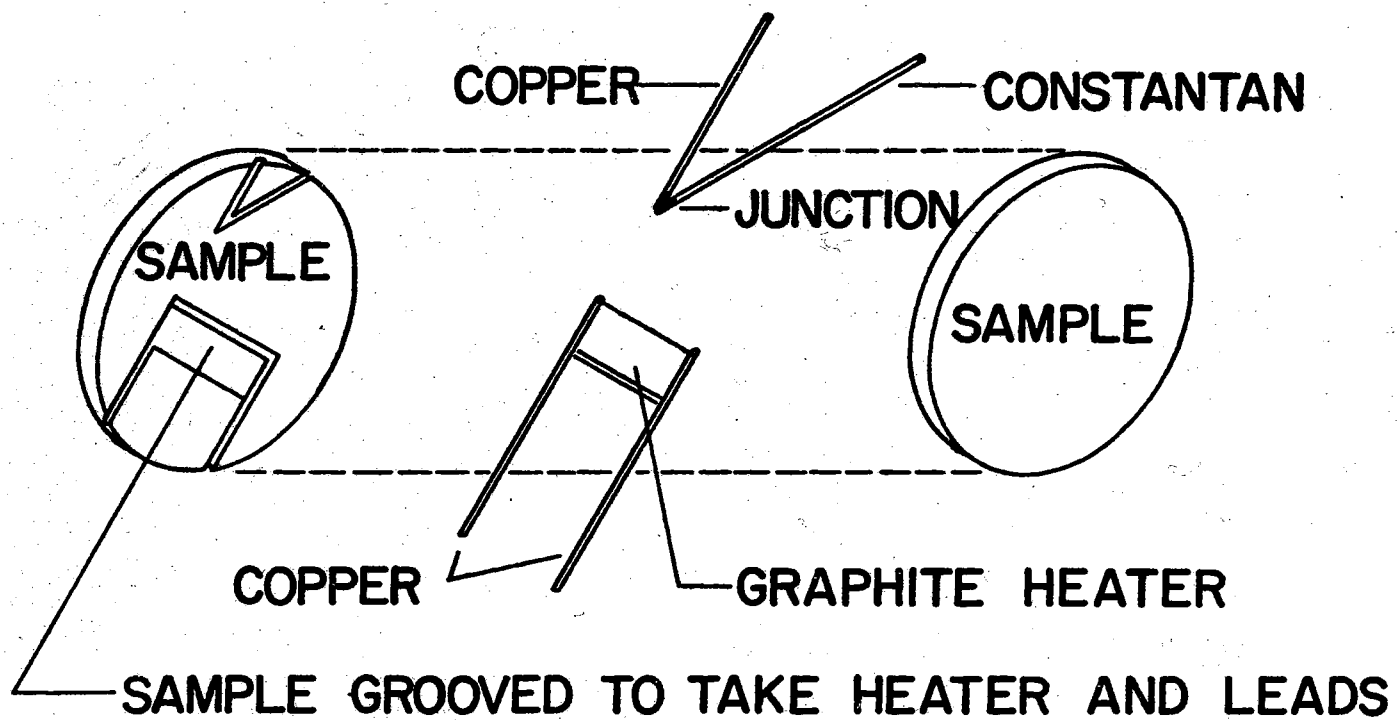


Figure 28. Construction of Sample Assembly.

small flat well to contain the heater plate. This was originally done by masking the sample and sandblasting it with No. 600 alundum powder. Later it was found more convenient to sandblast the well to proper depth and then to adjust the depths of the grooves with the aid of a Gulton Model DS-10 ultrasonic drill. This technique allowed the heater and the differential thermocouple junction to be sealed inside the material to be tested. The sample was then mounted to the calorimeter by means of the electrical connecting wires. Thus both the heat capacity of the sample and the conductive losses to the calorimeter were kept at a minimum relative to the mass of the material to be tested.

The sample heater was made of carbon. Originally the heaters were polished into shape from small pieces of graphite rod, but it was found that the use of pieces of carbon arc rod gave higher resistances for the required dimensions, which facilitated measurement of heater power. A typical heater had dimensions of 4 mm x 8 mm x 0.1 mm and a resistance in the range from one to five ohms. This heater plate was then mounted in the well provided in the sample and connections made to the #30 copper lead wires with silver paint. The use of a heater element in the shape of a flat plate allowed a large area of contact between the sample and the heater and resulted in more uniform heating.

The heater was connected to a six volt battery and control was achieved by means of a ten ohm wire-wound potentiometer. Typical heating conditions consisted of a voltage of about 0.30 volts across the heater and a current of 0.15 amperes through it. Under these conditions the minimum power deviations obtainable were of the order of 0.3 milliwatts. The voltage across the heater was measured by means of a microammeter fitted with various series resistances to provide the optimum

range of measurement, and the current was measured by means of a Simpson Model 269 milliammeter.

The temperature of the sample was measured with a copper constantan thermocouple junction planted in the sample. This junction was made by spot welding a piece of #30 constantan wire to a piece of #30 copper wire and was fitted in the grooves shown in Figure 28. The copper wire was grounded to the copper of the calorimeter through the threaded central ground plug. The constantan led to the reference junction of the differential thermocouple which was fitted into one of the vacuum feedthroughs as shown in Figure 27. It was found that the thermal resistivity of the glass portion of the feedthrough allowed this junction to heat slightly during the nonadiabatic runs. In order to give better thermal contact between this junction and the calorimeter, a cap was built to fit the exterior central pin of the feedthrough. A thin mica sheet between the cap and the calorimeter cover gave good thermal contact while providing electrical separation.

After insertion of the thermocouple junction and the heater, the two discs comprising the sample were bonded together with Duroplastic epoxy.

Measurement Techniques

Preliminary Measurements

Preliminary measurements were made on each sample by observing the exponential rise and fall of the temperature of the sample when power was applied to the sample heater and the calorimeter was kept at room temperature. This technique allowed the sample heater to be calibrated and permitted the determination of the conduction losses

between the sample and the calorimeter. From these measurements it was also possible to determine the room temperature specific heat of the sample material.

If a sample of material is originally at a temperature higher than its surroundings, and if it is postulated that conduction losses are much larger than radiation losses from the sample, the following condition must hold:

$$c \frac{dT}{dt} + a (T - T_0) = 0$$

where c = sample heat capacitance

T = sample temperature

T_0 = surrounding temperature

a = thermal loss constant (quantity of heat lost per unit time per unit temperature difference.)

Solving this equation for T ,

$$T = T_0 + \Delta T e^{-at/c}$$

where ΔT is the difference of temperature at time zero. This implies that under the stated conditions, the sample will cool exponentially with the exponential time constant determined by the ratio c/a .

Likewise, if the sample and its surroundings are initially at the same temperature and power is applied to the sample, the following relation holds:

$$c \frac{dT}{dt} + a (T - T_0) - Q/t = 0$$

where Q/t is the thermal power being applied to the sample.

Solving this equation for T ,

$$T = T_0 + (T_f - T_0) e^{-at/c}$$

where T_f represents the equilibrium temperature at which the thermal

losses equal the power input. From this it can be seen that under these latter conditions the temperature will rise exponentially to a final equilibrium temperature, and that the exponential time constant will be the same as that for the cooling curve.

Thus by observing a cooling curve for a given sample mounted in the calorimeter, the ratio of the loss factor to the heat capacity of the sample can be determined. By observing the equilibrium temperature obtained by a given power input, the loss factor can be found from the relation:

$$a = \frac{Q/t}{(T_f - T_o)}$$

The heat capacity of the sample is then the product of this loss factor and the exponential time constant.

In making these measurements, the output of the differential thermocouple was connected to the vertical input of a Moseley Autograf Model 2A X-Y Recorder. The horizontal input was connected to an internal 750 second time base. Thus the actual exponential heating and cooling curves were plotted by the recorder.

Cooling curves were observed over a range of twenty degrees for the accurate determination of the time constant. Then heating curves were observed for various power inputs. Since the time constant of heating was already known, it was only necessary to record a heating curve for a short time in order to calculate the final equilibrium value of the temperature. When these equilibrium temperatures were plotted as a function of power, the result was a straight line whose slope gives the loss factor. Figures 29 and 30 represent such a plot together with a plot of the cooling curve for a quartz sample which was

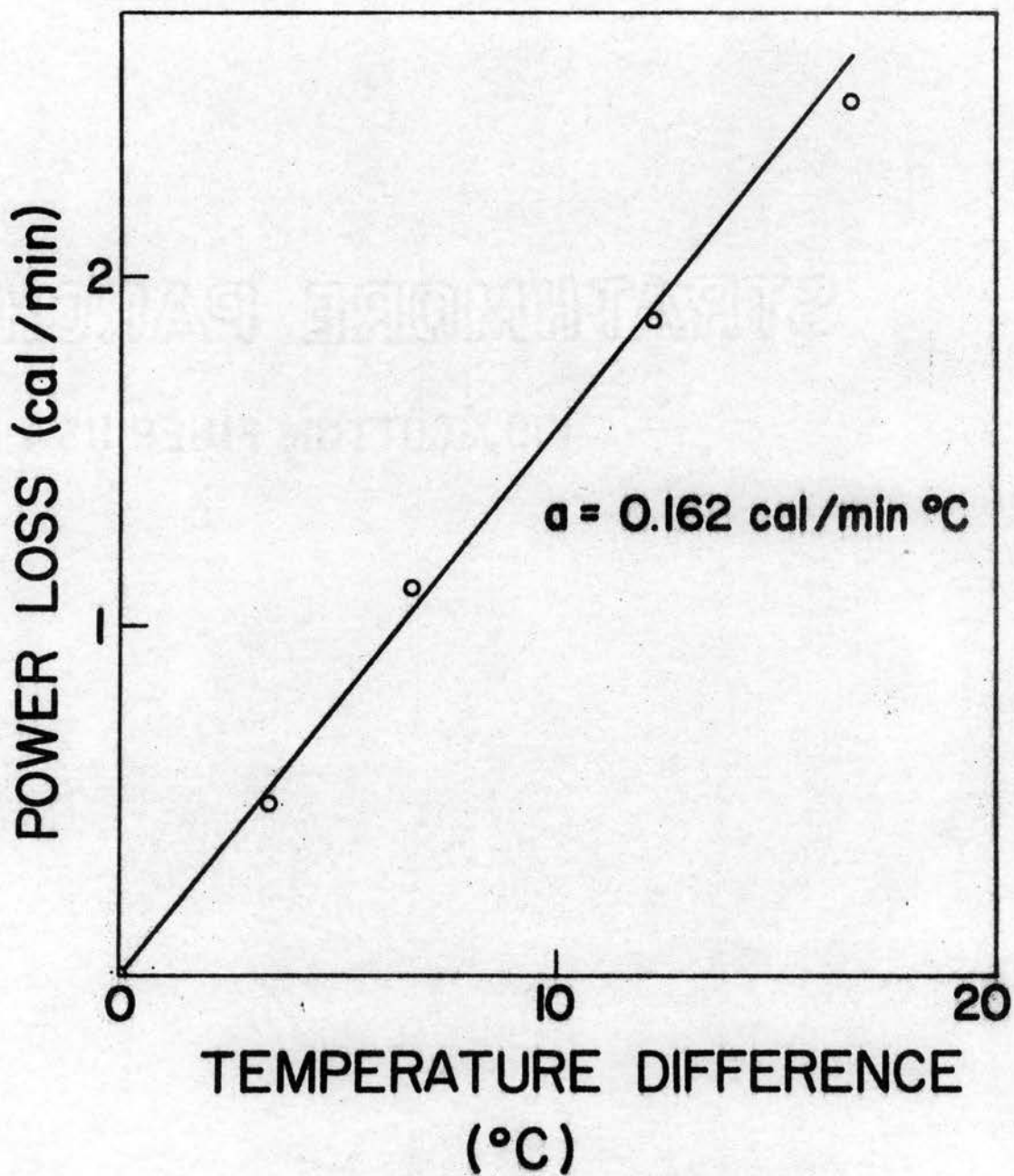


Figure 29. Determination of Loss Factor in Preliminary Measurements.

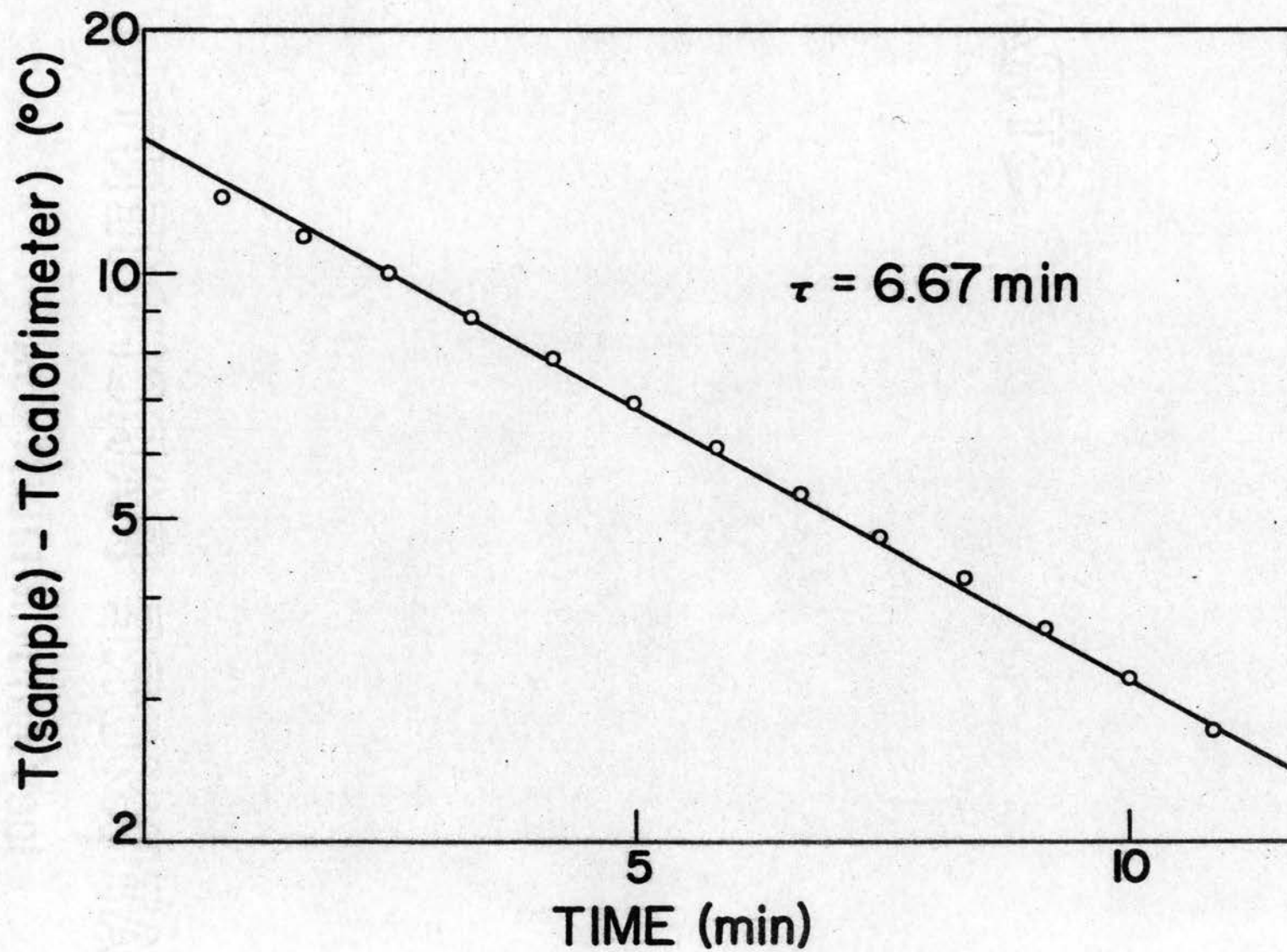


Figure 30. Exponential Cooling Curve for Quartz Check Sample.

used to check the system. The cooling curve has been plotted on a logarithmic scale to verify the assumption that the loss is primarily through conduction. The value of the specific heat of quartz given by these plots is 0.187 as compared to a handbook value of 0.181. As was stated earlier, it was found that the reference junction of the differential thermocouple tended to heat slightly above the actual calorimeter temperature during nonadiabatic measurements. This caused the reading of the difference temperatures between the sample and the calorimeter to be slightly low, giving erroneously high loss constants. This in turn led to values of the specific heat of the sample which ranged from five to ten per cent high. After installation of the cap to improve thermal contact between the reference junction and the calorimeter, this error was reduced to approximately two per cent.

Adiabatic Measurements

The most precise measurements of this thermal study were those made under adiabatic conditions. As outlined in the introduction to this chapter, these conditions were achieved by using a differential thermocouple as a null detector and varying the input power to the sample to maintain it at the same temperature and the same rate of temperature change as the calorimeter.

In making these measurements, it was found most convenient to apply a constant amount of power to the oil bath throughout a complete run. This caused the rate of heating of the oil to increase during the early part of a run until a steady set of heating conditions was obtained, and then to decrease slowly throughout the rest of the run as losses to the surroundings became greater. The reason that a

constant input power was chosen lay in the high thermal mass of the calorimeter and the oil bath. In contrast to the sample, which could achieve a stable set of thermal conditions within 40 seconds after an input power change, the transient effects of an input power change to the oil bath did not disappear for several minutes. However, the same high thermal mass which prolonged these transients acted to prevent the growth of heating instabilities under the constant input power conditions.

The sensitive detection of adiabatic conditions was accomplished by connecting the differential thermocouple directly into a Leeds and Northrup Type K-3 potentiometer. At its most sensitive settings this potentiometer gave approximately the sensitivity of its Leeds and Northrup Model 2430 galvanometer (one-tenth microvolt per division) and the versatility of the potentiometer circuit was invaluable during periods of instability, troubleshooting, etc. Using this instrument it was possible to keep the temperature of the sample within 0.05°C of that of the calorimeter during all measurements, and to match the two heating rates to within $0.01^{\circ}\text{C}/\text{minute}$. From the loss factors found in this study, a temperature difference of 0.05°C represents a deviation from the measured input energy to the sample of only 0.2 milliwatts, which is about the same as the sensitivity of setting the input power. This number represents a deviation of less than one per cent of the smallest heating rate normally used during the measurements.

During these first measurements with this system it was felt advisable to use manual control of the sample power. In this manner it was possible to better compensate for the magnitudes and rates of change which were occurring in the samples, and to adjust to the

transient behavior and sensitivities of balance which were characteristic of the system. In experimental studies where a large number of measurements were to be made, however, it would be advantageous to automate the sample power supply to allow adiabatic measurements to be made and recorded automatically. The block diagram of a preliminary system for this purpose is given in Figure 31. An amplifier having the characteristics necessary for the detection and control of a temperature null between the sample and the calorimeter has already been designed by Dauphinee and Woods (8). A schematic for this amplifier is given in Figure 32. A prototype of this amplifier was built, but was not used in any of the measurements reported here.

During measurements under adiabatic conditions the horizontal section of the X-Y recorder was again operated on the 750 second time base. The vertical section was connected to the calorimeter thermocouple, which was balanced against a reference junction at 0° C. Thus the curves obtained from the X-Y recorder were direct plots of the calorimeter temperature against time. The rate of change of temperature could then be obtained by measuring the slope of these curves. This rate of change of temperature was thus determined as a function of the calorimeter temperature.

The electrical power input to the sample which was necessary to maintain it at the same temperature as the calorimeter was listed on the X-Y recorder curves at intervals of from one to five degrees. From this data a plot could be constructed which showed this power as a function of the calorimeter temperature. The ratio of the value of the power applied to the sample to the corresponding rate of change of temperature gives the heat capacity of the sample.

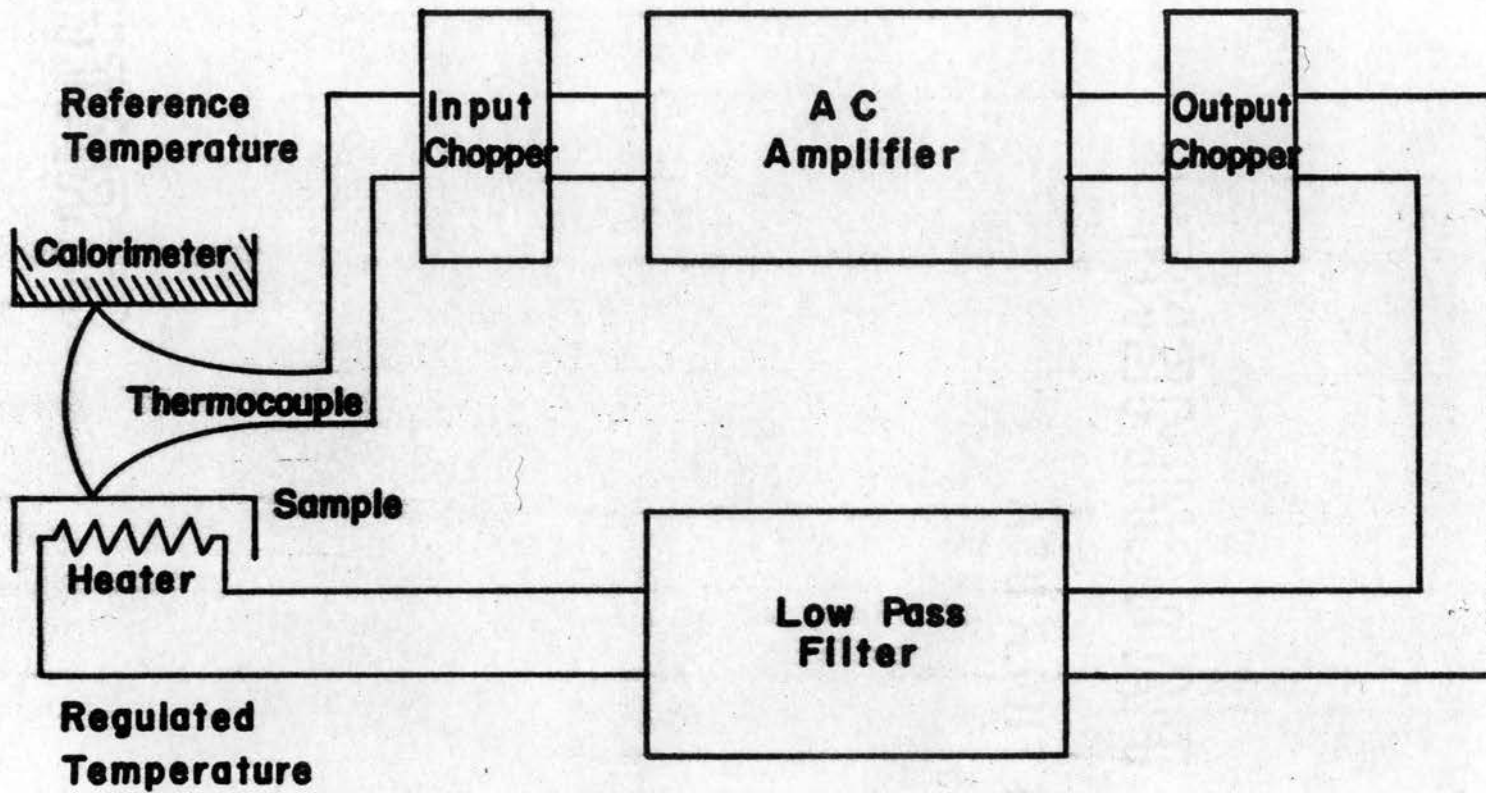


Figure 31. Block Diagram of Automated Thermal Measurement Apparatus.

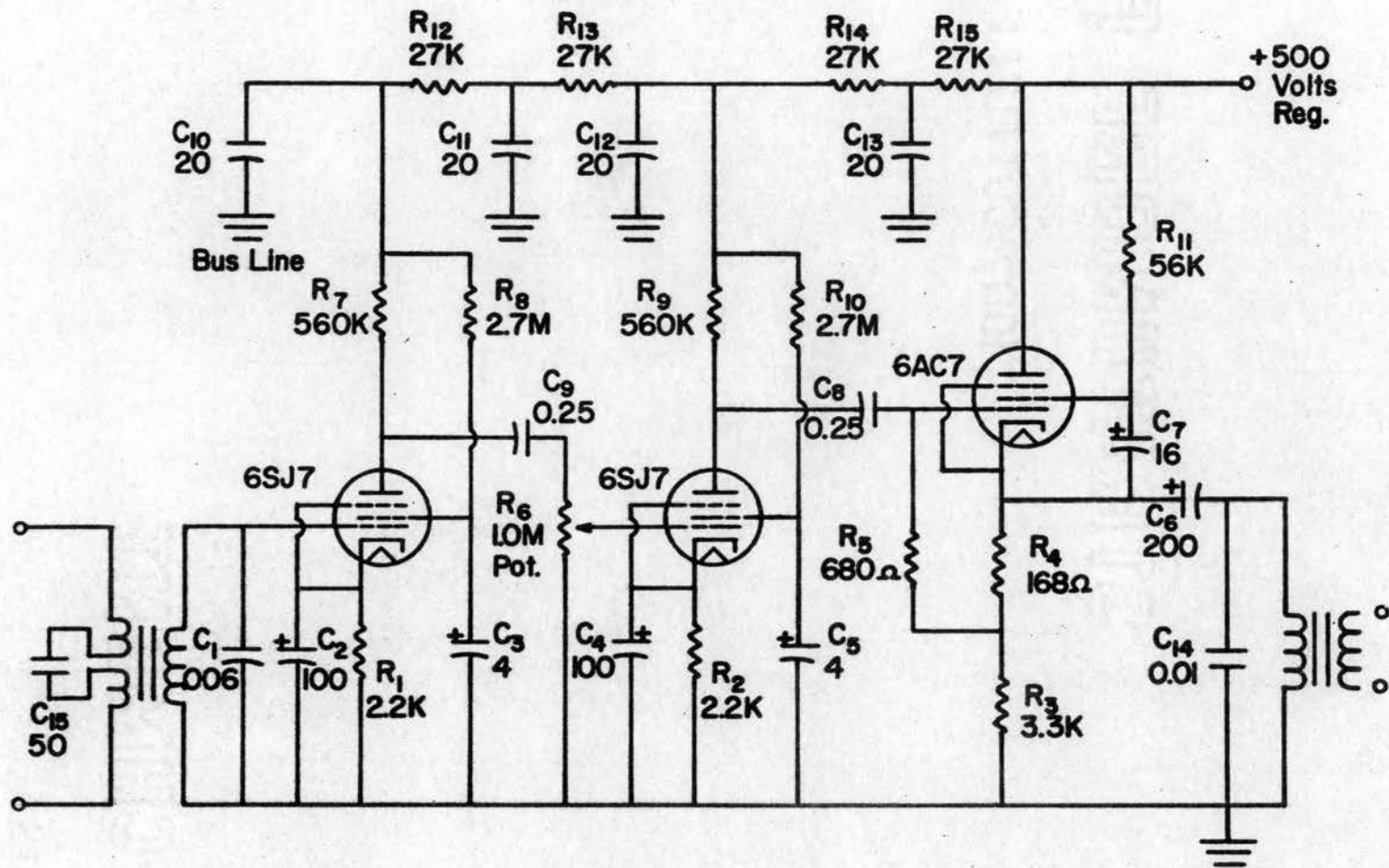


Figure 32. Amplifier Schematic for Automated System (All Capacitances in mfd).

Figure 33 shows a typical plot of input power and rate of change of temperature as a function of temperature. The effect of the heat of transition at the Curie temperature is evident from this graph. In order to calculate this heat of transition, the excess power applied to the sample, represented by the peak in the power curve near the Curie temperature, was plotted as a function of time. The area under this curve thus gives the total excess energy applied to the sample during the transition. Dividing this energy by the mass of the sample gives the transition energy in units of calories per gram, which can be converted to calories per mole by multiplying by the effective molecular weight of the solid solution.

Experimental Results

Table IV lists the characteristics of the samples which were obtained by the preliminary measurements. The sample mass listed is that of the two ceramic discs after sandblasting and cleaning. The tare heat capacity for each sample was calculated by multiplying the masses of the thermocouple wires, the heater connecting wires, the heater plate, and the epoxy binder by their respective specific heats. Although the specific heat of the epoxy was not known exactly, a value of 0.35 calories per gram per degree Centigrade was picked as being typical of this material. The exponential time constants and loss factors were determined from the curves shown in Figures 34 and 35. The heat capacity of each sample was determined as outlined above, and the specific heats calculated from the relationship:

$$\text{Specific heat} = \frac{\text{Sample heat capacity} - \text{Tare heat capacity}}{\text{Sample mass}} \times \text{Mol. wt.}$$

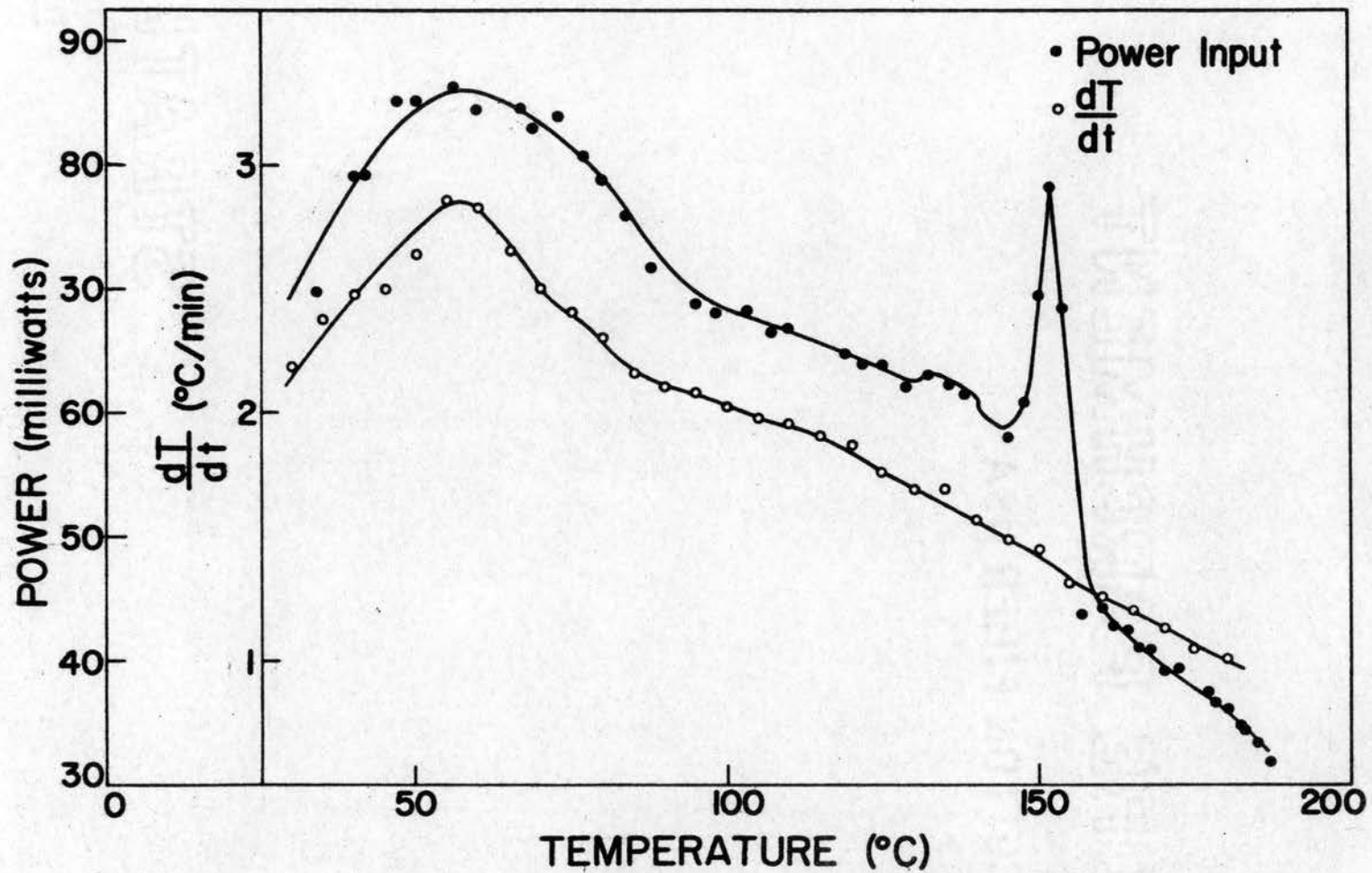


Figure 33. Input Power and Rate of Change of Temperature as Function of Temperature for PZST.

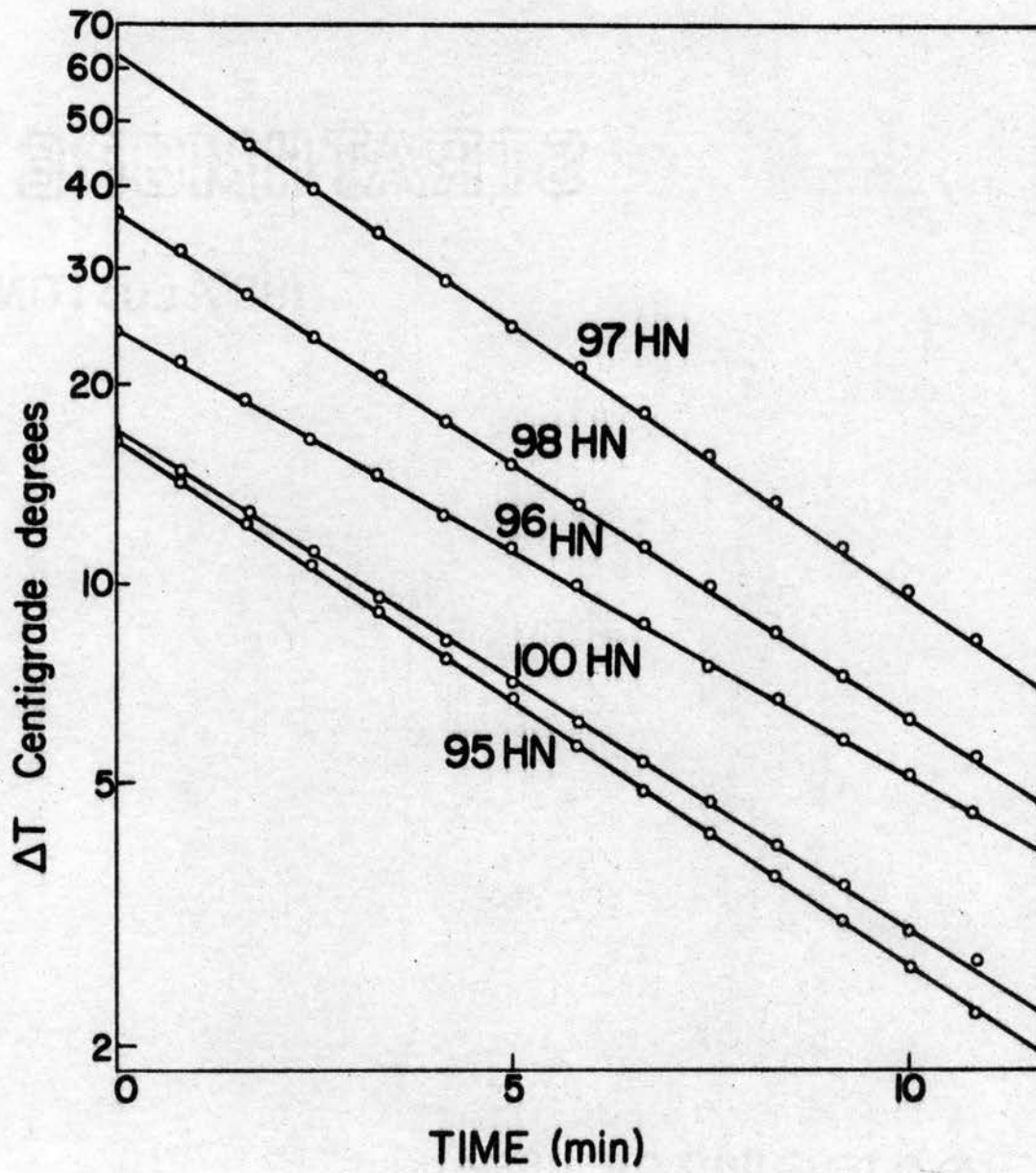


Figure 34. Exponential Cooling for Lead Hafnate Titanate Samples.

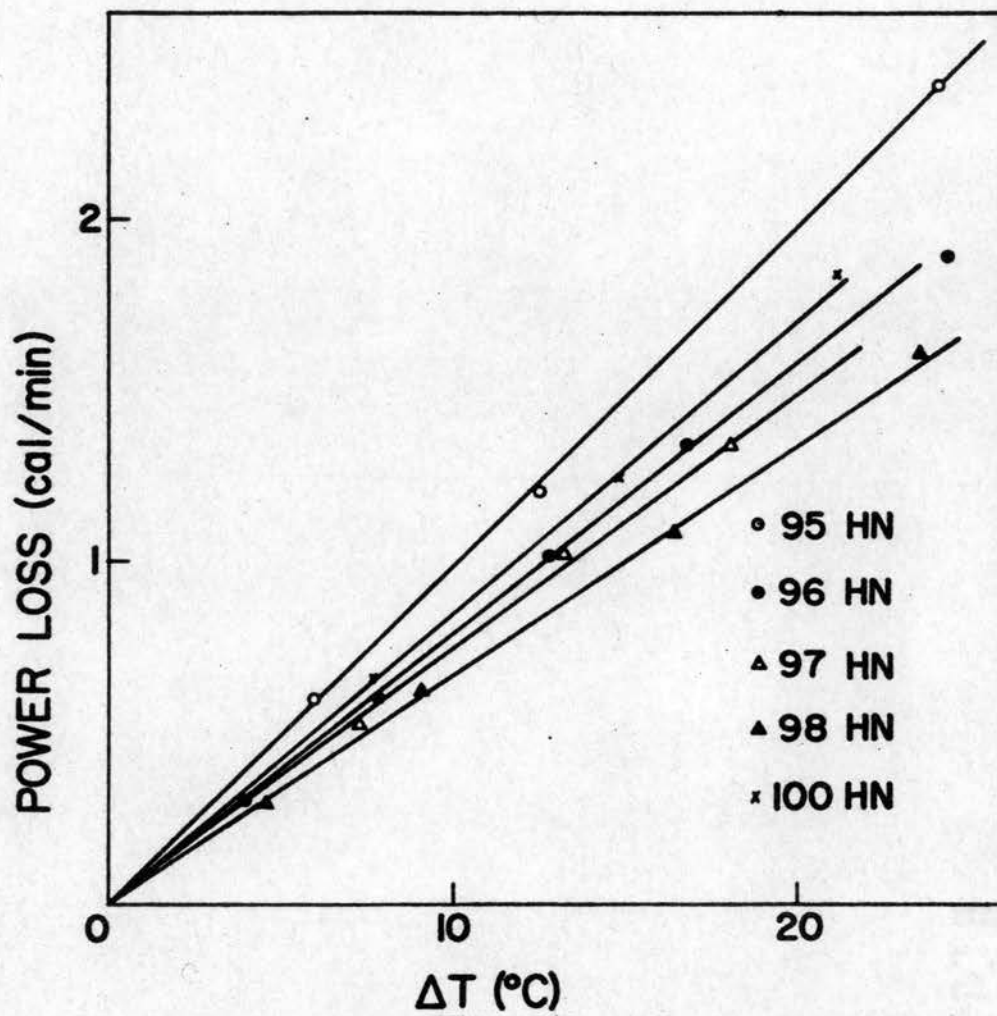


Figure 35. Measurement of Thermal Loss Factor for Lead Hafnate Titanate Samples.

TABLE IV
DATA FROM PRELIMINARY THERMAL MEASUREMENTS

Sample	Sample mass (gm)	Tare heat Capacity (cal/gm ^o C)	Exponential Time Constant (min)	Loss Factor (cal/min ^o C)	Heat Capacity (cal/ ^o C)	Specific Heat (cal/gm ^o C)(cal/mol ^o C)	
95HN	6.91	0.027	5.50	0.100	0.550	0.076	32.1
96HN	7.72	0.020	6.48	0.075	0.490	0.061	25.8
97HN	6.23	0.028	5.30	0.079	0.420	0.063	26.7
98HN	7.04	0.028	5.61	0.067	0.375	0.049	20.8
100HN	7.28	0.028	5.78	0.085	0.495	0.064	27.3

Figures 36, 37, 38, 39, 40, and 41 show the variation of specific heat with temperature for the materials used in this study as determined from the adiabatic measurements. Each figure shows the characteristic spike expected of a first order transition at the Curie temperature. The variations below this temperature are much more diffuse and thus less susceptible to interpretation. The 96/4 lead hafnate titanate does not show a spike in specific heat at the FE-AFE transition, but rather exhibits a general rise in the specific heat, as if the transition is blending with the Curie transition. The PZST sample shows a very small diffuse peak in the power input curve near the FE-AFE transition temperature. The other materials show certain broad peaks and rises, but nothing which can be quantitatively studied.

Figure 42 shows a typical power vs. time plot used to calculate the transition energy in this type of measurement. Table V lists the pertinent data for these calculations and the heats of transition obtained from them. An estimate was also made of the energy involved

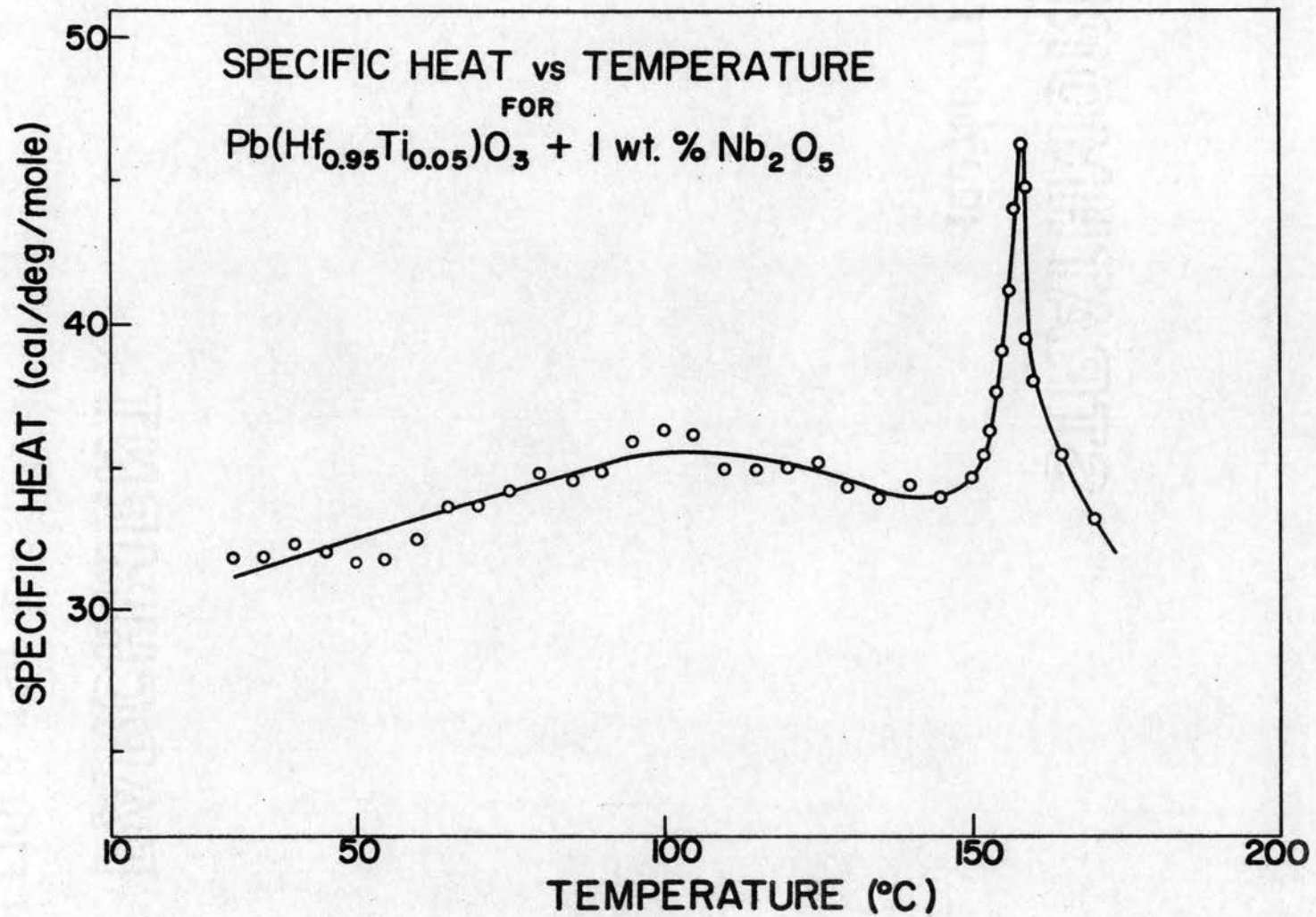


Figure 36. Specific Heat vs. Temperature for $\text{Pb}(\text{Hf}_{0.95}\text{Ti}_{0.05})\text{O}_3 + 1 \text{ wt. \% Nb}_2\text{O}_5$.

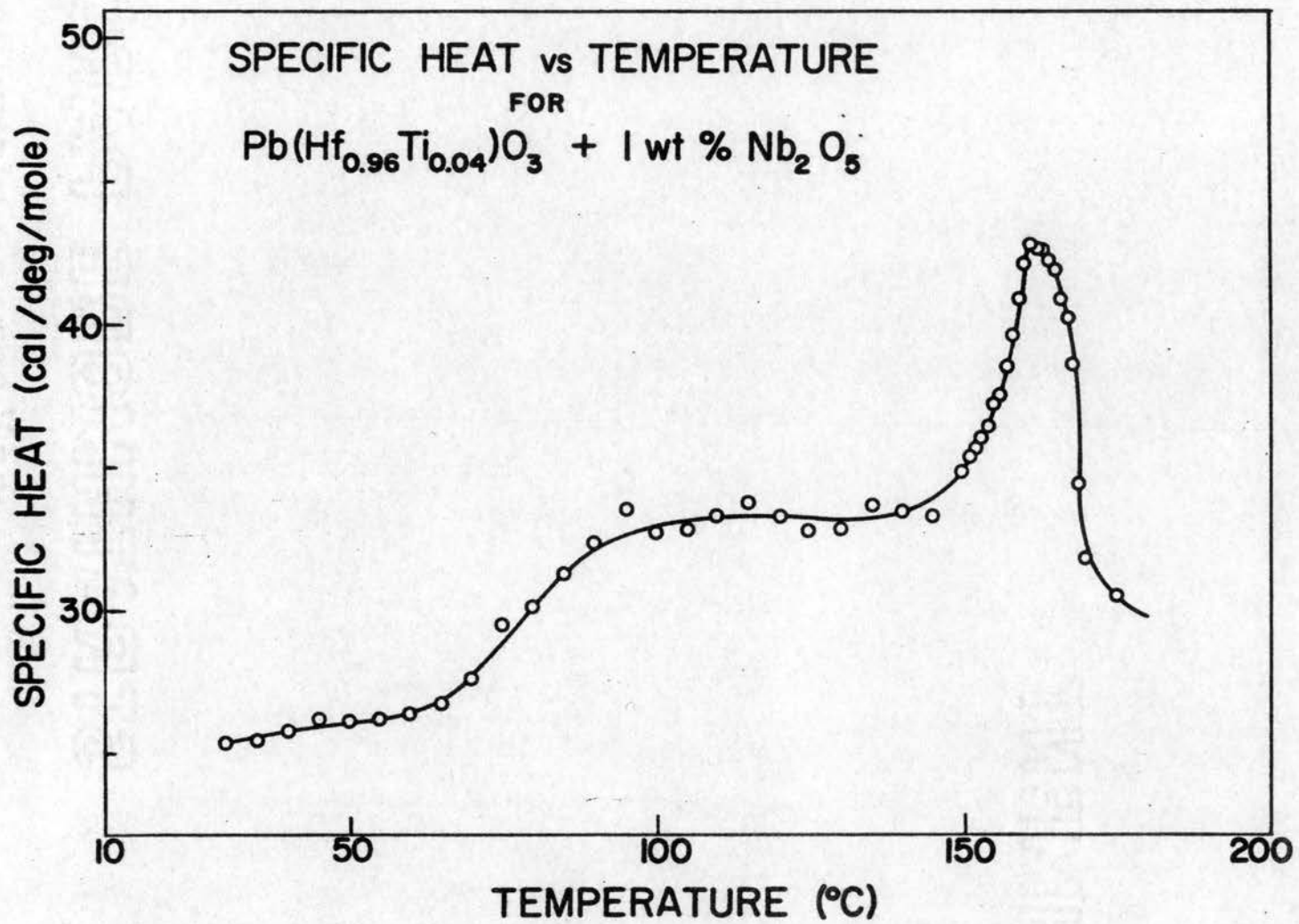


Figure 37. Specific Heat vs. Temperature for $\text{Pb}(\text{Hf}_{0.96}\text{Ti}_{0.04})\text{O}_3 + 1 \text{ wt. } \% \text{Nb}_2\text{O}_5$.

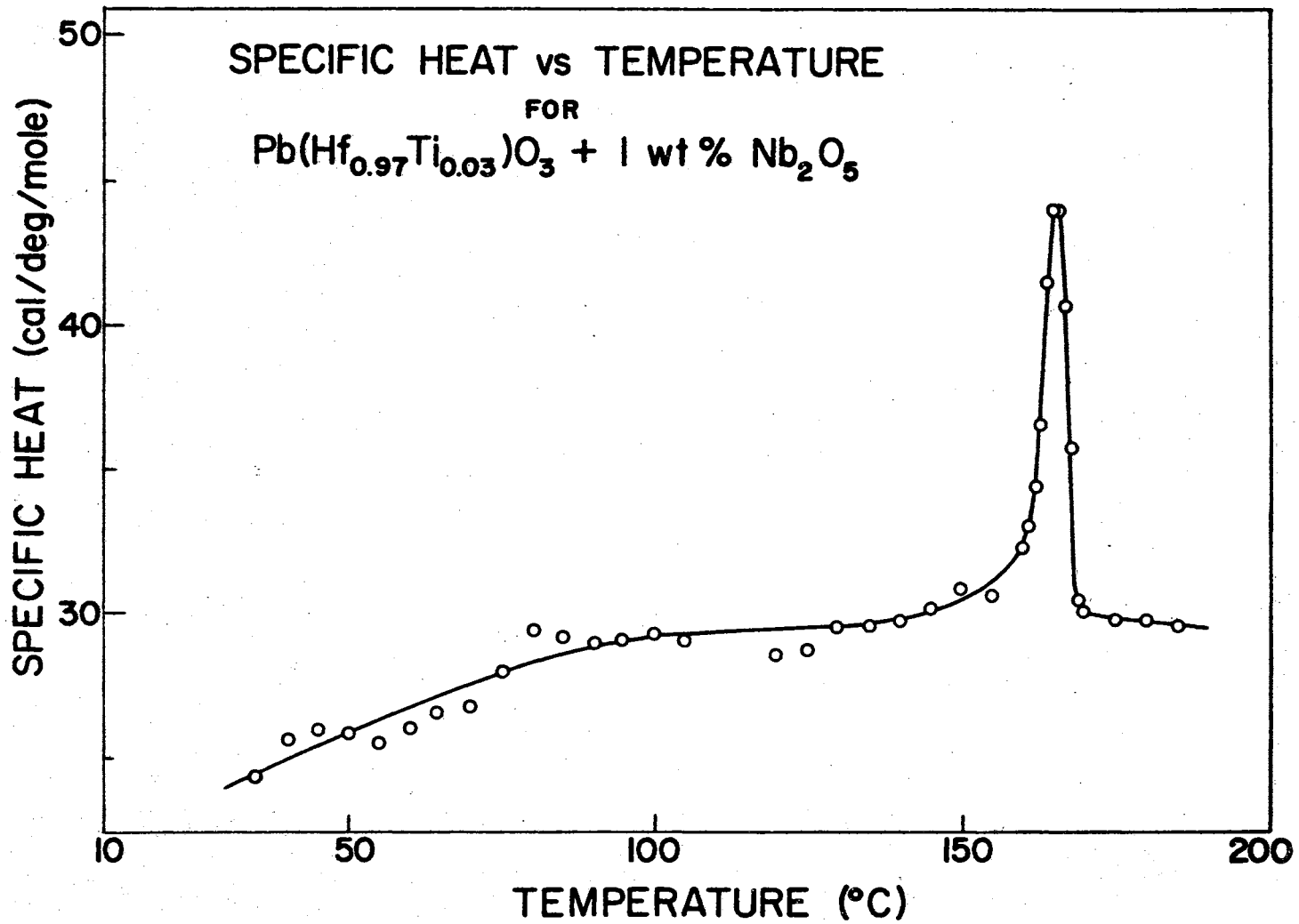


Figure 38. Specific Heat vs. Temperature for $\text{Pb}(\text{Hf}_{0.97}\text{Ti}_{0.03})\text{O}_3 + 1 \text{ wt. } \% \text{Nb}_2\text{O}_5$.

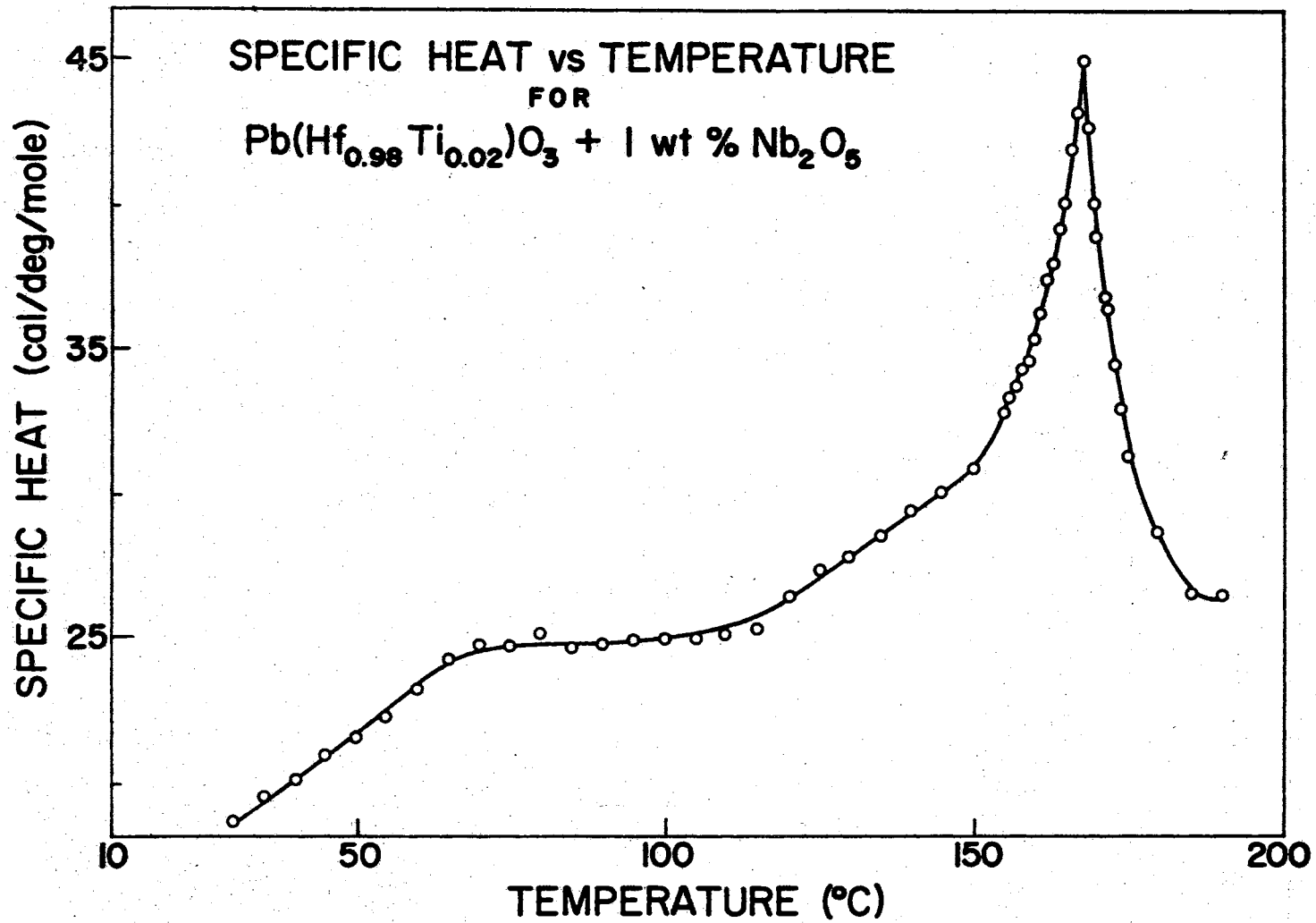


Figure 39. Specific Heat vs. Temperature for $\text{Pb}(\text{Hf}_{0.98}\text{Ti}_{0.02})\text{O}_3 + 1 \text{ wt. } \% \text{Nb}_2\text{O}_5$.

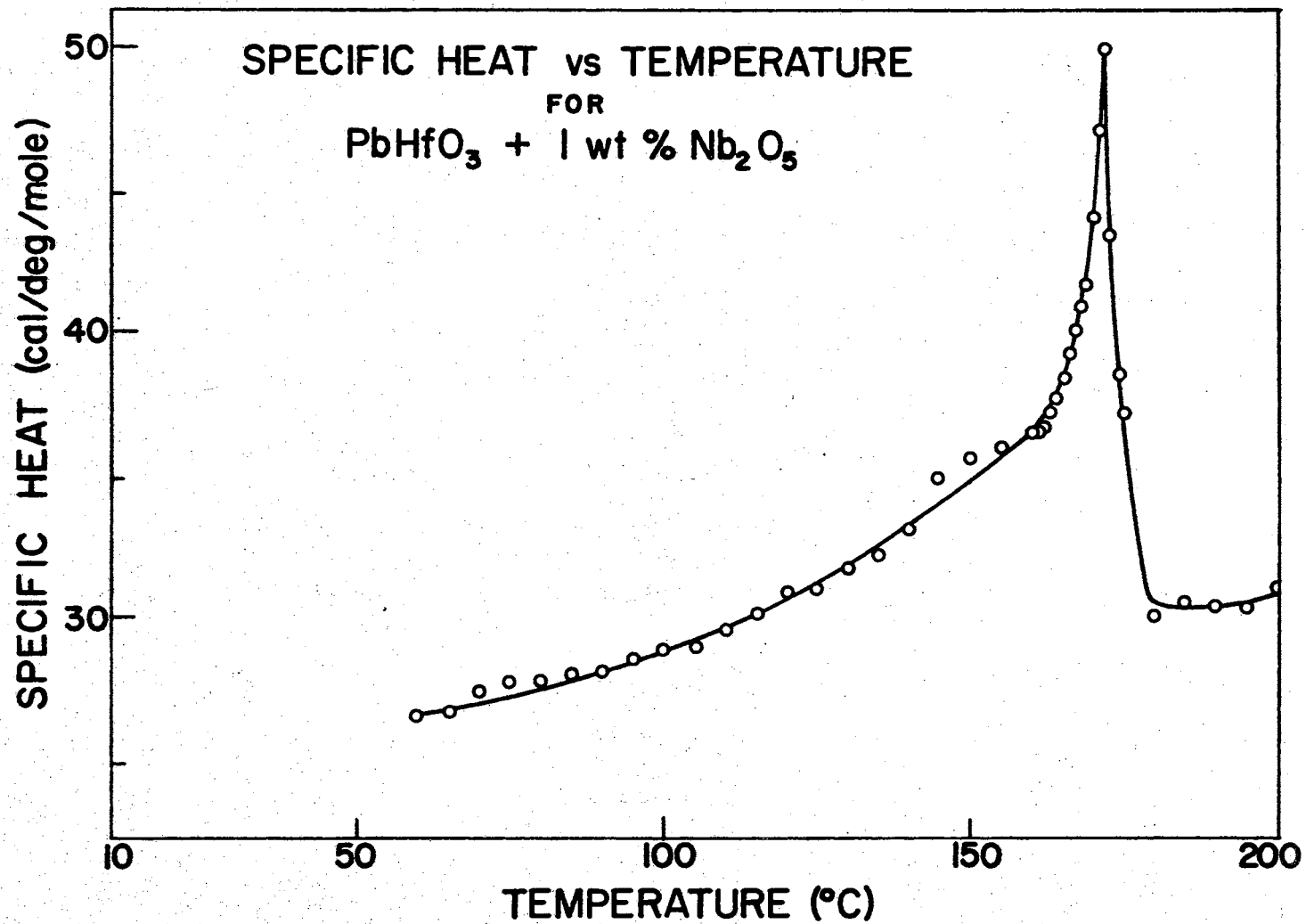


Figure 40. Specific Heat vs. Temperature for $\text{PbHfO}_3 + 1 \text{ wt. } \% \text{ Nb}_2\text{O}_5$.

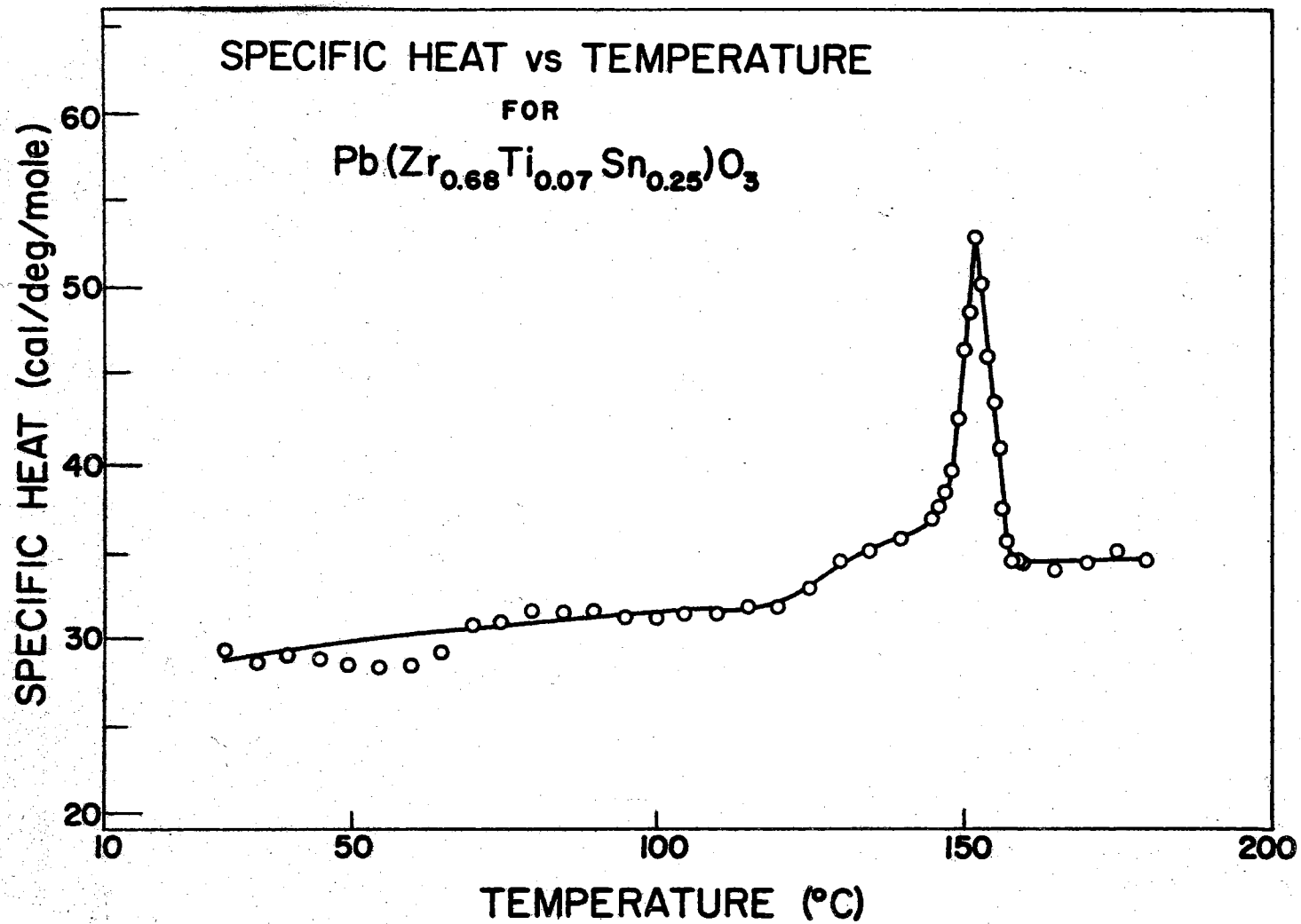


Figure 41. Specific Heat vs. Temperature for PZST.

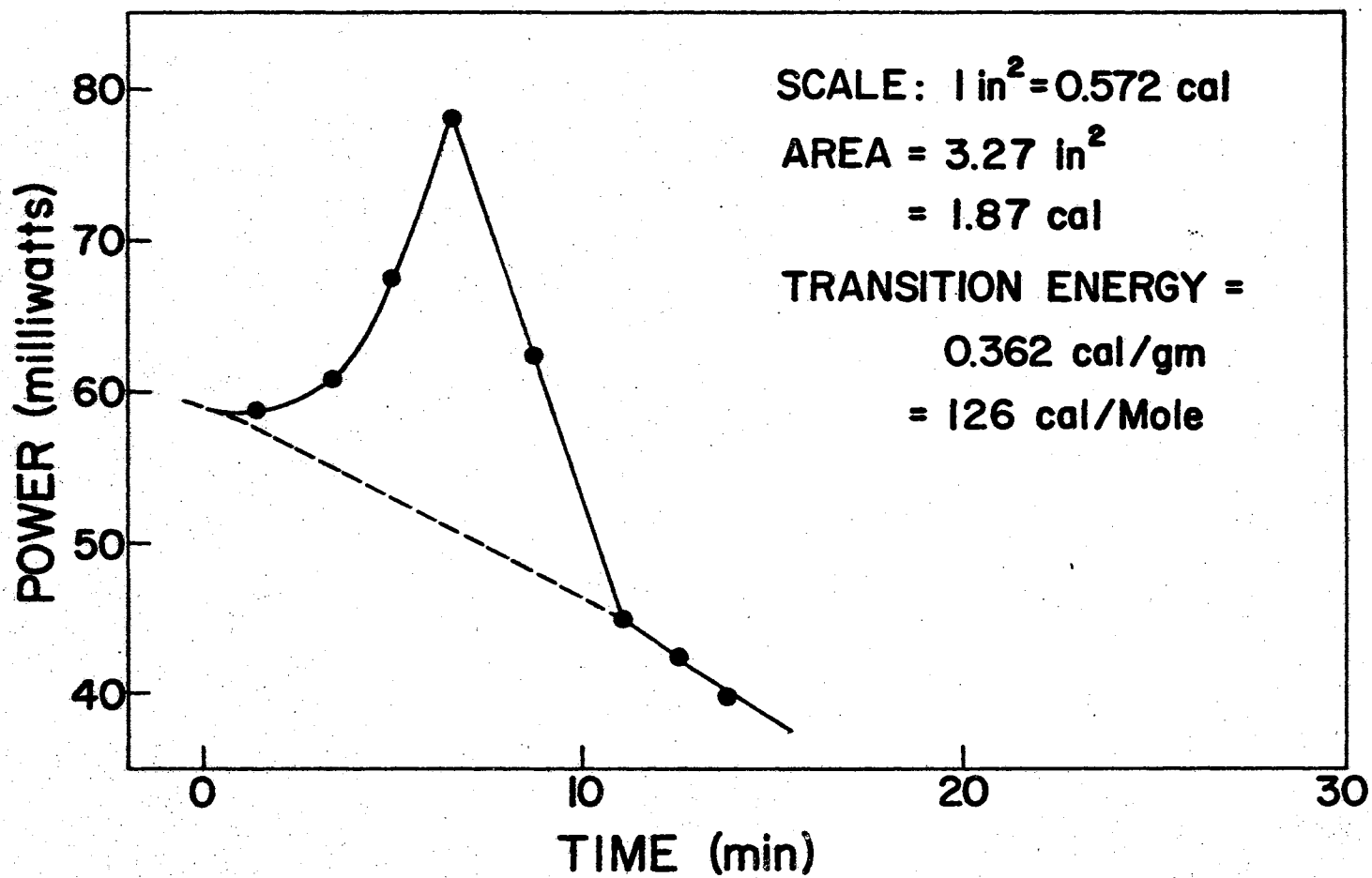


Figure 42. Excess Power vs. Time Plot Used to Calculate Curie Transition Energy for PZST.

in the FE-AFE peak in the PZST sample. Because of the blending of this transition with the Curie transition, this estimate is of limited accuracy but does indicate a very small heat of transition at the FE-AFE transition temperature.

The heats of transition calculated for these materials are smaller than those reported for lead zirconate and its solid solutions. This fact will be discussed later together with a comparison of the techniques used in obtaining them. The heat of transition of the 96/4 material probably appears higher than that of the other members of this family of compositions because of the blending of the FE-AFE transition with the Curie transition.

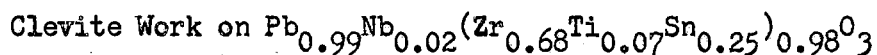
TABLE V
HEAT OF TRANSITION DATA

Sample	Sample Mass (gm)	Transition Temperature	Excess Heat (cal)	Heat of Transition (cal/gm)(cal/mol)		ΔS (cal/mol °C)
95HN	6.91	160	1.53	0.222	94	0.22
96HN	7.72	163	2.40	0.311	133	0.31
97HN	6.23	167	1.49	0.240	102	0.23
98HN	7.04	170	1.60	0.228	97	0.22
100HN	7.28	172	1.58	0.218	93	0.21
PZST (Curie)	5.17	152	1.87	0.362	126	0.30
PZST(FE-AFE)	5.17	130	0.079	0.015	5.3	0.013

CHAPTER VII

RESULTS OF RELATED WORK

This chapter presents certain results obtained during recent studies by other groups which either extend the present study or which can be useful in the interpretation of the present results. Some of the results of the study by Sawaguchi (24) on lead zirconate titanate are also presented and will be used for comparison with the conclusions obtained for lead zirconate titanate stannate and lead hafnate titanate in the next chapter.



A great deal of work on the lead zirconate titanate stannate compositions has been done during the last few years by the Electronic Research Division of Clevite Corporation of Cleveland, Ohio. The work of interest to this study has been selected from three reports by Berlincourt (2, 3, 4) of the Clevite group.

The work at Clevite has included a study of the characteristics of the FE-AFE transitions in the lead zirconate titanate stannate composition used in the present study and has obtained interesting results concerning the pressure vs. volume relationships in this composition. X-ray studies have shown the AFE phase to be the phase of minimum volume with a change of about 0.36% occurring during transitions between the FE and AFE phases. The change in volume produced in a sample of this

material by the application of hydrostatic pressure was also determined. Again the volume difference between the phases was found to be about 0.35% with the transition occurring at a pressure of 38,000 psi.

Figure 43 compares the polarization changes produced in this composition by variation of temperature and pressure. It can be seen that while the general shapes of the curves are the same, almost twice as much depoling takes place before the abrupt transition when the temperature is varied as occurs before a pressure induced transition.

Figure 44 indicates the variation of transition pressure of poled ferroelectric samples as a function of a biasing electric field. Because of the oriented condition of the specimen, the transition pressure for the FE-AFE transition decreases with negative bias until the bias field reaches the coercive field and switching takes place. For the AFE-FE transition there is no original orientation of the polarization and the phase boundary is symmetrical.

A great deal of work has been done by this group in the analysis of the double hysteresis loops characteristic of field induced AFE-FE transitions. Loops taken for PZST about 8 C° above the FE-AFE transition are quite broad, giving E_f equal to about 8 Kv/cm and E_a about 4 Kv/cm.

Figure 45 is a temperature vs. field phase diagram obtained by field variation at constant temperature. This is in contrast to the technique used in the present study and described in Chapter IV, which involved the variation of temperature at constant field. It is interesting to note that the shape of the curve representing the AFE-FE transition with increasing field is similar to that which was shown earlier for the FE-AFE transition with increasing temperature.

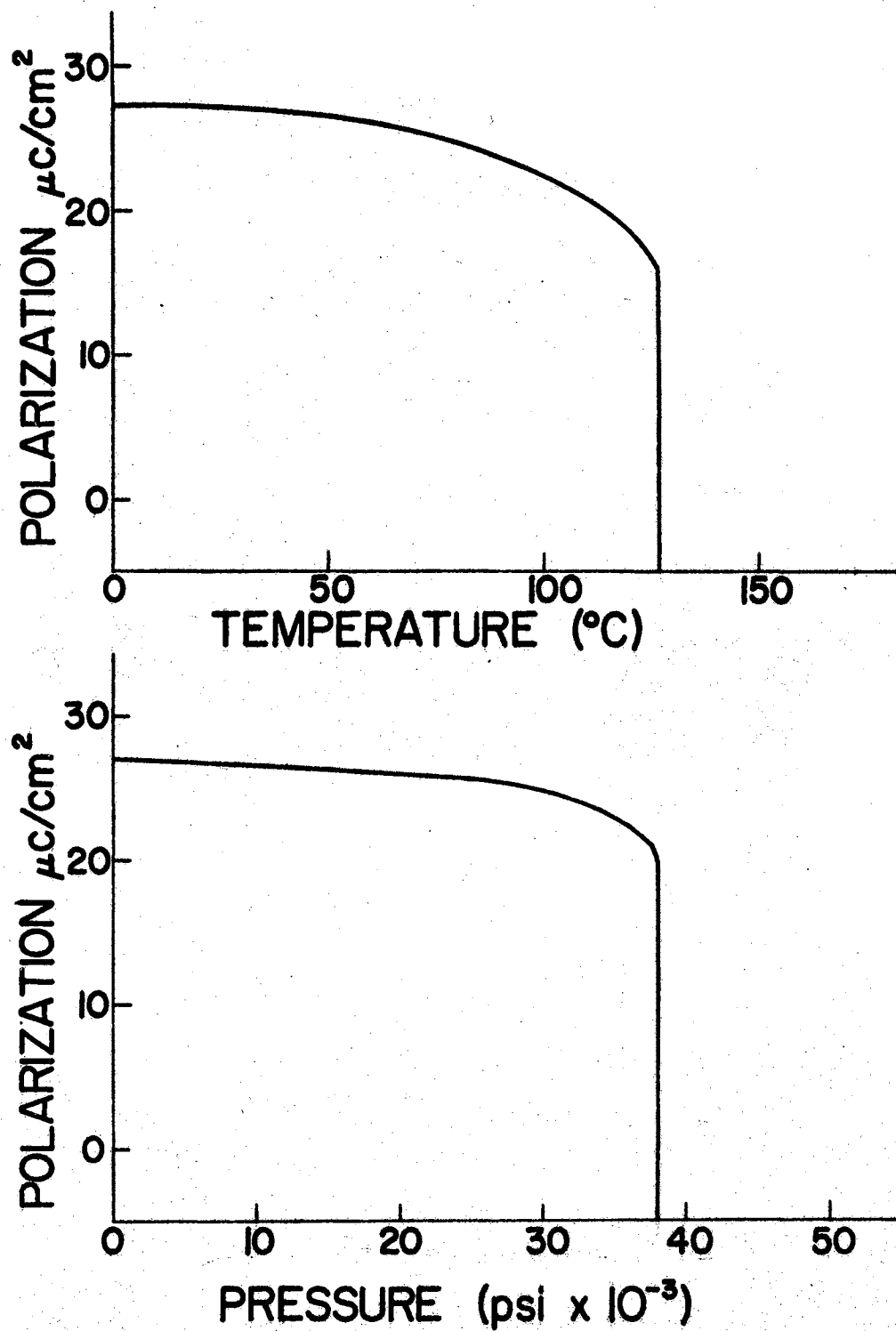


Figure 43. Polarization vs. Temperature and Pressure for PZST. (After Berlincourt (3)).

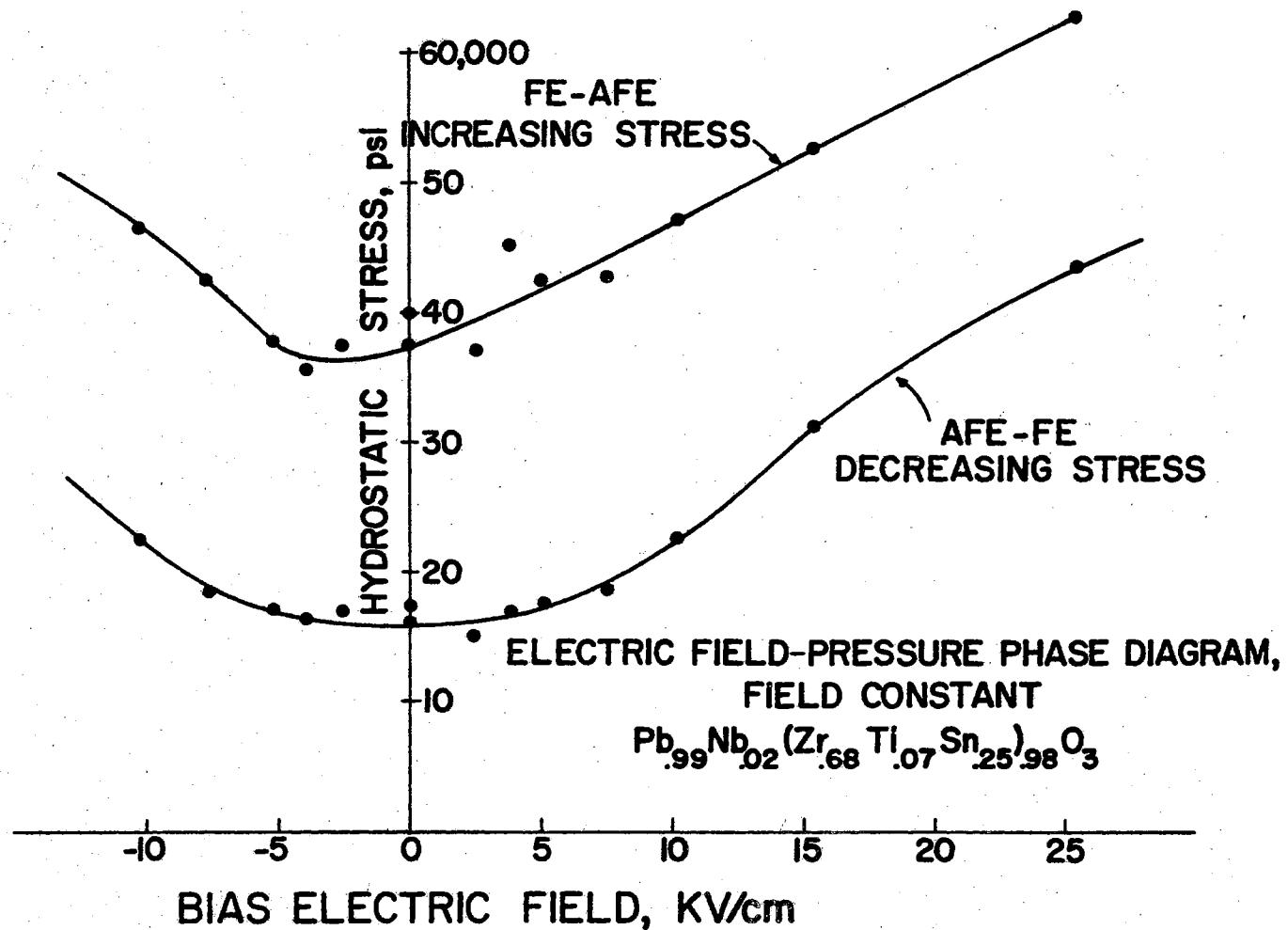


Figure 44. Electric Field-Pressure Phase Diagram for PZST (After Berlincourt (4)).

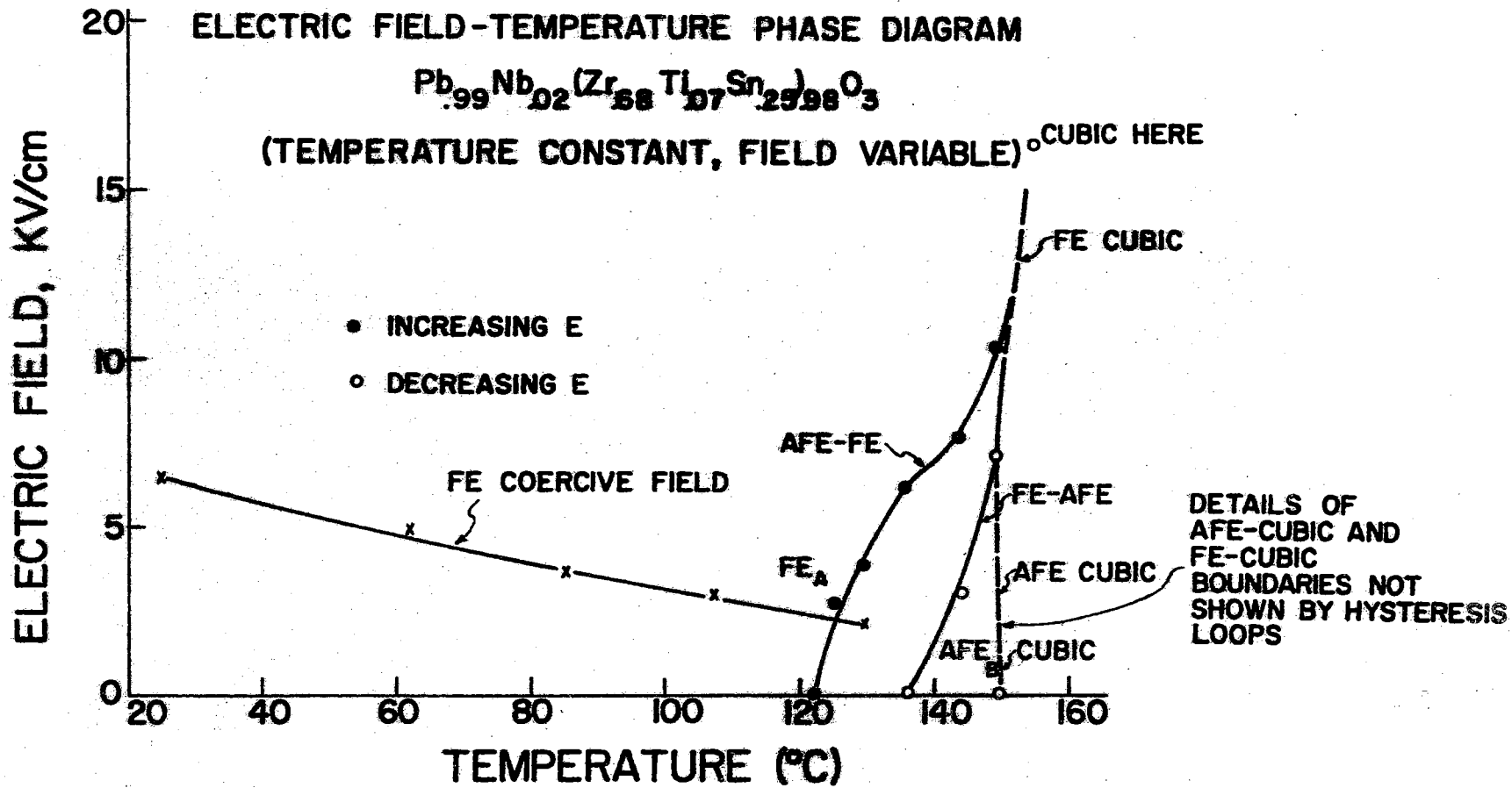


Figure 45. Electric Field-Temperature Phase Diagram for PZST. (After Berlincourt (5)).

Clevite Lead Zirconate Titanate Stannate Compositional Studies

In addition to the work on $\text{Pb}_{0.99}\text{Nb}_{0.02}(\text{Zr}_{0.68}\text{Ti}_{0.07}\text{Sn}_{0.25})_{0.98}\text{O}_3$, the group at Clevite has devoted a great deal of work to compositional studies in the lead zirconate titanate stannate family. One such study was devoted to the compositions containing 25 mole per cent stannate ion but with a variation of the zirconate to titanate ratio. In addition to the 68/7 composition, the 70/5 composition was found to show both AFE and FE phases. In the 70/5 composition the AFE phase exists over a much wider temperature range than in the 68/7 composition. With zero bias the FE-AFE transition occurs at about 65°C and the Curie transition at 160°C . With increasing bias the region of stability of the AFE phase decreases and this phase is not present at biases greater than 20 Kv/cm. The 70/5 composition showed good characteristics in the FE-AFE transition but was extremely sluggish in the reverse reaction.

The FE-AFE boundary curves in the temperature vs. composition diagrams were found to be approximately parallel for 15, 25, and 30 mole per cent stannate ion. This indicates that the reversal of slope discussed earlier, which occurs as a result of the addition of tin to lead zirconate titanate compositions, is completed with less than 15 mole per cent tin. It was found that for a given molar fraction of titanium ion, the addition of tin tends to favor the AFE phase.

A study of the minor additions used to increase resistivity revealed that La^{3+} , which goes substitutionally into the A position, tends to favor the antiferroelectric state, while Nb^{5+} , which enters the B position, favors the ferroelectric state. Both additions tend to depress the Curie temperature.

Sandia Studies on Lead Hafnate Titanate Compositions

Studies at Sandia by Hall, Dungan, et al (10, 12) have continued to reveal new characteristics of the lead hafnate titanate compositions.

Measurements of the variation of E_f and E_a as functions of temperature for the 97/3 and 98/2 compositions revealed that at most temperatures the double hysteresis loops were quite broad and that reliable estimates of the free energy difference between the phases can only be obtained near the transition temperature. However, it should be noted that at temperatures more than 50 degrees below the zero bias transition temperature, the phase change could be produced by fields less than 20 Kv/cm.

Samples having the same compositions as those used in the present study were prepared using a higher purity HfO_2 than had previously been employed (13). The electrical properties of the samples were quite similar to those previously tested, but the compositional boundary between the FE and the AFE phases covered a much smaller range. Using the purer material, the 96/4 composition was ferroelectric between room temperature and the Curie temperature while the 98/2 composition was antiferroelectric over the same region. An AFE-AFE transition was also observed which had not been reported previously.

Lead hafnate titanate samples without the niobium addition were also prepared. This modification increased the Curie temperature to the 200° C region and moved the AFE-FE phase boundary to the 95/5 composition.

Dungan and Stark (10) have investigated the lead hafnate titanate stannate compositional family and find it to be strikingly similar to the lead zirconate titanate stannate family.

Hall, in his Ph. D. dissertation (14), investigated compositions in the lead zirconate hafnate titanate series. In his study of the temperature vs. composition relations for materials having equal molar parts of zirconium and hafnium, he found that the FE-AFE phase boundary had been displaced so as to enlarge the antiferroelectric stability region, but that the boundary slope was still in the same direction as in the lead zirconate titanate compositions. In an extension of this work, he has found that this slope does not appear to reverse until the compositions contain about 80 mole per cent hafnium. Thus the influence of the zirconium ion on the relative stability of the various phases seems to be stronger than that of the hafnium ion.

Sawaguchi (24), in his study of the high zirconium regions of the lead zirconate titanate series, was able to construct a relative free energy diagram for this system. From calorimetric data, he found that the entropy difference between the two AFE phases ($0.22 \text{ cal/mol } ^\circ\text{C}$) was much larger than the difference between the high temperature AFE phase and the FE phase ($0.073 \text{ cal/mol } ^\circ\text{C}$). These in turn were both smaller than the entropy difference observed at the Curie transition ($0.51 \text{ cal/mol } ^\circ\text{C}$).

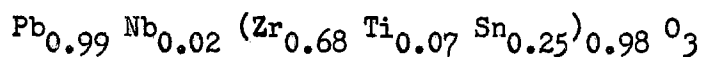
From the double hysteresis loops exhibited near the transition temperature, Sawaguchi was able to calculate the difference in free energy between the FE and AFE phases in PbZrO_3 . The calculations show a free energy difference of about 3 cal/mole at 215°C which decreases to 1 cal/mole near 230°C . From this he concluded that the FE and AFE phases would have equal free energies at about 240°C . Unfortunately, the paraelectric phase becomes dominant below this temperature so that an AFE-FE transition is not actually observed.

From the work with $\text{Pb}(\text{Zr}_{0.97}\text{Ti}_{0.03})\text{O}_3$ and $\text{Pb}(\text{Zr}_{0.98}\text{Ti}_{0.02})\text{O}_3$, Sawaguchi also determined that additions of lead titanate to lead zirconate decreases the free energy of the FE phase relative to the cubic phase at a rate of 0.5 cal/mol-at% and increases the free energy of the two AFE phases at rates of 5.8 cal/mol-at% and 2.3 cal/mol-at% relative to the cubic phase.

CHAPTER VIII

CONCLUSIONS

Free Energy Relationships in



The most complete set of data available for any of the compositions used in this study is that on the PZST samples. For this material one now has thermal, electrical, and pressure relationships which involve all three phases. This composition also gave the sharpest transitions and thus the most reliable phase diagrams of all the materials studied. For all of these reasons, the free energy relationships for this composition will be discussed first and the ideas thus obtained then applied to the discussion of the other compositions.

As was shown in Chapter III, the calculation of free energy involves a knowledge of the extensive variables -- volume, polarization and entropy. From the Berlincourt data the molar volume of this composition is found to be about 42 cm^3 and the volume in the AFE phase is approximately 0.35% less than that of the FE phase. The variation of polarization with temperature and pressure was indicated in Figure 43, while the polarization dependence on electric field can be obtained from the plots of dielectric susceptibility vs. field and a knowledge of the spontaneous polarization by using the relation,

$$P(E) = P_s + \int_0^E \epsilon_0 \chi(E) dE$$

The calculation of the absolute entropy, however, is a much greater problem. This requires a knowledge of the specific heat at all temperatures above absolute zero. The variation in the vicinity of absolute zero is quite important and is thus far not available. For this reason the absolute entropy of this system cannot presently be calculated and relative entropies must be used to determine the free energy diagrams. The entropy differences between the phases at the transitions are given in Table V.

A correlation of the results of the various measurements is useful as a check on the experimental values obtained. The electrical and thermal data can be compared by using the relationship:

$$\left(\frac{\partial T}{\partial E}\right)_p = - \frac{V\Delta P}{\Delta S}$$

Using the values $V = 42 \text{ cm}^3/\text{mole}$

$$\Delta P = - 16 \times 10^{-6} \text{ coul/cm}^2$$

$$\Delta S = 0.013 \text{ cal/mole } ^\circ\text{C}$$

a value of $(\partial T/\partial E)_p = 12.3 \text{ } ^\circ\text{C/cm/Kv}$ is obtained. This compares with a value of about $9 \text{ } ^\circ\text{C/cm/Kv}$ which is obtained from the central slope of the FE-AFE phase boundary in Figure 10. The discrepancy seems to indicate that the value of entropy measured was slightly low. This is quite possible since, as was pointed out earlier, the peak used in the calculation of that value was quite small and diffuse. It would seem a value of about $0.02 \text{ cal/mole } ^\circ\text{C}$ might be more accurate for this transition.

The above relation also applies to the ferroelectric Curie transition at high fields. Here the polarization used consists of the spontaneous polarization plus that induced by the field. Using a value of ΔP equal to about $22 \times 10^{-6} \text{ coul/cm}^2$ and a value of $\Delta S = 0.30 \text{ cal/mole } ^\circ\text{C}$ (the entropy difference between the phases at zero field), a value of

0.74 C°cm/Kv is calculated. This compares with a value of 0.80 C°cm/Kv measured just above the triple point in the PZST phase diagram. In view of the assumptions made, this would seem to be very good agreement.

A comparison of the transition temperature vs. field phase diagrams obtained by varying the temperature in one case and the field in another leads to some interesting conclusions concerning the hysteresis in these transitions. Figure 46 compares the FE-AFE transition with increasing temperature to the AFE-FE transition with increasing field. Since these transitions are in opposite directions, the true phase equilibrium conditions must lie somewhere between them. But a comparison of this figure with Figures 10 and 45 indicates that the true equilibrium line lies much closer to the transition observed with increasing intensive parameter than to that observed with decreasing intensive parameter. Thus the shapes of the curves in Figure 46 are more representative of the shape of the phase equilibrium line than are those for the reverse transitions. The rapid decrease of the slope of the FE-AFE transition as this transition approaches the Curie point would seem to indicate that these two transitions tend to blend causing the change of entropy at the FE-AFE transition to increase rapidly.

The results obtained with hydrostatic pressure can be compared with the electrical results by the relation:

$$\left(\frac{\partial p}{\partial E}\right)_T = \frac{V\Delta P}{\Delta V}$$

Using the values $\Delta P = 22 \times 10^{-6}$ coul/cm²

$$\Delta V/V = 0.35\%$$

a value of 62.8 coul/m² is found for $(\partial p/\partial E)_T$. This compares with a value of 65.4 coul/m² observed in Figure 44.

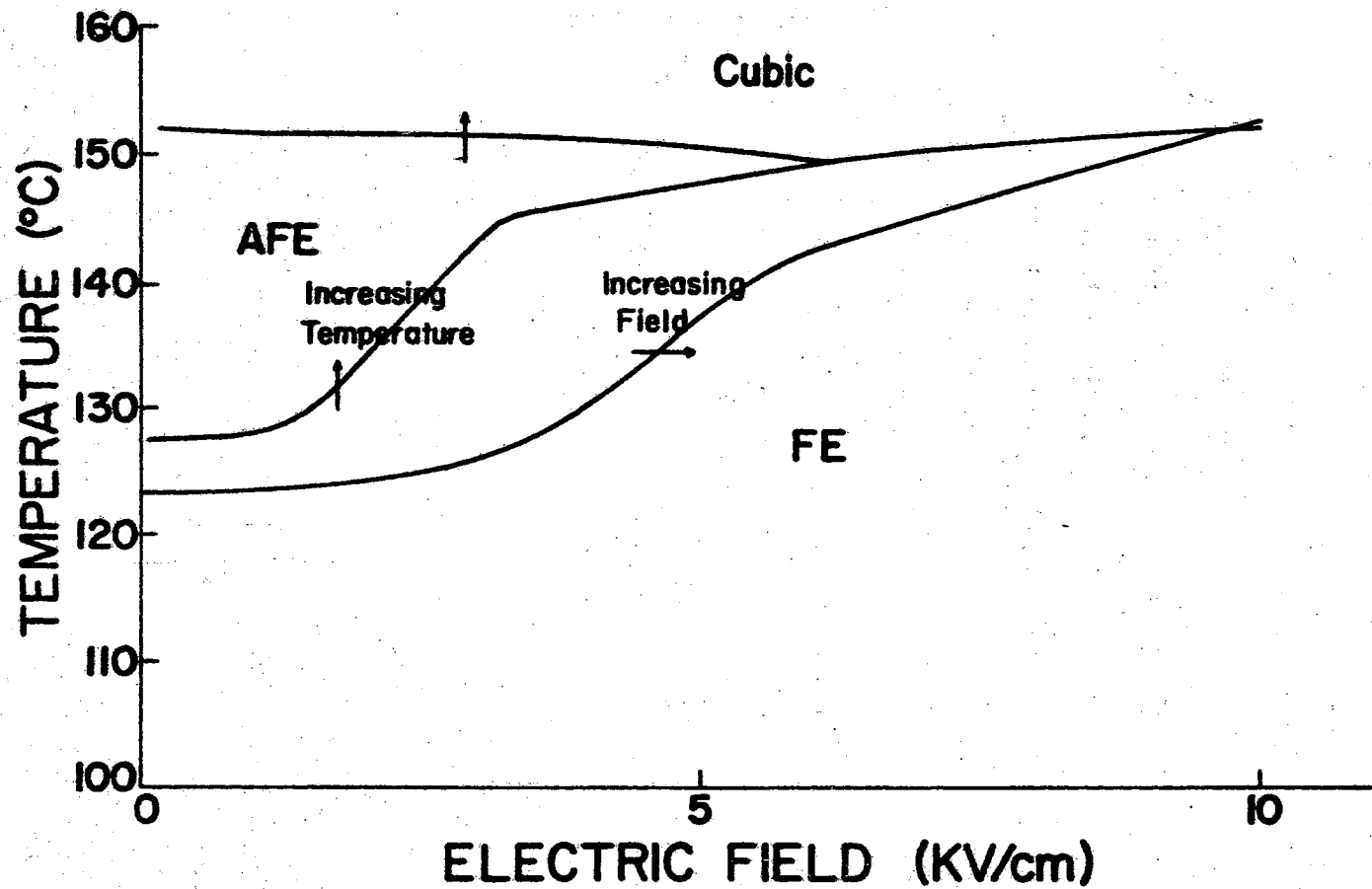


Figure 46. Comparison of Transitions Observed with Increasing Temperature and Increasing Field for PZST.

From the pressure induced transition data it is possible to estimate the free energy difference between the FE and the AFE phases at room temperature. Sawaguchi (24) has shown that the free energy difference between two phases observed during a forced ferroelectric transition is essentially the product of the intensive variable necessary to force the transition and the corresponding change of extensive parameter. Authors following him seem to have followed this method of calculation (e. g., the difference in free energy between the phases in the double hysteresis loop is represented by an area equivalent to the average field at the transition multiplied by the change in polarization). An assumption that the difference in entropy and internal energy between the two phases are approximately constant over the temperature range considered, on the other hand, leads to a correction of the above value by a factor of $\Delta S(T - T_0)$, where ΔS is the observed entropy difference, T is the temperature of the forced transition, and T_0 is the temperature of the transition with the intensive parameter equal to zero. Over the temperature ranges used in this study, however, this correction amounts to less than 20% of the principal term, so that the Sawaguchi assumption will be used in subsequent calculations. The values given for free energy differences between the phases should therefore be understood to give at least a reasonable approximation to the true free energy difference.

Using the above approximation, Berlincourt's pressure induced transition data gives:

$$\begin{aligned}\Delta G \text{ (molar)} &= p\Delta V \\ &= 38 \times 10^3 \text{ psi} \times 15 \times 10^{-8} \text{ cm}^3 \\ &= 9.4 \text{ cal/mole}\end{aligned}$$

While this is only an estimate, it is comparable to the values of difference of free energy between the ferroelectric and antiferroelectric

phases observed by Sawaguchi in lead zirconate titanate solid solutions. Because of the possible presence of hysteresis, this value should be taken to represent an upper limit to the free energy difference between the phases.

An estimate of the free energy difference at 135° C may be obtained from the field induced hysteresis loops of Berlincourt. Since these loops are broad, this estimate is of limited accuracy but a maximum and minimum value can be established from E_f and E_a for the transition. Again using the previous assumptions, the maximum value of the change of molar free energy (given by $\Delta P E_f V_m$) is 0.96 cal/mole, while the minimum value for this quantity (given by $\Delta P E_a V_m$) is 0.48 cal/mole.

In order to establish free energy differences involving the paraelectric phase, the entropy difference at the transition must be used, since this is the only information at hand regarding this phase. The entropy difference of 0.30 cal/mol °C indicates that the free energy of the cubic phase falls quite rapidly below that of the AFE phase above the Curie temperature. Extrapolations of this difference to temperatures far from the Curie point depends on a knowledge of the curvature of the free energy lines as a function of temperature. The curvature of these lines is given by the relation:

$$\left(\frac{d^2G}{dT^2}\right)_{E,p} = -\left(\frac{\partial S}{\partial T}\right)_{E,p} = -\frac{C_p}{T}$$

Thus from the measurement of specific heat, the curvature of the free energy lines can be found, and the relative free energy curves calculated. Figure 47 shows a plot of C_p/T calculated from the curve of Figure 41. The points in the vicinity of the Curie transition have been left out

since the change of entropy in this region has been calculated as the entropy change at the transition. This plot indicates that the curvature of the free energy lines is almost constant over the entire range, decreasing only about 15% between 30° C and 170° C. There is no noticeable abrupt change of curvature for the material in the cubic phase.

Figure 48 is a construction of a relative free energy diagram using the above curvatures and the free energy differences given earlier. In this diagram the free energies of the different phases have been matched at most probable transition points between the various phases, the slopes have been adjusted to give differences of free energy comparable to those found for the forced transitions, and curvatures have been matched to those found in Figure 47. The entropy difference relative to the entropy of the FE phase at 100° C has been used for the temperature-entropy product term. Therefore in order to show the true variations of free energy which occur in the various phases with temperature a further slope equivalent to the absolute entropy of the FE phase at 100° C must be superimposed on each of the curves. Even without this slope the free energy change for each phase is about 150 cal/mole over the 50 C° range while the greatest measured difference in free energy between two phases in the same range is less than 10 cal/mole. From this it can be seen that the variation of free energy with temperature completely dominates all other variations in all three phases and that the differences in free energies between the phases are quite minor compared to this variation.

In order to show more clearly the free energy relationships explaining the experimental findings, plots of the free energies of the AFE and

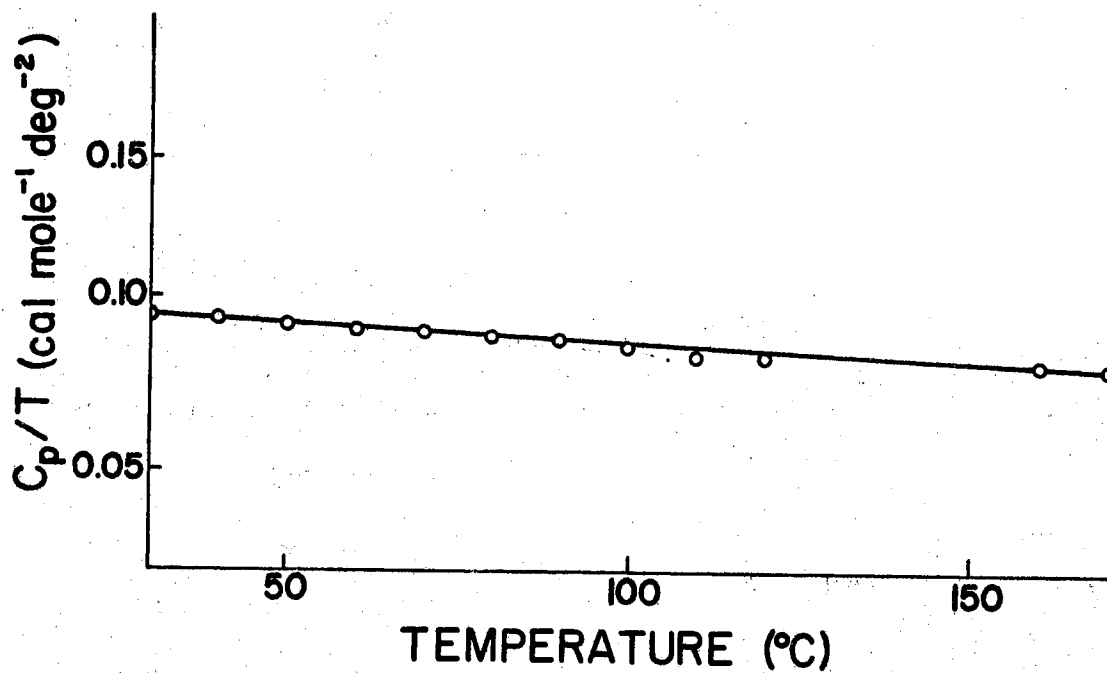


Figure 47. C_p/T for PZST Sample.

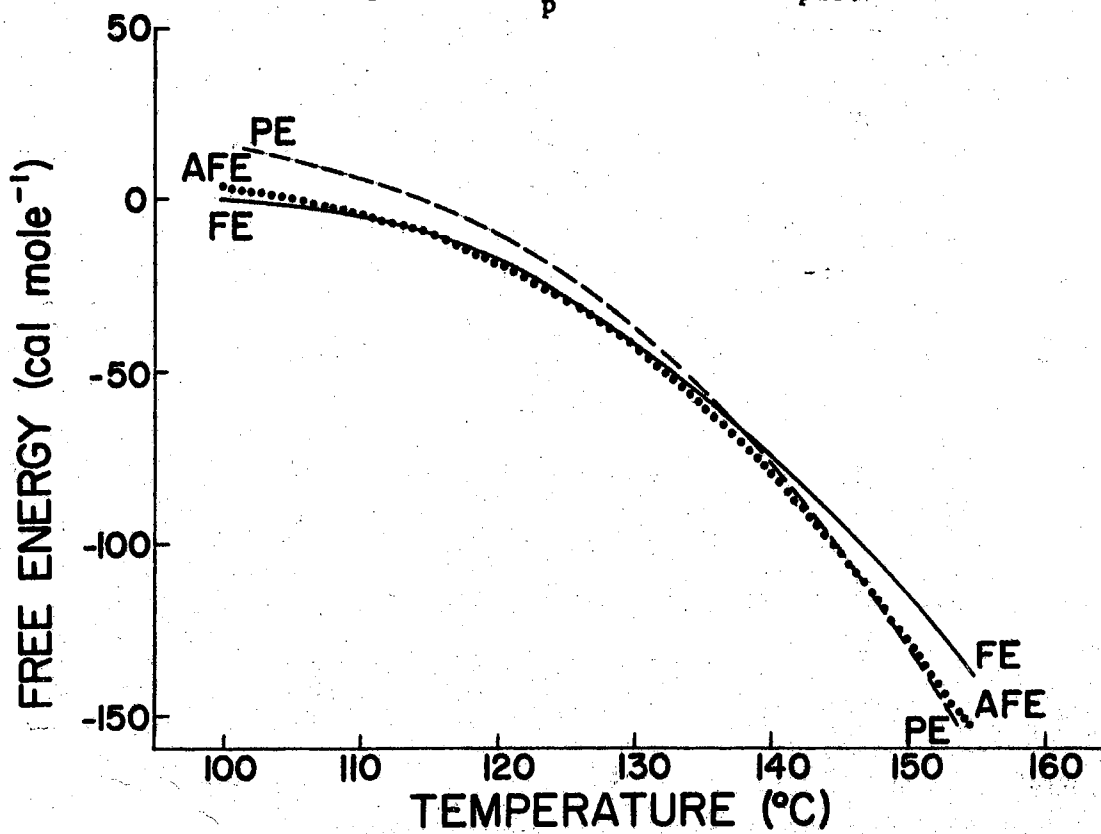


Figure 48. Free Energy vs. Temperature for PZST. (Relative to FE Phase at 100°C)

PE phases may be made relative to that of the FE phase at all temperatures. These are shown in Figures 49 and 50. The phase relationship pictured in Figure 49 is for zero pressure and field. The FE-AFE equilibrium point has been set at 125° C to be consistent with the hysteresis observed in Figure 10. The AFE-PE equilibrium has been placed at the Curie temperature observed with rising temperature because of the small hysteresis connected with this transition. If the assumption is made that the curvature of the free energy vs. temperature is approximately the same in all three phases, the relative free energies may be approximated by straight lines. The slopes of these lines have been chosen to fit the entropy differences noted at the transitions and the free energy differences found at temperatures near the normal transitions, but can be considered only semi-quantitative. Lines have been drawn at the observed FE-AFE and AFE-PE transitions to show the probable free energy differences over which hysteresis effects can occur. These differences are approximately 0.10 cal/mole at the FE-AFE transition and about 1.75 cal/mole at the reverse transition.

Figure 50 represents the relative free energies at a field of 5 Kv/cm. This field lowers the free energy of the FE phase approximately 1 cal/mole relative to the other phases and lowers the PE phase line slightly with respect to the AFE phase line. Here the AFE-PE transition was observed at a temperature corresponding to a free energy difference of about 1.25 cal/mole. This decrease of energy difference necessary to cause the transition was probably due to the orienting nature of the applied field. The FE-AFE transition occurs at a temperature where the PE phase becomes energetically competitive, leading to the possibility of a blending of the transitions. At fields greater than about 7 Kv/cm

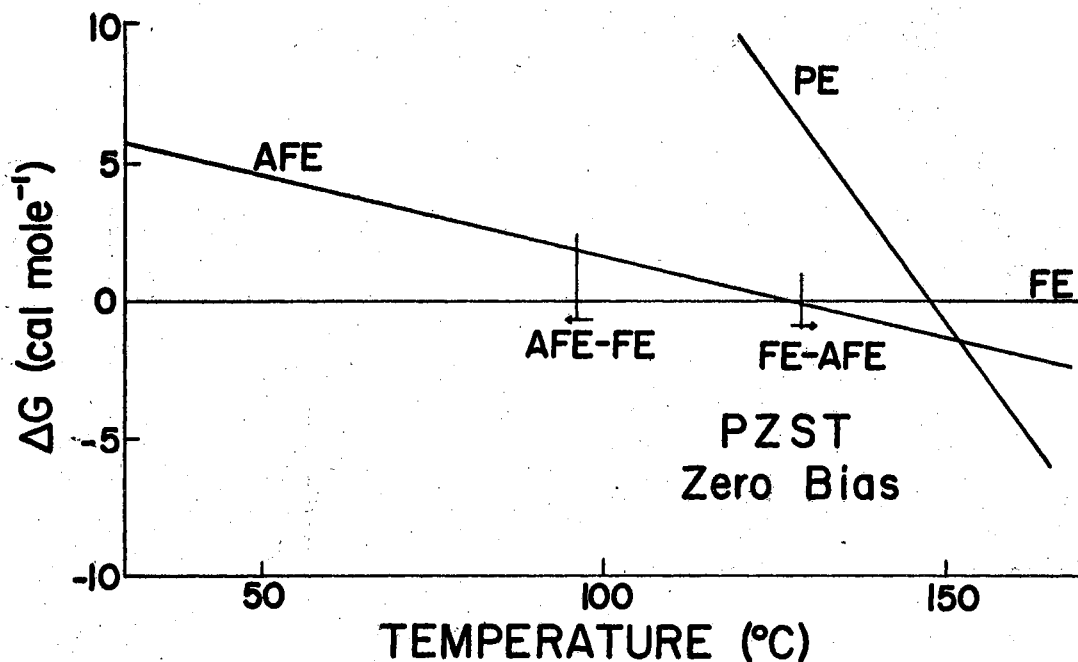


Figure 49. Relative Free Energies of the Various Phases for a PZST Sample at Zero Field.

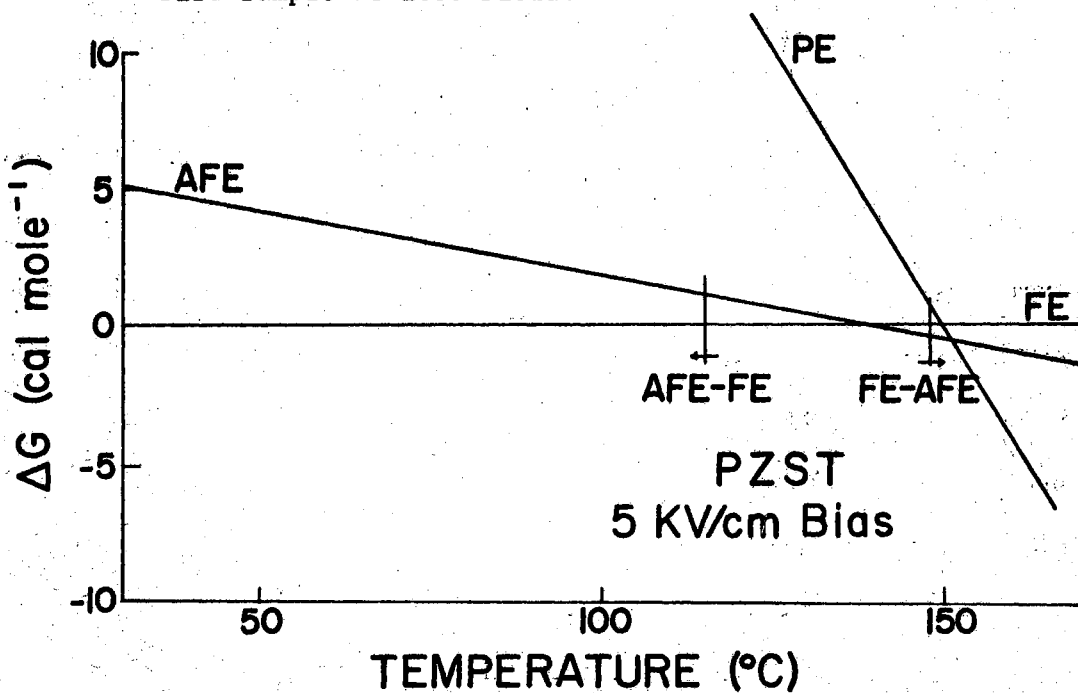


Figure 50. Relative Free Energies of the Various Phases for a PZST Sample with External Field of 5 KV/cm.

the AFE phase disappears completely since the junction of the FE free energy curve and the PE free energy curve occurs below the AFE free energy curve.

From this treatment it can be seen that although the absolute values of the free energies cannot be calculated exactly and approximations must be made in order to calculate the free energy differences between the phases, the behavior of the relative free energies of the various phases leads to an explanation of the dependence of transition temperature and hysteresis characteristics on the external electric field.

Results for the Lead Hafnate Titanate Samples

As has been pointed out previously, the lead hafnate titanate samples gave less quantitative information regarding free energies since the transitions tended to be more diffuse. Thus a quantitative discussion of the relative free energies of these materials would not be productive with the present results. Qualitatively, the fact that AFE-FE transitions have been induced at temperatures as much as fifty degrees below the normal transition temperature shows that the phases are more nearly equal in free energy than corresponding phases in the PZST material. Thus, in these materials too, the free energies and the entropies of the FE and AFE phases show only a very slight variation.

Qualitative Theory of FE-AFE Transitions in Lead Perovskites

From the preceding discussions it appears that the reversal of the direction of phase transformation with rising temperature in these ferroelectric materials does not represent a drastic difference in the thermodynamic character of the material but rather a relatively minor

difference which changes the delicate balance of thermodynamic parameters from one mode of behavior to another. Regardless of whether the transition with rising temperature is FE-AFE or AFE-FE, both the free energies and the entropies of the two phases are nearly equal under conditions of room temperature, atmospheric pressure, and zero electric field. If the free energy of the FE phase is lower than that of the AFE phase at room temperature and the entropy of the FE phase is higher than that of the AFE phase, the FE phase will prevail at all temperatures between room temperature and the Curie temperature. If the entropy of the AFE phase happens to be greater than that of the FE phase, there is a possibility that the AFE phase will become energetically favorable below the Curie temperature and an FE-AFE phase transition may occur. Likewise, a room temperature dominance of the AFE phase coupled with a slightly higher entropy in the FE phase leads to the possibility of an AFE-FE transition. Since the free energies involved are small, the entropy differences necessary are extremely minute.

It is interesting here to compare the energies associated with the FE-AFE transitions with those observed in other common transformations. Chemical transformations are accompanied by energy changes of the order of 10^4 to 10^6 calories per mole. For example, the heat of combustion of carbon is about 8000 calories per gram, or 100,000 calories per mole. Changes of state normally involve changes of energy two orders of magnitude smaller than this. For example, the energy change during the melting of ice is about 1440 calories per mole. Thus it can be seen that the energy differences involved in FE-AFE transformations (about 10 calories per mole) are quite small when compared with most transformation energies.

By using the above considerations, the relationship between the FE and AFE phases with regard to free energy and entropy may be outlined for the lead perovskite compositions used in this study.

In both pure lead zirconate and pure lead hafnate, the AFE phase is the phase of minimum free energy. The free energy difference between the FE and AFE phases at room temperature is great enough that differences in entropy cause no AFE-FE phase transformations below the Curie temperature. However, the difference between the zirconium ion and the hafnium ion is great enough to cause a difference in the entropy relationships between the two phases. In lead zirconate the entropy of the FE phase is greater than that of the AFE phase, while in lead hafnate the opposite is true. These differences are brought out by the addition of the titanium ion. The addition of a small amount of titanium to lead zirconate produces a situation in which the AFE phase is still dominant at room temperature but the larger FE phase entropy can lead to an AFE-FE phase transformation at higher temperatures before the paraelectric phase becomes dominant. In lead hafnate, on the other hand, certain amounts of titanium ion produce a condition in which the FE phase is dominant at room temperature but the higher entropy of the AFE phase causes an FE-AFE transformation to take place below the Curie temperature. Thus, this small entropy difference between the phases in the two materials produces radically differing behavior.

The addition of a small amount of stannate ion to lead zirconate titanate increases the entropy of both phases but affects the AFE phase more than the FE phase, causing the AFE phase to become the phase of highest entropy. Again when enough titanate ion is available to cause the FE phase to be only slightly dominant at room temperature, the

greater entropy of the AFE phase is sufficient to cause an FE-AFE transformation to occur at higher temperature. Thus the behavior of this material is found to be similar to that of lead hafnate titanate rather than lead zirconate titanate.

This behavior of the FE and AFE phases would therefore seem to emphasize that the only drastic difference between the two phases is in the electrical properties. The fact that the unit cell polarizations sum in the case of ferroelectric materials and cancel in antiferroelectrics leads to large variations in behavior with only minor structural and energy differences. This in turn explains the great influence that structural and thermal parameters exert on the observed properties of these materials.

Resume of Experimental Techniques

Dielectric Measurements

The most important results of the dielectric portion of this study lie in the use of the equivalent conductance as a technique for the study of FE-AFE phase transitions and in the measurement of the dielectric saturation associated with the peaks of dielectric constant in the vicinity of the Curie transition.

As has been pointed out previously, the use of equivalent conductance in the place of the more conventional $\tan \delta$ allows a truer observation of the actual loss mechanism in the dielectric material. By eliminating the effects of the rapidly changing dielectric constant in the vicinity of a transition, it becomes easier to distinguish between the various types of transition which occur, and allows a better estimate of transition temperatures.

The effect of dielectric saturation at high electric fields has a pronounced bearing on the application of these materials in thermal-to-electric energy conversion. The highest dielectric constants observed in this study were found under triple point conditions, that is, near that temperature and field at which the FE, AFE, and cubic phases show nearly equal free energies. Unfortunately, this is also the region where the dielectric constant is most degraded by the application of a further electric field. Thus the conversion efficiencies and amplifications to be gained by thermally changing the dielectric constant are lessened and stability becomes a problem. Because of the absorption of charge in the unit cells of the FE phase as the temperature of the material decreases from the Curie temperature, it seems that the best amplification characteristics will be found by using the change of dielectric constant of an AFE material in these parametric devices. Results of the present study indicate that amplifications of three to five should be possible with the present materials.

Thermal measurements

This study has indicated that while thermal measurements are much less sensitive than electrical measurements in the vicinity of an FE-AFE transition, they nevertheless reveal valuable information concerning the energy relationships between the phases. The interpretation of thermal data with regard to accurate determination of excess specific heat and heats of transition will require further study with improved ceramics and single crystals. As was pointed out earlier, in this study only the excess heat occurring in the spike at the transition was used in calculating the heats and entropies of transition. Materials exhibiting

sharper transitions should cause these peaks to be more pronounced and thus give more accurate results.

A final result of this study is the indication that in many cases, what has been considered as a single phase sample may actually contain two or more phases coexisting over a temperature range which extends many degrees away from the "transition temperature." One cause of this behavior lies in the ceramic nature of the material with the accompanying stresses and variations of particle size and texture. Another cause probably lies in the lack of true chemical homogeneity throughout the samples. Since the electrical character of these materials shows such a strong dependence on structural characteristics, very slight compositional variations will spread transitions appreciably, causing a blending of transition characteristics when more than one transition is occurring in any small temperature region. As material processing techniques are improved, the experimental techniques described in this report will allow much information to be gained about the thermodynamic characteristics of ferroelectric and antiferroelectric phase transitions in lead perovskites.

BIBLIOGRAPHY

1. Anderson, J. A., Rept. Nat. Res. Council, April 1918.
2. Berlincourt, D. A., Research on Piezoelectric Materials and Phenomena, Annual Progress Report (1961).
3. Berlincourt, D. A., Research on Piezoelectric Materials and Phenomena, Fifth Progress Report (1961).
4. Berlincourt, D. A., and H. H. A. Kreuger, Phase Transitions in $Pb(Zr, Sn, Ti)O_3$ Compositions (1962).
5. Buerger, M. J., "Crystallographic Aspects of Phase Transformations", Phase Transformations in Solids, John Wiley and Sons, New York (1951).
6. Cady, W. G., Rept. Nat. Res. Council, May 1918.
7. Cross, L. E., and B. J. Nicholson, Phil. Mag. 46, 453 (1955).
8. Dauphinee, T. M., and S. B. Woods, Rev. Sci. Instr. 26, 693 (1955).
9. Devonshire, A. E., "Theory of Ferroelectrics", Advances in Physics 3, 85 (1954).
10. Dungan, R. H., and A. H. Stark, Investigation of Solid Solutions in the Antiferroelectric Region of the $PbHfO_3$ - $PbTiO_3$ - $PbNb_2O_6$ System, Sandia Corporation Technical Memorandum 224-62(11), (1962).
11. Goodman, G., J. Am. Ceram. Soc. 43, 105 (1960).
12. Hall, C.A., Preparation and Investigation of Solid Solutions in the High Hafnate Region of the $PbHfO_3$ - $PbNb_2O_6$ - $PbTiO_3$ System, Sandia Corporation Technical Memorandum 21-6(11), (1962).
13. Hall, C. A., personal communication.
14. Hall, C. A., Ph. D. dissertation, University of Illinois, 1962.
15. Jaffe, B. R., S. Roth, and S. Marzullo, J. Res. Nat. Bur. Stand. 55, 239 (1955).
16. Jaynes, E. T., Ferroelectricity, Princeton University Press, Princeton, (1953).

17. Jona, F., and G. Shirane, Ferroelectric Crystals, The McMillan Co., New York (1962).
18. Kanzig, W., "Ferroelectrics and Antiferroelectrics", Solid State Physics 4, 1, Academic Press, Inc., New York (1957).
19. Megaw, H., Ferroelectricity in Crystals, Methuen and Co., Ltd., London (1957).
20. Megaw, H., Acta Cryst. 2, 187 (1954).
21. Roth, R. S., J. Res. Nat. Bur. Stand. 58, 75 (1957).
22. Sachse, H., Ferroelectrika, Springer-Verlag, Berlin (1956).
23. Sanderson, R. T., Chemical Periodicity, Reinhold Publishing Co., New York (1960).
24. Sawaguchi, E., J. Phys. Soc. Japan 8, 615 (1953).
25. Sawyer, C. and C. Tower, Phys. Rev. 35, 267 (1930).
26. Shirane, G., and R. Pepinsky, Phys. Rev. 91, 812 (1953).
27. Shirane, G., R. Pepinsky, and B. C. Frazer, Acta Cryst. 2, 131 (1956).
28. Sykes, C., Proc. Roy. Soc. 148, 422 (1935).
29. Wells, A. F., Structural Inorganic Chemistry, Oxford University Press, London (1962).

VITA

John Willard Northrip

Candidate for the Degree of

Doctor of Philosophy

Thesis: THERMODYNAMIC CHARACTERISTICS OF FERROELECTRIC AND ANTI-FERROELECTRIC TRANSITIONS IN LEAD PEROVSKITES

Major Field: Physics

Biographical:

Personal Data: Born in Tulsa, Oklahoma, July 7, 1934, the son of J. Willard and Vivian A. Northrip.

Education: Attended grade school in Tulsa, Oklahoma and West Plains, Missouri; graduated from West Plains High School in 1951; received the Bachelor of Science degree from Southwest Missouri State College, with majors in Mathematics and Physics, in August, 1954; received the Master of Science degree, with a major in Physics, from Oklahoma State University in May, 1958; completed requirements for the Doctor of Philosophy degree in August, 1964.

Professional experience: Served in the United States Navy as an electronics technician from 1954 to 1956; worked as a staff member in the Applied Research Department of Sandia Corporation, Albuquerque, New Mexico, from 1958 to 1960; member of the American Physical Society, the American Association for the Advancement of Science, and Sigma Xi.